ALMA MATER STUDIORUM · UNIVERSITÀ DI BOLOGNA

SCUOLA DI INGEGNERIA E ARCHITETTURA
Corso di Laurea Magistrale in Ingegneria Civile

DIPARTIMENTO DI INGEGNERIA CIVILE, CHIMICA, AMBIENTALE E DEI MATERIALI

Tesi di Laurea in
Dinamica delle Strutture

Forests as a natural seismic metabarrier: analysis of interaction between trees and Rayleigh waves

RELATORE: CANDIDATA:

Chiar.mo Prof.   Flaminia Cabras
Alessandro Marzani

CORRELATORI:

Dott. Andrea Colombi
Chiar.mo Prof. Richard Craster

Contents

Abstract

The present thesis describes a sensitivity analysis over design parameters carried out through finite element simulations on seismic metamaterials, locally resonant structures able to affect the propagation of waves passing through them. Locally resonant metamaterials represent a particular type of resonant scattering, which is very powerful mean for stopping (bandgaps) and redirecting elastic waves at different length scales.

This work, carried out at the Imperial College London, is inserted as part of the the META-FORET project, a large-scale wave experiment, which aims to demonstrate the effectiveness of metamaterials in geophysics. In particular, this project proved that a dense forest of tree can behave as a natural seismic metamaterial for Rayleigh surface waves. Thus creating anomalous dispersion curves and bandgap, frequency regions where the wave propagation is forbidden. These regions are associated with compressional and flexural resonances of the trees.

Therefore I studied the same phenomena with time-domain numerical simulations, implemented in MATLAB. In particular, the simulation is performed with the spectral element method, a popular and efficient formulation of the finite element method that provides a numerical solution of partial differential equations. I analyzed the interaction between seismic metamaterials and the Rayleigh waves in one-dimensional and two-dimensional domain, neglecting the horizontal component to maintain the physical and numerical complexity low. This method is really efficient to conduct a sensitivity analysis, in order to identify which parameters influence the behavior of metamaterials and drive benchmarks.

Acknowledgments

Chapter 1

Introduction

This work aims to investigate the effective properties of metamaterials at the geophysical scale. I analyzed, through numerical simulations, the interaction between the seismic Rayleigh waves and seismic metamaterials, which are governed by locally resonant structures [18]. In particular, I numerically tackled a problem similar to the experiment performed in the META-FORET project [26], which studies the interaction between a forest of pine trees and Rayleigh waves. This project proved the presence of bandgaps, frequency ranges where the wave propagation is forbidden, for Rayleigh waves associated with compressional and flexural resonances of trees. Thus, a forest can control the elastic wave propagation for specific frequency range , acting as a natural seismic metamaterial. These important results may contribute to pave the way of seismic waves control. Therefore, I adapted a MATLAB code, already implemented by Prof. Jean Paul Ampuero, to analyze the wave propagation through locally resonant metamaterials. It has been used the spectral element method (SEM), which is an efficient type of finite element method for solving partial differential equation. I studied the same phenomena in both 1D and 2D fields, performing a sensitivity analysis over design parameters. Thus, I analyze which parameters influence the metamaterials' behavior to evaluate and improve the wave control capacities. Furthermore, starting from the time domain signal, I analyze the 1D and 2D problems in the frequency and wavenumber-wavenumber domain to individuate the presence of bandgap, slow waves and dynamic anisotropy.

1.1 Introduction to metamaterials and wave propagation engineering

Metamaterials are usually defined as artificially materials that are designed to have innovative properties not usually found in nature. This field nowadays forms a major emerging research area. Elastic or electromagnetic metamaterials for example can be made from composite materials such as metals ore plastics. Indeed, their properties derive from their physical macro structure, and not by their chemical composition. Metamaterials are artificial media structured on a size scale smaller than the wavelength of the wave propagation phenomenon they have influence on. Their structure arranged in a specific shape, size and geometry makes them capable to manipulate waves by blocking, absorbing, reflecting or banding. These materials can be designed to have a negative refractive index for a specific range of frequencies, predicted by Veselago[30] and revisited by Pendry [21]. Thus, it was developed in optics and electromagnetism a material having both
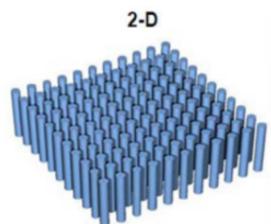

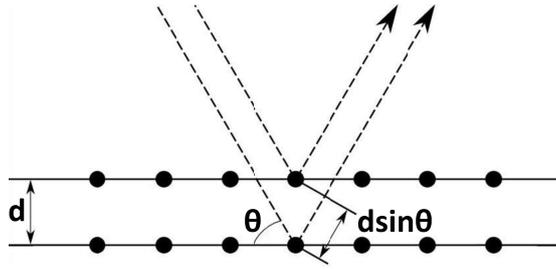Figure 1.1: Example of periodic structure

Figure 1.2: Bragg diffraction: two rays approach to a crystal modeled as a set of discrete parallel planes and they are scattered off two different atoms. The rays have the same wavelength comparable to the atomic distance and the ray is scattered when $d\sin(\theta)$ is equal to an integer multiple of the wavelength [31].

negative permittivity and permeability, using a sub-wavelength periodic structure[21] .

The study of metamaterials starts in 1987 with a research on photonic crystal conducted by Eli Yablonovitch [34] and Sajeev John [11], who studied these periodic optical structures in more than one dimension. Particularly, they show how their periodic form can manipulate the light propagation, through permitted and forbidden electronic energy bands. Forbidden bands of wavelength are called photonic bandgaps, which are the key concept for metamaterials.

The bandgaps in photonic crystal arise due to the Bragg diffraction, which occurs when electromagnetic waves, which wavelength is comparable to lattice's constant distance between elements, are scattered from lattice planed of the photonic crystal. Indeed, these crystals produce peaks of reflected radiation at certain incident angles and wavelengths comparable to atomic spacing. By modeling a crystal as a set of discrete parallel planes separated by a constant distance d, the phenomena is explained by the Bragg's law:

$$2d\sin(\theta) = n\lambda \tag{1.1}$$

Where:

- θ = scattering angle ;

- d = distance between parallel planes of a crystalline system;

- $n \simeq$ positive integer;

- λ = wavelength of incident wave.

Thus, the Bragg diffraction occurs when radiation has a wavelength comparable to the lattice spacing. The photonic crystal reflects the incident wave like a mirror and a bandgap appears in the dispersion relation around the frequency referred to λ .

Few years later, the same concept was applied to elastic acoustic waves. Thus, emerged the concept of phononic crystals, which are artificial periodic composite materials able to open bandgaps in the dispersion relation for a specific range of frequencies [15] [22]. The existence of these bandgaps is related to the interference of the scattered waves phenomena from the periodic structure and it occurs when the periodicity of the structure is comparable to the wavelength of the wave they have influence on. The phononic crystals have many potential applications [27] .

Seismic metamaterials are the mostly recently developed and meant to control seismic elastic waves, applying the metamaterials and phononic concepts at geophysical scale. Yet it results complicated to design a periodic structure with dimensions comparable to the typical earthquake wavelengths, which are from meters to decameters, referring to the frequency range relevant for Earthquake engineering applications. Therefore, unlike the Bragg-type scattering that occurs in phononic crystals, seismic metamaterials are made by locally resonant structures, a particular type of resonant scattering [18]. Generally, this kind of structure is smaller than the wavelength of the phenomena they influence and able to create hybridization gaps in low-frequency ranges. It is important to distinguish it from non-resonant inclusions, where the propagation can be described
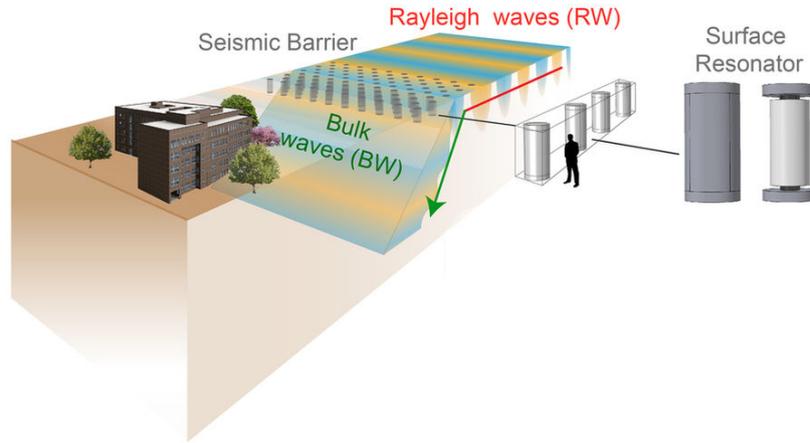
Figure 1.3: Representation of the resonant metabarrier[20]
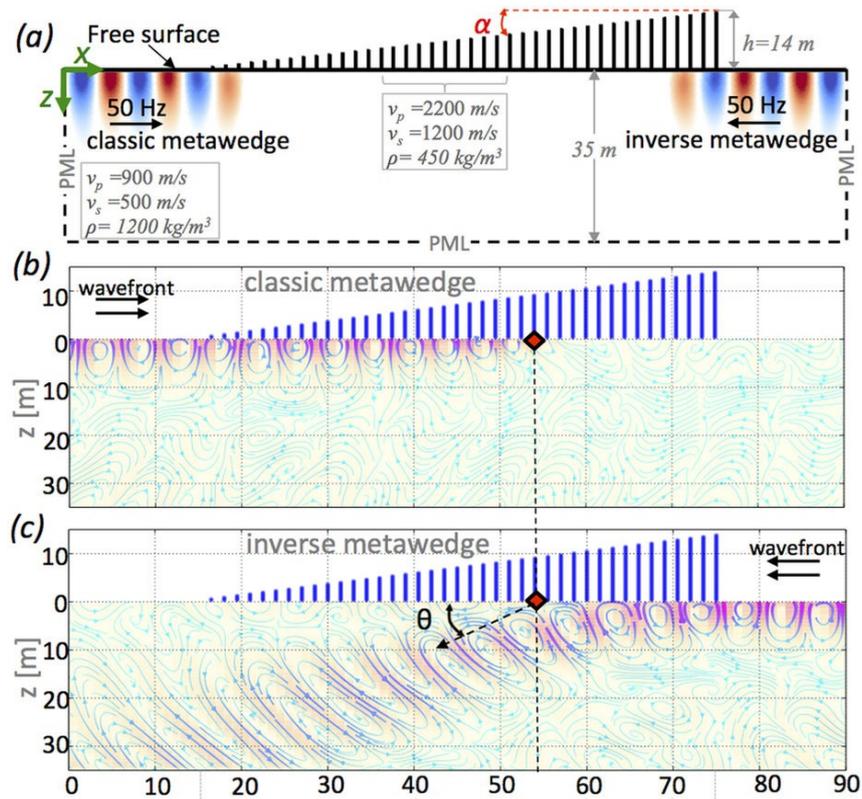
Figure 1.4: (a) Geometry of the problem: side view of the metawedge and wave front for both cases of classic and inverse matawedge. (b) Wave propagation for classic metawedge, the wavefront hits the shortest resonator. (c) Wave propagation for inverse metawedge, the wavefront hits the tallest resonator. In (b) and (c) the colorscale and linewidth of the elastic stream lines indicates the magnitude of the amplitude [5].

by general effective media theory [17]. Thus, the wave attenuation is due to the collective effect of local resonant units instead of periodic layout [15]. The distance between resonators has to be smaller than $\lambda/2$, where λ is the wavelength of the wave they manipulate.

In the last years, many experiments proved the validity of seismic metamaterials concepts. For example, Palermo et al. [20] proposed a seismic metabarrier able to convert seismic Rayleigh waves into shear bulk waves. The metabarrier is made by sub-wavelength resonant structures buried under the soil surface, composed by a cylindric mass suspended by elastomeric springs, shown in the Fig 1.3. The same result was proved with a scaled experimental model. In one of the last experiment it was proved by Colombi et al. [5] that the optical rainbow effect (spatial selection of frequency according to the wavelength) for electromagnetic metasurface could be created at the geophysical scale as "seismic rainbow effect". The optical rainbow effect[29] consists in a graded wedge of sub-wavelength resonators that can trap and spatially segregate the different frequencies (or colors) of light. The same concept it was applied to design a metasurface capable of controlling the flow of Rayleigh waves. Thus, it was developed a seismic metawedge made by a graded array of vertical resonators in 2D, designed referring to the first vertical resonance of an array of rods, that depends on the rods' length (Fig.1.4). When the waves hit the short edge (classic metawedge) the wave is trapped (Fig.1.4b), after traveling few meters inside the metawedge waves are reflected by the graded resonators, showing the same rainbow phenomena proved in acoustic. When Rayleigh waves hit the high edge (inverse metawedge),they are converted into shear waves, which propagate into the substrate. The results in terms of displacements are shown in the Fig 1.4.

1.2   Seismic waves

An earthquake is the shaking of the earth's surface and it is generated by a quick release of energy accumulated by the continuous sliding of tectonic plates. The large quantity of energy released during an earthquake generates seismic waves, mechanical motion that travel through the Earth's layers, from the hypocenter to the surface.[28] There are different kind of seismic waves and the main distinctions is between body waves, which travel through the interior of the Earth, and surface waves, which travel along the Earth's surface and are the most destructive for humans.

The body waves start traveling from the hypocenter and the main types are:

- **Primary waves**: P-waves are compressional longitudinal waves, whose particle motion is in the same direction of the wave propagation. The particles invested by P-waves change their volume with compressions and dilations. This kind of waves can propagate through any type of material and fluids and are the first recorded by seismometers. Indeed, P-waves are the fastest and their speed increases with the density of the medium (330 m/s in air and 5000 m/s in granite).

- **Secondary waves**: S-waves are shear transverse waves, whose particle motion is perpendicular to the direction of wave propagation. S-waves cannot propagate in fluids, as fluids do not stand shear stresses, and their speed is typically 60 % of that of P-waves in any given materials. The particle invested changes their shape, but their volume is unchanged.

The surface waves arise from the interaction of the elastic waves and the free surface, they are composed of P and S waves in a linear combination. Their amplitudes decrease exponentially with depth within a medium. I consider here mainly two types of surface waves:

- **Rayleigh waves**: Rayleigh waves travel along the surface of solid and include both longitudinal and transverse motions. In an elastic, isotropic and homogeneous medium there is no dispersion, but in a solid whose density or sound velocity changes with depth Rayleigh waves become dispersive. They are slower than body waves and their speed is typically 90 % of that of S-waves.

- **Love waves**: Love waves are horizontally polarized surface waves and they arrequire a velocity structure that varies with depth and cannot exist in a uniform half-space. They usually travel slightly faster than Rayleigh waves and the particle motion describes a horizontal line perpendicular to the direction of the wave.

Body waves

P Wave

expansions, compressions

undisturbed medium

S Wave

wavelength

Surface waves
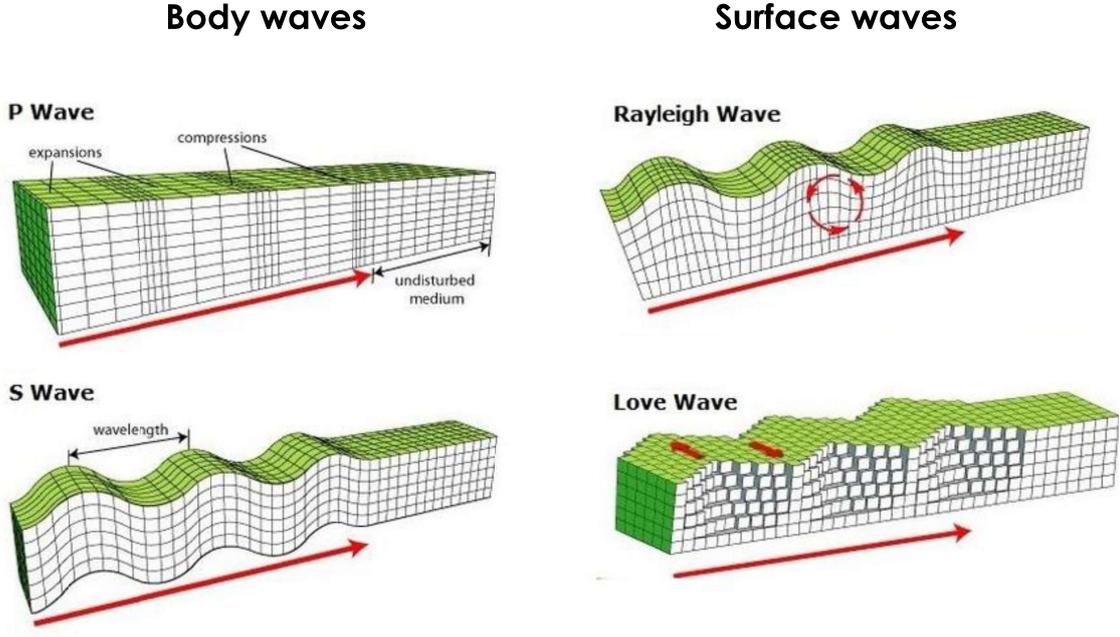
Rayleigh Wave

Love Wave

Figure 1.5: Particle elliptic motion and wave direction of the main types of seismic waves: Primary waves, Secondary waves, Rayleigh waves and Love waves

1.2.1 Rayleigh waves

The Rayleigh waves are a combination of P and SV waves that travel on the surface and could be studied at the top of a homogeneous half-space[28]. We consider the free surface at z=0 and the motion in x-z plane.

The waves can be described by P and SV potentials that satisfy the free surface boundary condition:

$$\Phi = A \exp\left(i(\omega t - k_x x - k_x r_\alpha z)\right) \tag{1.2}$$

$$\Psi = B \exp\left(i(\omega t - k_x x - k_x r_\beta z)\right) \tag{1.3}$$

Where:

- ω is the angular frequency

- k_x is the horizontal component of the wave vector that describes the direction of wave propagation, with this geometry k_x is the same for P and SV waves.

- $r_\alpha = \frac{k_{z\alpha}}{k_x} = \sqrt{\frac{c_x}{\alpha^2} - 1} = \cot i$, is the ratio of vertical to horizontal wavenumber. α is the medium velocity for the P waves and c_x is the apparent velocity, the velocity at which a plane wave appears to travel along a horizontal surface and is defined as $\frac{v}{\sin i} = \frac{\omega}{k_x}$ where i is the incident angle for the P waves.

- $r_\beta = \frac{k_{z\beta}}{k_x} = \sqrt{\frac{c_x}{\beta^2} - 1} = \cot j$, is the ratio of vertical to horizontal wavenumber. β is the medium velocity for the SV waves and c_x is the apparent velocity, the velocity at which a plane wave appears to travel along a horizontal surface and is defined as $\frac{v}{\sin j} = \frac{\omega}{k_x}$ where j is the incident angle for the SV waves.

To describe the energy trapped near the surface are applied the following conditions:

1. the energy cannot propagate away the surface;
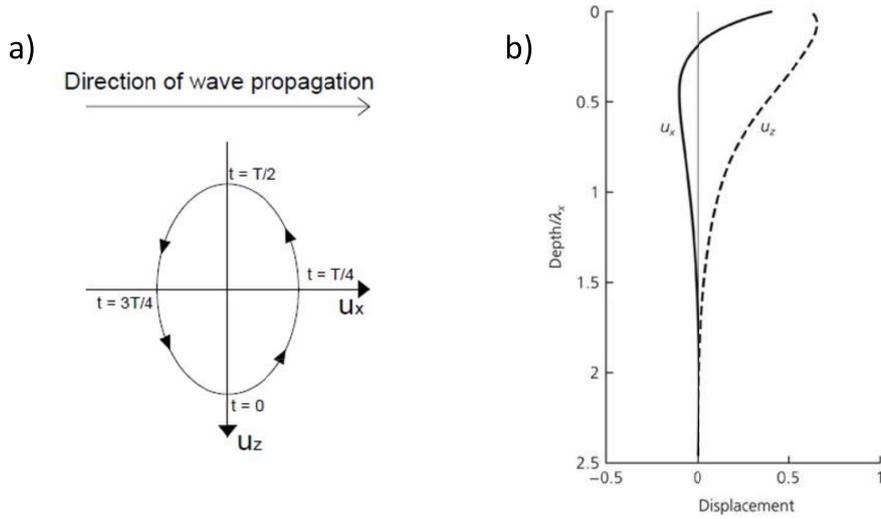
2. free surface boundary condition;

Figure 1.6: Rayleigh waves. (a) Particle elliptic motion and wave direction. (b) Variation with depth of the Rayleigh wave's components in an Poisson solid halfspace. Here u_x and u_z are plotted normalized by the horizontal wavelength and both of them decay with depth.

For this type of wave, the displacements decay with the depth as $\exp(-k_x z)$, so the depth significant for displacements is proportional to its horizontal wavelength and the exponential $\exp(ik_x r_\alpha z)$ and $\exp(ik_x r_\beta z)$ must have negative real exponents. Because of $r_\alpha = \sqrt{\frac{c_x}{\alpha^2} - 1}$ and $r_\beta = \sqrt{\frac{c_x}{\beta^2} - 1}$, it is necessary to fix an apparent velocity smaller than the shear velocities $c_x < \beta < \alpha$ so that the square roots become imaginary with the following choice of sign:

$$r_\alpha = -i\sqrt{1 - \frac{c_x}{\alpha^2}} \tag{1.4}$$

$$r_\beta = -i\sqrt{1 - \frac{c_x}{\beta^2}} \tag{1.5}$$

To satisfy the second condition, we impose the tangential stress and the normal stress at z = 0 :

$$\sigma_{xz}(x,0,t) = 2\mu\epsilon_{xz} = \mu\left(\frac{\partial u_x}{\partial z} + \frac{\partial u_z}{\partial x}\right) \tag{1.6}$$

$$\sigma_{zz}(x,0,t) = \lambda\theta 2\mu\epsilon_{zz} = \lambda\left(\frac{\partial u_x}{\partial x} + \frac{\partial u_z}{\partial z} + \mu\left(\frac{\partial u_x}{\partial z}\right)\right) \tag{1.7}$$

Expressed in terms of potential, without incident wave:

$$\sigma_{xz}(x,0,t) = 2r_\alpha A + (1 - r_\beta^2)B = 0 \tag{1.8}$$

$$\sigma_{zz}(x,0,t) = [\lambda(1 + R_\alpha) + 2\mu R_\alpha^2]A + 2\mu R_\beta^2 B = 0 \tag{1.9}$$

Using the expressions $r_\alpha = \sqrt{\frac{c_x}{\alpha^2} - 1}$ and $r_\beta = \sqrt{\frac{c_x}{\beta^2} - 1}$, we obtain a linear homogeneous system for A and B:

$$2\sqrt{\left(\frac{c_x^2}{\alpha^2} - 1\right)}A + \left(2 - \frac{c_x^2}{\beta^2}\right)B = 0 \tag{1.10}$$

$$\left(\frac{c_x^2}{\beta^2} - 2\right)A + 2\sqrt{\left(\frac{c_x^2}{\beta^2} - 1\right)}B = 0 \tag{1.11}$$

From this system of equations it is possible to compute the coefficients A and B in terms of the shear velocity c_x:

$$B = A\left(2 - \frac{c_x^2}{\beta^2}\right)/(2r_\beta) \tag{1.12}$$

We find the nontrivial solution from the former system of equation imposing the determinant zero, obtaining:

$$(2 - \frac{c_x^2}{\beta^2})^2 + 4 \sqrt{(\frac{c_x^2}{\beta^2} - 1)} \sqrt{(\frac{c_x^2}{\alpha^2} - 1)} = 0 \tag{1.13}$$

Only one of the four roots satisfy the equation and the requirement $0 < c_x < \beta$. Imposing the values of velocity for P and SV waves referred to a Poisson solid with $\frac{\alpha^2}{\beta^2} = 3$, the last equation becomes:

$$(\frac{c_x^2}{\beta^2})[\frac{c_x^6}{\beta^6} - 8\frac{c_x^4}{\beta^4} + \frac{56}{3}\frac{c_x^2}{\beta^2} - \frac{32}{3}] \tag{1.14}$$

Finally, taking the real part of the exponential and setting the velocities' values referred to a Poisson solid, we obtain:

$$u_x = Ak_x \sin(\omega t - k_x x)[\exp(-0.85k_x z) - 0.58\exp(-0.39k_x z)] \tag{1.15}$$

$$u_z = Ak_x \cos(\omega t - k_x x)[-0.85\exp(-0.85k_x z) + 1.47\exp(-0.39k_x z)] \tag{1.16}$$

Both components are harmonic waves propagating in x direction, which exponentially decay with depth. The Fig. 1.6 shows how the components of the displacement decrease with depth.
For $z = 0$ the displacements are:

$$u_x = 0.42Ak_x \sin(\omega t - k_x x) \tag{1.17}$$

$$u_z = 0.62Ak_x \cos(\omega t - k_x x) \tag{1.18}$$

The two components are out of phase and the amplitude of the displacement in z-direction is about 1.5 times the amplitude in x-direction, so the particle motion at the free surface describes a retrograde ellipse as function of time (see Fig. 1.6). Furthermore, the displacement in radial and vertical directions are the sine and cosine function of the same argument, thus when u_x has a maximum u_z is zero and vice versa. This feature of the Rayleigh wave motion is particularly relevant for the analysis presented in this study. I will discard the dependence with depth and discard the u_x component. The coupling between rods and elastic halfspace in Fig 1.4, can be described using only u_z and the vertical motion of the resonator [7].

1.3 Frequency domain analysis

Under certain circumstances, the wave propagation can be efficiently described making use of the frequency domain representation of a time domain signal. In the frequency domain the signal's energy is described as a complex function of frequency. At each value of frequency corresponds a complex number representing the magnitude, that is the amplitude of that component, and the angle, that is the relative phase. A time domain signal can be converted in the frequency domain through mathematical operators, called transform. One of the most used is the Fourier Transform, which decomposes a time function into the frequencies that determine it.

1.3.1 The Fourier Transform

A non-periodic waveform can be transformed from a function of time to a function of frequency by using the Fourier integral:

$$F(\omega) = \int_{-\infty}^{\infty} f(t)e^{-i\omega t}dt \tag{1.19}$$

The waveform becomes a complex function of angular frequency and has the dimension of displacements multiplied by time. In order to transform $x(t)$ using the Fourier Integral, the function must be non periodic and must respect Dirichlet conditions [25]:

- For $-\infty \leq t \leq \infty$, $x(t)$ must contain a finite number of maxima and minima;

- If $x(t)$ contains discontinuities, they must be in finite number over the range $-\infty \leq t \leq \infty$;

- The function $x(t)$ must be integrable in the sense that

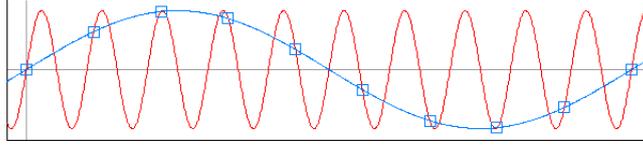$$\int_{-\infty}^{\infty} |x(t)|dt < \infty \tag{1.20}$$

Figure 1.7: Example of aliasing due to insufficient sampling: two different sinusoids can fit the same set of samples.

In the same manner, using the Fourier Inverse Transform, $F(\omega)$ can be inverse transformed back to the time domain function $x(t)$:

$$f(t) = \frac{1}{2\pi} \int_{-\infty}^{\infty} F(\omega)e^{i\omega t}d\omega \qquad (1.21)$$

In the frequency domain $F(\omega)$ is described by magnitude and phase diagrams and is a complex number which contains a real and imaginary part:

$$F(\omega) = \int_{-\infty}^{\infty} f(t)e^{-i\omega t}dt = Re(\omega) + iIm(\omega) \qquad (1.22)$$

Furthermore, in the analysis of seismic data by computer, the ground motion is represented by a signal consisting of the ground motion measured at discrete N points in time and $F(\omega)$ can be written as a summation, called Discrete Fourier Transform:

$$F(\omega) = \Delta t \sum_{n=0}^{N-1} f(n\Delta t)e^{-i\omega n\Delta t} \qquad (1.23)$$

Where N is a even number. The DFT operates on a finite sequence set of data where each point is discretely and evenly spaced in time [28]. In the same way, we can compute the Inverse Discrete Fourier Transform (IDFT) by approximating the inverse Fourier transform integral with discrete summation:

$$f(n\Delta t) = \frac{1}{2\pi} \sum_{k=0}^{N-1} F(k\Delta\omega)e^{i(k\Delta\omega)(n\Delta t)}\Delta\omega \qquad (1.24)$$

Thus, a continuous function of ω is approximated in a sum of values at discrete frequency points, that produces a spectrum periodic in angular frequency with a period of $2\pi/\Delta t$. So $\Delta\omega$ is divided into N points:

$$F(\omega) = F(k\Delta\omega) \quad for \ \ k = 0, 1..N - 1$$

With:

$$\Delta\omega = 2\omega_N/N = 2\pi/N\Delta t = 2\pi/T$$

Where $T = N\Delta T$ is the total length of the signal. In this way, it is obtained the Discrete Fourier Transform (DFT):

$$F(k\Delta\omega) = \Delta t \sum_{n=0}^{N-1} f(n\Delta t)e^{-ik\Delta\omega n\Delta t} = \Delta t \sum_{n=0}^{N-1} f(n\Delta t)e^{-ikn2\pi/N} \qquad (1.25)$$

That gives the values at angular frequencies:

$$0, \Delta\omega, 2\Delta\omega, ...(N/2)\Delta\omega, ...(N - 1)\Delta\omega$$

The first part of the values represents the positive angular frequency, the second part, after the Nyquist angular frequency $(N/2)\Delta\omega$, corresponds to the negative angular frequencies. Furthermore the Nyquist angular frequency is the highest that can be solved. On other hand, the resolution depends inversely on the total length ($T = N\Delta T$), because it is given by the spacing among angular frequency points ($\Delta\omega = 2\pi/(N\Delta t)$). During the sampling process, it is important to avoid the aliasing phenomena, which consists in the spectra overlap. Hence it is required to sample the signal densely, choosing a sampling interval Δt that corresponds to a Nyquist Frequency ($f_N = 1/(2\Delta t)$)

higher than the highest frequency component of the signal.

In the numerical simulations presented in this work, I analyze the signal in the frequency domain after having applied the Fast Fourier Transform (FFT), which is a smart discrete formula of the Fourier Transform already implemented in MATLAB and it makes possible to analyze digital signal without an hight computational cost. The FFT is a clever method to compute the DFT with less operations, indeed the DFT requires N^2 operations to evaluate N points, instead of the FFT which requires only $N \log_2 N$ operations [28]. That method requires N to be an integral power of 2 and the value usually taken is between 256 and 4096. The FFT, to compute the transform of function $f(n)$ recorded for a series of points ($n = 0, 1, ..., N-1$), splits the total number of points (N) into two sub-series :odd-numbered points series and even-numbered points series, as follows:

$$a(n) = (f(0), f(2), ...) = f(2N)$$

$$b(n) = (f(1), f(3), ...) = f(2N+1)$$

$$for \quad n = 0, 1, ...N/2 - 1,$$

Thus the DFT series is divided into two sub-series:

$$A(k) = \sum_{n=0}^{N/2-1} a(n)e^{-4\pi i k n/N} \qquad (1.26)$$

$$B(k) = \sum_{n=0}^{N/2-1} b(n)e^{-4\pi i k n/N} \qquad (1.27)$$

Furthermore, the original DFT ($F(k) = \sum_{n=0}^{N-1} f(n)e^{-i2\pi k n/N}$) can be written as:

$$F(k) = \sum_{n=0}^{N/2-1} [a(n)e^{-i2\pi k(2n)/N} + b(n)e^{-i2\pi k(2n+1)/N}] \quad for \; k = 0, 1, ...N/2 - 1 \qquad (1.28)$$

$$F(k) = A(k) + e^{-i2\pi k/N}B(k) \quad for \; k = 0, 1, ...N/2 - 1 \qquad (1.29)$$

The second N/2 are computed from replacing k by k+N/2:

$$F(k + N/2) = A(k + N/2) + e^{-2\pi i(k+N/2)/N}B(k + N/2) \qquad (1.30)$$

But it can be found from the first, using:

$$F(k + N/2) = A(k) - e^{-2\pi i k/N}B(k) \qquad (1.31)$$

Because the sub-series are periodic with a period equal to their length N/2 :

$$A(k + N/2) = A(k) \qquad B(k + N/2) = B(k) \qquad (1.32)$$

Using the exponential property:

$$e^{-2\pi i(k+N/2)/N} = e^{-\pi i}e^{-2\pi i k/N} = -e^{-2\pi i k/N} \qquad (1.33)$$

Thus with this method (doubling method)it is possible to compute the transform of an N-points series from the transforms of its two N/2-points sub-series. Applying the doubling method recursively a series of length $N = 2^n$ can be calculated by $n = \log_2 N$ steps. The same algorithm could be used to take the inverse transform.

Therefore, in this work, I use the frequency spectrum to investigate the bandgap, due to the interaction with seismic metamaterials, and to measure the relative drop of amplitude as a function of frequency.

1.3.2 Frequency-wavenumber analysis

To understand the metamaterials' effective properties and to individuate bandgaps generated by them, it is necessary to study the wave propagation in the frequency-wavenumber domain. A frequency-wavenumber diagram is a plot of wavenumber k, which represents the opposite of wave length $k = \frac{1}{\lambda}$, as function of frequency and it is used to examine the direction and apparent velocity of seismic wave. A dispersion relation relates the wavelength or wavenumber of a wave to its frequency and it describes the effect of dispersion in a medium of a wave traveling within that medium. Dispersion occurs when waves composed by different wavelengths have different propagation velocities inside the medium, so that a wave packet of mixed wavelengths tends to spread out in space. Therefore, the dispersion curve is linear only when the medium is elastic, homogeneous and isotropic. The speed of the wave is a function of the wavelength and it is related to the frequency, or the angular frequency as [3]:

$$v(\lambda) = \lambda f(\lambda) \tag{1.34}$$

$$\omega(k) = v(k)k \tag{1.35}$$

The use of $\omega(k)$ to describe the dispersion relation has become standard because phase velocity $(v = \omega/k)$ has convenient representations via this function.

Thus, it is possible to derive the dispersion curve of the recorded wave field. To pass from the time domain to the wavenumber-frequency domain it is necessary to apply the 2D Discrete Fourier Transform (DFT) that is defined as:

$$F(k,l) = \sum_{m=0}^{M-1} \sum_{n=0}^{N-1} f(m,n) e^{-i2\pi(\frac{k}{M}m + \frac{l}{N}n)} \tag{1.36}$$

Where:

- $F(k,l)$ is the discrete representations of the signal in the wavenumber-frequency domain;

- $f(m,n)$ is the discrete representations of the signal in the space-time domain;

- N and M are the number of point of the discrete signals for spatial and time domain .

In this work, I applied the 2D Fast Fourier Transform (FFT2) to obtain the signal in the frequency-wavenumber domain. The 2D Fourier Transform is already implemented in MATLAB and it permits to compute the 2D Discrete Fourier Transform reducing the computational cost.

The FFT2 returns the two-dimensional Fourier transform of a matrix using a fast Fourier transform algorithm, which is equivalent to computing the FFT twice and is defined as follows:

$$Y_{p+1,q+1} = \sum_{j=0}^{m-1} \sum_{k=0}^{n-1} \omega^{mk} \omega^{nl} X_{j+1,k+1} \tag{1.37}$$

Where:

$$\omega_m = \exp(-2\pi i/m)$$
$$\omega_n = \exp(-2\pi i/n)$$

Therefore, I used the frequency-wavenumber representation to show the dispersion relation of the wave propagation and to individuate the presence of bandgaps, related to the interaction with seismic metamaterials. In this domain, it is easy to individuate the range of frequency where the wave propagation is forbidden.

1.4 META-FORET project

The META-FORET project is a large-scale wave experiment, which aims to demonstrate the effectiveness of metamaterials in geophysics [26]. Thus, the main purpose it to apply the metamaterials concept discovered for electromagnetic and acoustic waves at the geophysical scale (see the website https://metaforet.osug.fr for further details).

This research can be identified as a part of the META-FORET project. One of the main project's
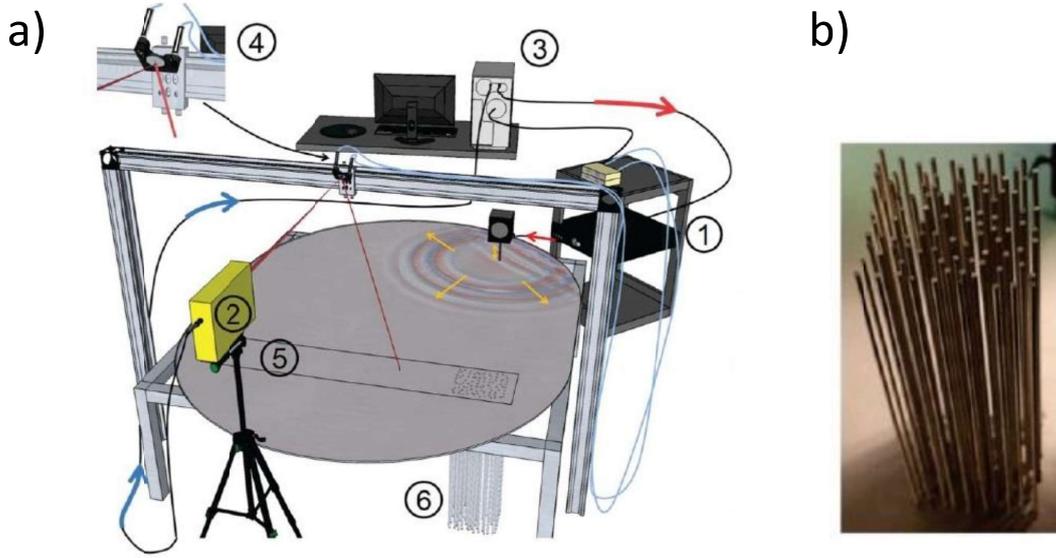
Figure 1.8: (a) Set of the laboratory experiment made by Philippe Roux and his team [33]. (b) Represents the detail of the aluminum plate coupled with 100 thin rods

goals is to analyze the behavior of seismic metamaterials using as a proxy a dense forest where each tree reacts as a resonator. Thus, forest can induce some frequency bandgaps where part of the seismic energy is blocked.

Before the experiment at the geophysics scale, the behavior of metamaterials has been studied at laboratory scale with two kind of experiments. In the first one, made by Rupin et al. [27], it has been studied the different behavior between an ordered and a disordered lattice of elements interacting with elastic waves propagating in solids. For this experiment soda cans were used as acoustic metamaterials and it was proved that their behavior is not effected by their order, and that is always true when metamaterials are governed by the resonance of their unit cells. Moreover, it was proved that a local modification can be realized without altering the properties of the rest of metamaterials. The second experiment, again at the laboratory scale but this time using elastic waves, has been made to investigate the elastic wave propagation in a thin aluminum plate coupled with a set of 100 long rods [33]. The rods of 61 cm ware attached perpendicularly to the thin plate of 1.5 x 1.5 m in a square of 20 X 20 cm, as it is shown in the Fig 1.8. In particular, it was analyzed the propagation of A0 Lamb waves through the system formed by the plate and the set of rods. The A0 Lamb waves were generated by a shaker in a range of frequency between 1-10 kHz. Thus, these thin rods, with a diameter of 6 mm, represent a set of quasi punctual resonators with a total size of 0.2 m comparable to the average out-of-plane flexural waves transmitted in the plate. The experiment proved the hybridization phenomenon [27] between the flexural A0 mode in the plate and the compressional resonances in the rods, as it is shown in the spatial representations of Fig 1.9. At the geophysical scale, it was analyzed the difference of wave propagation between an open field and a forest. It was chosen the Landes forest, a pine forest placed in southwest France, with a density of 800 trees per hectare and an average height of 15 m. For the signal recording, a seismic array, made by more than 1000 geophones, was placed in a regular grid of 120 m x 120 m with a spacing of 4 meter in both x and y direction. Thus the geophones covered a length of 90 m of forest and 30 m of an adjacent agricultural field. The set of the experiment and its location is shown in the Fig 1.10 .

The spacing it was chosen to match the half-wavelength spatial sampling requirement to avoid the aliasing phenomena, referred to a surface wave velocity between 150 m/s and 300 m/s and a range of frequency between 10 Hz and 100 Hz. Thus it is obtained the following range of wavelength:

$$\lambda = \frac{v}{f} = \frac{[150 - 300]m/s}{[10 - 100]Hz} = [1.5 - 30]m$$
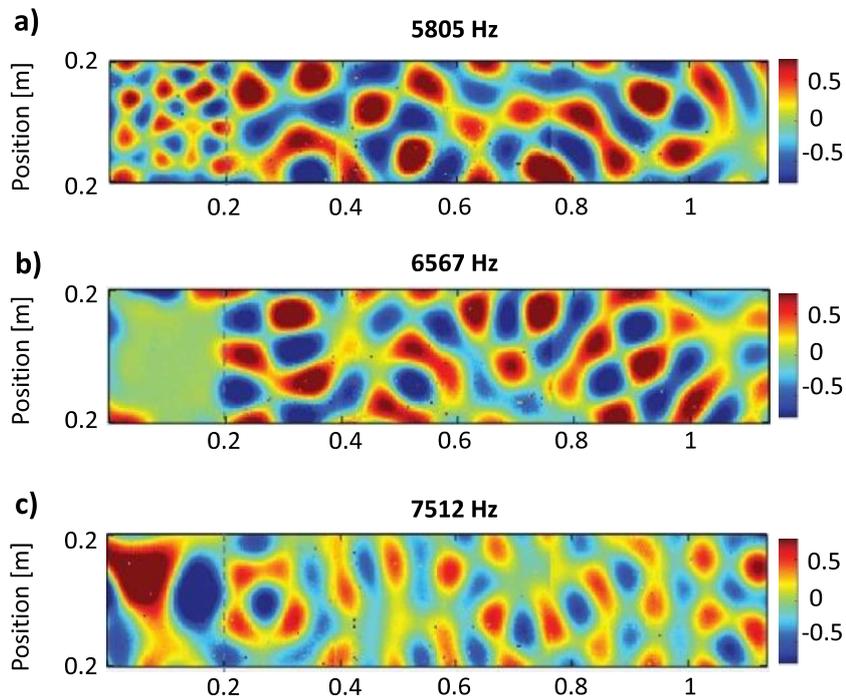
Figure 1.9: Spatial representation (x-y) of the velocity in the plane, where the left part of the domain between 0-0.2 meters is coupled with the rods. The snapshots are measured for the same instant of time and filtered for different range of frequency. (a) Snapshot filtered for the range of frequency before the stop band and the subwavelength mode of the wave that propagates through metamaterials. (b) Snapshot filtered in the frequency bandgap generated by the rods, there is not wave propagation through metamaterials. (c) Snapshot filtered after the stop band shows the supra-wavelength mode propagation inside metamaterials [33].
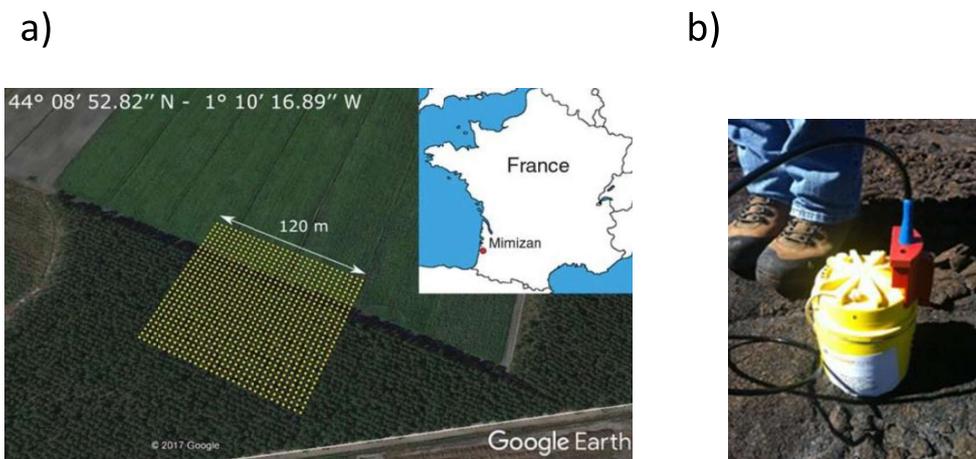

Figure 1.10: (a) Position of geophones, set in a grid of 120X120 m with a spacing of 4 m, covering 90 m of foresta and 30 m of agricultural field and the experiment's location in southwest France. (b) Example of the gephones used to the seismic signal recording
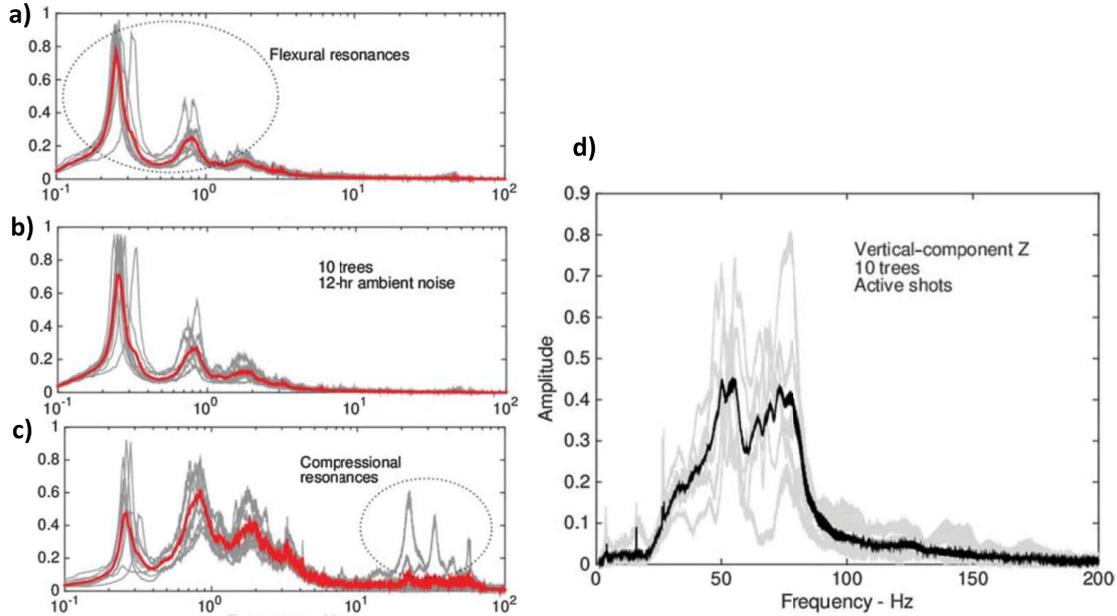
Figure 1.11: Normalized frequency spectra from recording of 10 instrumented trees. (a-c) Normalized Fourier spectra for both flexural components (north-sud direction (a) e and east-west direction (b)) and for the vertical component (c), from ambient vibration recording during the night. Gray curves are the average Fourier spectra of night recording and the red curve is the average response of the trees. It appears to be sensitive to tree characteristics and predominant for frequencies higher than 10 Hz. (d) Normalized Fourier spectrum from recording the vertical response of the 10 different trees during the active source produced by the shaker. It shows that the amplitude is gathered between 20 and 100 Hz with a maximum around 50 Hz. The gray curves are the single tree response with and the average response is represented by the black line.

The chosen spacing of 4 meters was suggested by preliminary numerical simulations [6]. The seismic network was composed by vertical-component geophones and three-component geophones, able to record signals in wireless mode continuously for two weeks.

Consequently, it was used a shaker to produce an active controlled source to measure the dispersion curves and to prove the results obtained previously in laboratory . The shaker generated 1-min long, 10-100 Hz frequency-modulated sweep function. The emission was recorded by each element of the seismic network. In combination, was performed another experiment to analyze the behavior of a single tree during the 12 hrs of ambient noise record at night and during a shaker source experiment. Thus, the experiment was performed using the three-component velocimeters and from the data collected was generated the normalized Fourier Spectra (see Fig. 1.11). The modal analysis of ambient noise record shows clear resonances for 0.3,0.9 and 2 Hz, which corresponds to the 3 first flexion modes of the trees.

The seismic data were collected by a 100-m-long line array of seismometers (GIIP) to analyze the response of the ground to the active source generated by the shaker. From the data collected it was generated the spatio-temporal representation of the seismic field for the vertical components, which shows three types of waves with different velocity:

1. P waves, which travels at 1000 m/s with a low-amplitude;

2. S waves, which travels at 400 m/s with a moderate-amplitude;

3. Rayleigh surface waves,which travels at 350 m/s with variable amplitude.

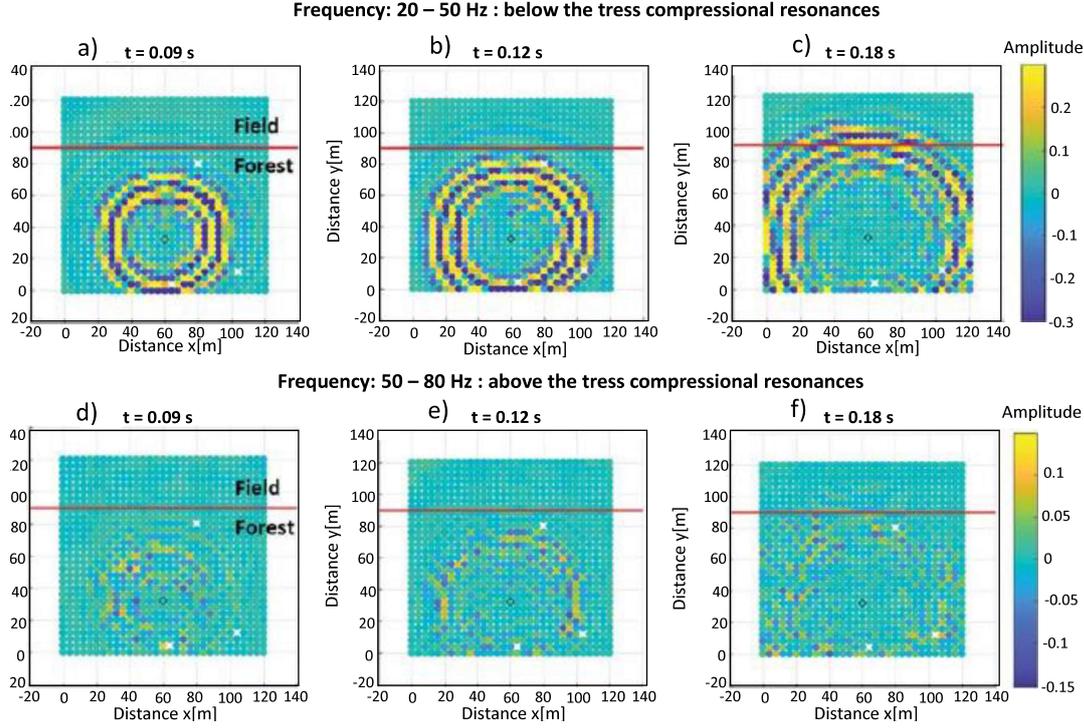Therefore, the amplitude of the Rayleigh waves depends on the frequency and on the interaction

Frequency: 20 – 50 Hz : below the tress compressional resonances

Frequency: 50 – 80 Hz : above the tress compressional resonances

Figure 1.12: (a-c) Spatial representation (x-y) of the seismic wavefield filtered between 20 and 50 Hz, for 3 different instants of time. The point source wave travels through the forest and the red line symbolizes the boundary between the forest and the open field. (d-f) Same representation for the seismic field filtered in the 50-80 Hz frequency, the wave propagations is dramatically damped by the local resonators.

with the forest. Indeed, when the waves penetrate in the forest, below 50 Hz the amplitude increases and above 50 Hz it is clearly damped by the interaction with trees. Indeed, the vertical component of tree's displacement has the higher value of amplitude for the range of frequency between 50-80 Hz, so trees behave as locally resonators for surface wave propagation above 50 Hz. This behavior is clearly shown in the Fig 1.12, which represents the wave propagation in x-y plane for different time instance. Therefore, from the data collected from the grid of sensors it was measured the dispersion curve inside the forest, for the frequency bands of both the shaker source and the ambient noise recordings, to underline the behavior of the trees acting as resonator. The dispersion curve in Fig. 1.13 shows a clear bandgap due to a hybridization phenomena for the Rayleigh wave between 45 and 60 Hz, that represents the frequency range related to the tree compressional resonances. Thus, the forest for a specific range of frequency acts like a metabarrier influencing the seismic wave, the reason why it is called "metaforest".

The same phenomena was studied through numerical simulations based on spectral element method (SEM) implemented in Fortran and MPI [6]. The phenomena was studied in 2D and 3D field with the SPECFEM3D software package reproducing 3D model mesh through the CUBIT software [23]. Thus, it was modeled a metaforest of trees on a sedimentary half-space with a constant height of 15 meters. Then, it was studied the interaction between Rayleigh waves and the Metaforest in a range of frequency of [20 100] Hz. The simulation shows how trees act as locally resonator creating a hybridization effect. The elements are sub-wavelength, i.e. with a spacing smaller than the wavelength of the propagating wave. Figure 1.14 shows the results of this numerical simulation, underlining the behavior of the resonant trees.
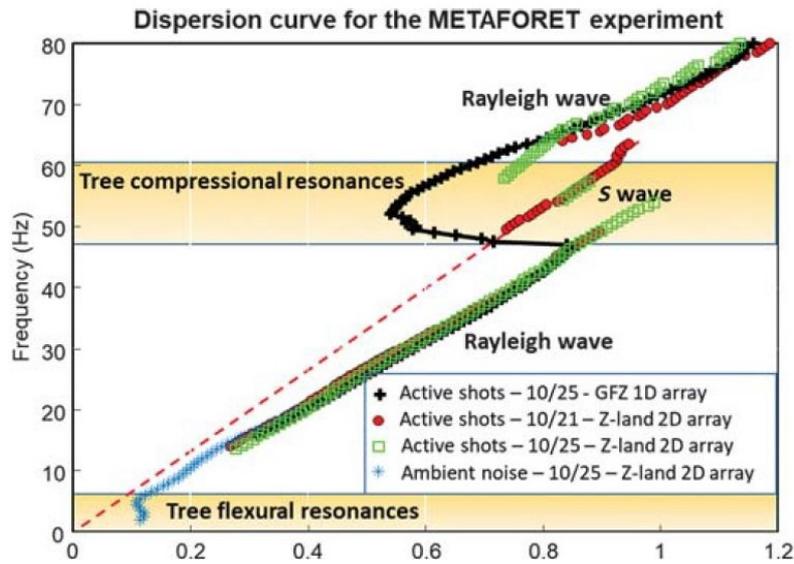
Figure 1.13: The dispersion curve for the METAFORET experiment is obtained in the the frequency - wavenumber domain. The blue line represents the ambient noise recording and it presents a bandgap at low frequencies (< 10 Hz) related to tree flexural resonances. The red, black and green curves show the result of active data analysis. The Rayleigh wave curve presents a large bandgap between 50 and 50 Hz in according with tree compressional resonances.
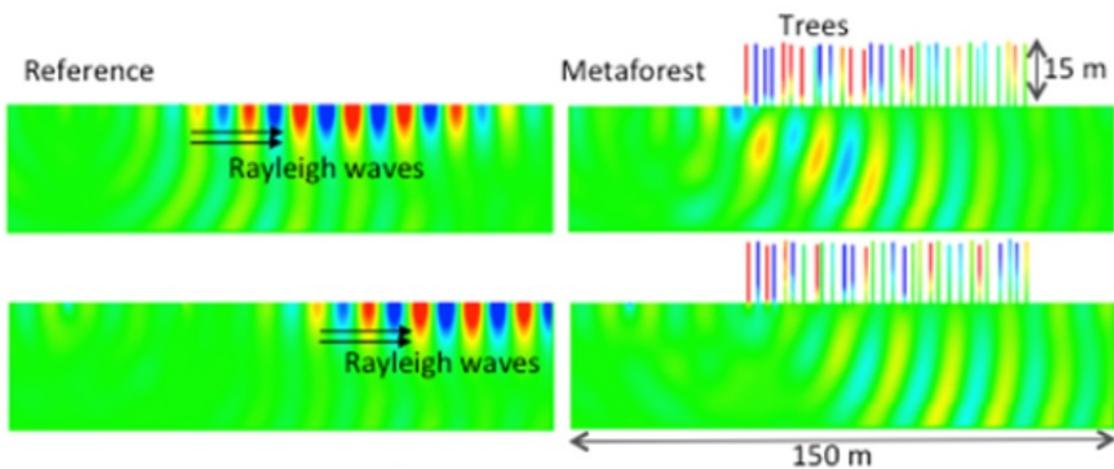

Figure 1.14: Preliminary 2D simulation on the mate-forest shows that elastic rods attached to a bulk elastic substrate can simulate the trees behavior. The simulation shows the hybridization phenomena due to trees acting as local resonators[6]

17

1.5   Goal of the thesis

In this research I study the behavior of rows of trees as seismic metamaterials, analyzing how they can control the Rayleigh waves for specific range of frequencies. The main goal of my research is finding a simple way to study this complex phenomena. Therefore, I implemented an efficient code in MATLAB to analyze the interaction between Rayleigh waves and trees. In this code, trees are approximated as simple vertical rods vibrating along the vertical axis, neglecting the presence of branches and considering only the first longitudinal mode of vibration. Thus, the roots system architecture is simplified as a clamped joint fixed at the ground. The pine tree, used in the current experiment, has the main root, which comprehends the half of the total volume, in the first 10 centimeter of soil. Thus, it is possible to reduce the roots system to a clamped joint. I used this code to carry out a parameter sensitivity analysis in both 1D and 2D domains. In particular I analyze the effect of the following aspects:

- Periodic and random distribution of elements;

- spacing between adjacent elements;

- effect of damping;

- constant height and graded arrays of elements;

- different kinds of wave source.

Chapter 2

Wave Propagation using the spectral element method

The first problem analyzed is the wave propagation in an elastic, isotropic and homogeneous medium [24]. In particular, the domain of the problem is defined by a one-dimensional truss coupled with a simple resonator, showed in the Fig. 2.1. The input wave is represented by the external time dependent point force $f(t)$ [N/m]. The system of equations which describes the problem is [12]:

$$\mu \frac{\partial^2 u}{\partial x^2} - \rho \frac{\partial^2 u}{\partial t^2} = f(t) - k_r(u - u_r) \tag{2.1}$$

$$M_r \ddot{u}_r = K_r(u - u_r) \tag{2.2}$$

Where:

- μ : linear shear modulus $[N/m]$;

- ρ : linear density of the medium $[kg/m]$;

- k_r: stiffness of the simple oscillator per unit length $[N/m^2]$;

- K_r: stiffness of the simple oscillator $[N/m]$;

- M_r: Mass of the simple oscillator $[kg]$;

- u and u_r : displacements of the truss and the resonator.

In this work, I study the Rayleigh wave propagation, referring to the non-dispersive vertical component and neglecting the horizontal one. Indeed, the seismic Rayleigh wave is characterized by a particle elliptic motion (see Fig. 1.6) with a strong, vertical component u_z, which results to be efficiently coupled to the vertical resonator [6]. In this way it is possible to analyze the phenomena in one-dimensional domain. Thus, I implemented a input Ricker wave to reproduce the Rayleigh waves' vertical component. The wave is described by the following expression:

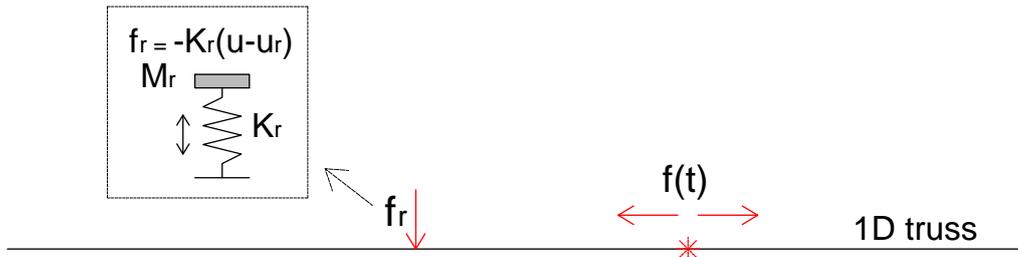$$F(t) = [2(\pi F0(t - t_0))^2 - 1] \exp^{-\pi F0(t - t0)} \tag{2.3}$$

Figure 2.1: Free body diagram for wave propagation 1D truss coupled with 1 resonator
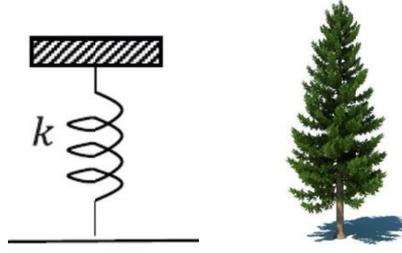
Figure 2.2: The resonator is computed referring to the mechanical characteristics of a pine tree along the longitudinal axis

The fundamental frequency $F0$ is set equal to 40 Hz to investigate the band frequency typical of the trees and $t_0 = \frac{1.5}{F_0}$ represents the delay.

The truss simulates a ground characterized by an elastic, homogeneous and isotropic material. The density, referring to an average soil, is set equal to 2000 Kg/m^3 and the shear velocity v_s is 300 m/s. For a Poisson ratio typical of this soil the Rayleigh wavespeed is almost equal to the shear velocity [6]. The shear modulus is easily computed as:

$$\mu = \rho v_s^2 = 180 * 10^6 \frac{N}{m^3} \tag{2.4}$$

The tree is represented as a homogeneous elastic vertical resonator with constant thickness (or cross section) referred to a pine tree with the following properties:

- height = 14m;

- density = 500 Kg/m^3;

- diameter = 0.4 m;

- Young's Modulus E = 3000 Mpa.

Thus, I obtain:

$$M_r = \pi(\frac{d}{2})^2 h\rho = 879.64 kg \tag{2.5}$$

$$K_r = \frac{EA}{h} = \frac{\pi(\frac{d}{2})^2}{h} = 3.385 * 10^7 N/m$$

K_r is the stiffness of the resonator and is defined as the force required for unit deformation of the structure in the longitudinal direction. Furthermore, I can compute the angular frequency and the frequency of the oscillator in the simple way:

$$\omega_r = \sqrt{\frac{K_r}{M_r}} = 247.43 \ rad/s \tag{2.6}$$

$$f_r = \frac{\omega_r}{2\pi} = 39.38 Hz$$

2.1 Spectral element method

The simulation is performed with the spectral element method, a popular and efficient formulation of the finite element method that provides a numerical solution of partial differential equations. In the spectral element method the element interpolation nodes are placed at the zeros of Gauss-Lobatto-Legendre orthogonal polynomials, to achieve the highest interpolation accuracy for a given number of nodes [2], as shows (see Fig 2.3). Indeed, in finite element analysis there are two ways to increase the accuracy of the numerical solution [14] [10] :

1. decreasing the element size;

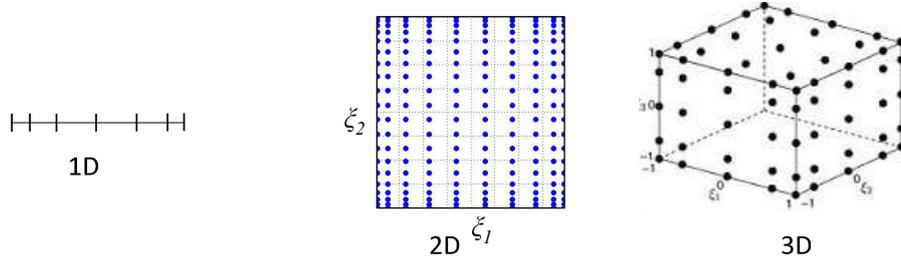2. increasing the order of polynomials expansion (p).

Figure 2.3: Gauss-Lobatto-Legendre point interpolations in 1D,2D and 3D domains

In the SEM the numerical error decreases faster than any power of $\frac{1}{p}$. Therefore, with this method is possible to obtain an accurate solution implementing a low order of polynomials expansion (few degrees of freedom of the system) [8] [16]. Furthermore, a finite element solution with evenly spaced interpolation nodes, for high polynomial orders, is more sensitive to numerical errors or fails.

The spatial domain is discretized in small elements and functions are defined at the element level in the interval $-1 \leq \xi \leq 1$ of the dimensionless axis. The mapping between global and local coordinates is mediated by the function:

$$x(\xi) = \frac{1}{2}(X_2^i - X_1^i) + \frac{1}{2}(X_2^i - X_1^i)\xi \qquad (2.7)$$

Where i is the generic element. For each element the displacement is expressed through basis functions ϕ :

$$u = \sum U_j \phi_j \qquad (2.8)$$

The basis functions are represented by Lagrange polynomials, which have unite values only at the integration point, as shows the Fig 2.4:

$$\phi_i \phi_j = \delta_{ij}$$

The domain of the problem is divided into non-overlapping elements, defined by their control nodes. So each element of the mesh contains a spectral sub-grid of Gauss-Lobatto-Legendre internal nodes. For example, if the polynomials implemented are of fifth degree, each element is described by 6 nodes (including the two geometrical end-nodes). For each node an integration weight, using the Lobatto integration quadrature:

$$\int_{-1}^{1} f(\xi)d\xi = \sum_{p=1}^{k+1} f(\xi = z_p)w_p \qquad (2.9)$$

Where:

- $k \geq 1$ is the selected order of the quadrature;

- z_p are the quadrature base points;

- w_p are the integration weights, given by: $w_p = \frac{2}{k(k+1)} \frac{1}{L_k^2(z_p)}$

The mass matrix for each element is diagonal and implemented in a vector form.

Furthermore, by introducing absorbing boundary conditions it is possible to fit a realistic physical situation[1] [14] [13]. These boundary conditions are derived for numerical wave simulation that minimize artificial reflection from the edges of the computation domain. Thus, since a numerical solution of wave propagation is implement in a unbounded domain, the wavefronts behave as outgoing object at the artificial boundaries[16].
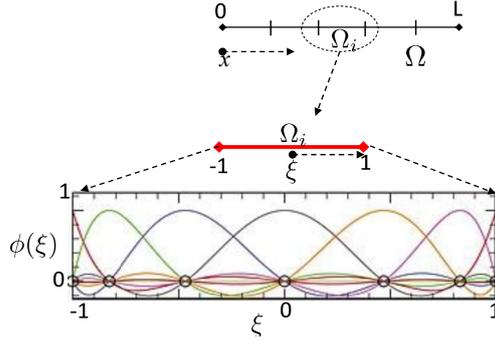
Figure 2.4: Mapping between local and global dimensionless coordinates and Legendre functions. Each Legendre function has the unit value for the interpolation point

2.2 Time discretization of the problem with the Newmark method

By SEM space-discretization, the 1D wave equation coupled with the resonator is reduced to:

$$M\ddot{u} + Ku = F(t) - K_r(u - u_r) \tag{2.10}$$

$$M_r\ddot{u}_r = K_r(u - u_r) \tag{2.11}$$

This system of equations is solved using the Newmark Method, that is a method of numerical integration applied to resolve differential equations and it is widely used for dynamic problems [9] [19] [10]. First of all the time interval is subdivided in many discrete time step with a constant time interval(Δt). Then from the results for the initial time step it is possible to to update the solution at any other instant in time. In this method, the acceleration is computed considering acceleration linear in time:

$$\ddot{u}(t) = a(t) = a_i + \frac{t - t_i}{\Delta t}(a_{i+1} - a_i) \tag{2.12}$$

Where Δt is the time step. The velocity and the displacement is computed by integrating acceleration:

$$\dot{u}(t) = v(t) = v_i + (t - t_i)a_i + \frac{(t - t_i)^2}{\Delta t}(a_{i+1} - a_i) \tag{2.13}$$

$$u(t) = u_i + (t - t_i)v_i + \frac{(t - t_i)^2}{2}ai + \frac{(t - t_i)^3}{6\Delta t}(a_{i+1} - a_i) \tag{2.14}$$

The expressions could be generalized using β and γ factors:

$$u_{i+1} = u_i + \Delta t v_i + \frac{\Delta t^2}{2}[(1 - 2\beta)a_i + 2\beta a_{i+1}] \tag{2.15}$$

$$v_{i+1} = v_i + \Delta t[(1 - \gamma)a_i + \gamma a_{i+1}] \tag{2.16}$$

Every algorithm is considered stable if small numerical error at the i-th time causes a smaller cumulative errors in the following time steps. The Newmark method is unconditional stable (the stability does not depend on the value of time step) if:

$$2\beta \geq \gamma \geq \frac{1}{2}$$

This code makes use of an explicit version of the method, with $\beta = 1/2$ and $\gamma = 1$, which respects the stability condition. The final expressions are:

$$u_{i+1} = u_i + \Delta t v_i + \frac{\Delta t^2}{2}a_{i+1} \tag{2.17}$$

$$v_{i+1} = v_i + \Delta t a_{i+1} \tag{2.18}$$

$$u_{r_{i+1}} = u_{r_i} + \Delta t v_{r_i} + \frac{\Delta t^2}{2}a_{r_{i+1}} \tag{2.19}$$
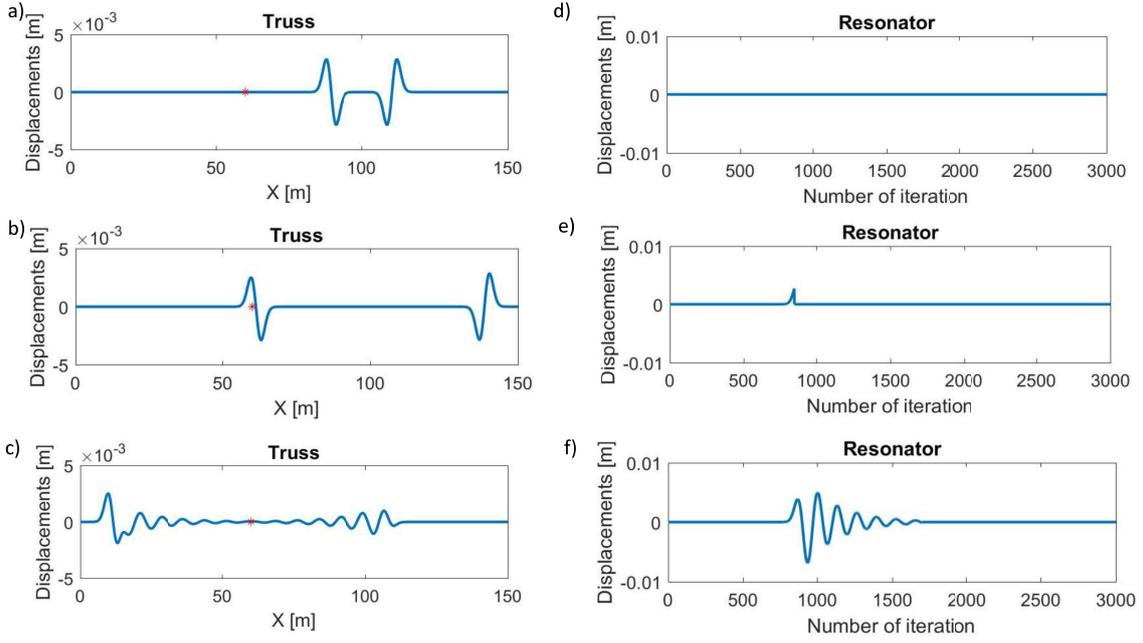
Figure 2.5: Results in time domain for 1D truss coupled with 1 resonator. (a-c) Wave transmission in the truss for different instants of time, the red star indicates the resonator's location. (d-f) Resonator's displacements for the same instants of (a-c).(a),(d) Configuration before that the wave hits the resonator, which is steady at the zero position. (b), (e) Moment of interaction between the resonator and the front wave, when the resonator starts to vibrate (e). (c), (f) Configuration after 1700 iterations: the truss displacement shows that a part of input wave energy is reflected by the resonator, which is almost stationary again.

$$v_{r_{i+1}} = v_{r_i} + \Delta t a_{r_{i+1}} \tag{2.20}$$

Thus, the two second order differential equations in terms of truss' displacement and resonator's displacement are converted into four first-order differential equation in terms of displacement and velocity of truss and resonator and solved with numerical integration. The acceleration term is updated at each iteration. The problem is computed introducing the mid-step displacement for both truss and resonator:

$$u_{mid} = u_i + \frac{1}{2}\Delta t v_i \tag{2.21}$$

$$u_{r_{mid}} = u_i + \frac{1}{2}\Delta t v_{r_i} \tag{2.22}$$

Then, I introduce the truss' force term related to the input wave and to internal force. The Newmark method is not initialized, because the initial conditions are in terms of displacement and velocity instead of acceleration and particularly they are:

$$u(0) = 0 \qquad \dot{u}(0) = 0 \qquad u_r(0) = 0 \qquad \dot{u}_r(0) = 0 \tag{2.23}$$

Where $u(0)$ and $\dot{u}(0)$ are the vectors of displacements and velocities of the truss for $t = 0$ and $u_r(0)$ and $\dot{u}_r(0)$ are the value of displacement and velocity of the resonator. Thus, it is necessary to compute the initial acceleration of truss and resonator imposing the balance equation for $t = 1$:

$$\ddot{u}(1) = \frac{F(t_1) - K_r u_1}{M} \qquad \ddot{u}_r(1) = \frac{K_r(u_1 - u_{r_1})}{M_r} \tag{2.24}$$

Furthermore, the resonator is connected with the truss, by imposing two boundary conditions in the point of attachment (see the Fig. 2.1):

1. continuity of displacements: $u_{truss} = u_{resonator}$

2. continuity of internal force $f_{truss} = f_{truss} + f_{resonator}$

At the point of attachment the resonator transmits a force to the truss that depends on difference of displacements in each time step: $f_{resonator} = -K_r(u_{truss} - u_{resonator})$. Where K_r is the stiffness of the resonator. Finally, the update of displacement and velocity is computed following the expressions:

$$v_{i+1} = v_i + \Delta t a_{i+1} \tag{2.25}$$

$$u_{i+1} = u_{mid} + \frac{1}{2}\Delta t v_{i+1} \tag{2.26}$$

$$v_{r_{i+1}} = v_{r_i} + \Delta t a_{r_{i+1}} \tag{2.27}$$

$$u_{r_{i+1}} = u_{r_{mid}} + \frac{1}{2}\Delta t v_{r_{i+1}} \tag{2.28}$$

2.3 Wave Propagation results in 1D truss coupled with 1 resonator

The transmission of the Ricker Wavelet in the truss is influenced by the presence of the resonator. Since the resonance frequency is contained in the input source time function resonance occurs. In this case, when the wavefront hits the resonator part of the wave energy is reflected to the opposite direction. The pictures in figure 2.5 are caught from the MATLAB video and represent the results in time domain and clearly show the resonance phenomena.

Together with time domain snaphot, I study the problem in the frequency domain, plotting the fast Fourier Transform of the truss' displacements. To analyze the problem in the frequency domain I use a "sweep" input wave, which is a modulated sinusoid and its frequency increases time by time. Moreover, the wave implemented increases amplitude until $t < \frac{16\pi}{\omega}$ and remains constant for $t \geq \frac{16\pi}{\omega}$ as it is explained in the following expressions:

$$F(t) = \frac{\omega t}{16\pi}\sin[2\pi(f_0 + bt)t] \qquad for \quad 0 \leq t < \frac{16\pi}{\omega} \tag{2.29}$$

$$F(t) = \sin[2\pi(f_0 + bt)t] \qquad for \quad t \geq \frac{16\pi}{\omega}$$

Where: f_0= 5 H, is initial input frequency; $b = 40$.

With this kind of input wave I get a better representation in both frequency and frequency-wavenumber domains. I want to compare the time domain results to the results in the frequency domain, which is computed by applying the Fast Fourier Transform (FFT) to the displacements of the truss. In this problem, I apply the FFT to the displacements of the truss recorded along an array of seismometers located between 20 and 80 meters. Furthermore, I use the absolute value of the FFT, that is the square root of the real and imaginary parts squared:

$$|FFT| = \sqrt{Re^2 + Im^2}$$

The Fig. 2.6 shows the frequency spectra obtained applying the FFT to the truss displacements, for the 1D problem without and with one resonator. The amplitude is expressed as a function of frequency and distance from the source. it is expressed in Decibel Unit, following the expression:

$$A[dB] = 20 * \log A \tag{2.30}$$

Through this comparison, it is easy to underline the resonator's behavior.

Afterwards, I study this problem in the frequency-wavenumber domain, as the analysis of the dispersion curve results essential to understand the metamaterials' behavior. The input wave used for this analysis is the same Sweep wave defined in the Eq. 2.29. I take the absolute value of the two-dimensional FFT, that is the square root of the real and imaginary parts squared. The Fig 2.6 shows the dispersion curve obtained for the truss alone and coupled with one resonator.
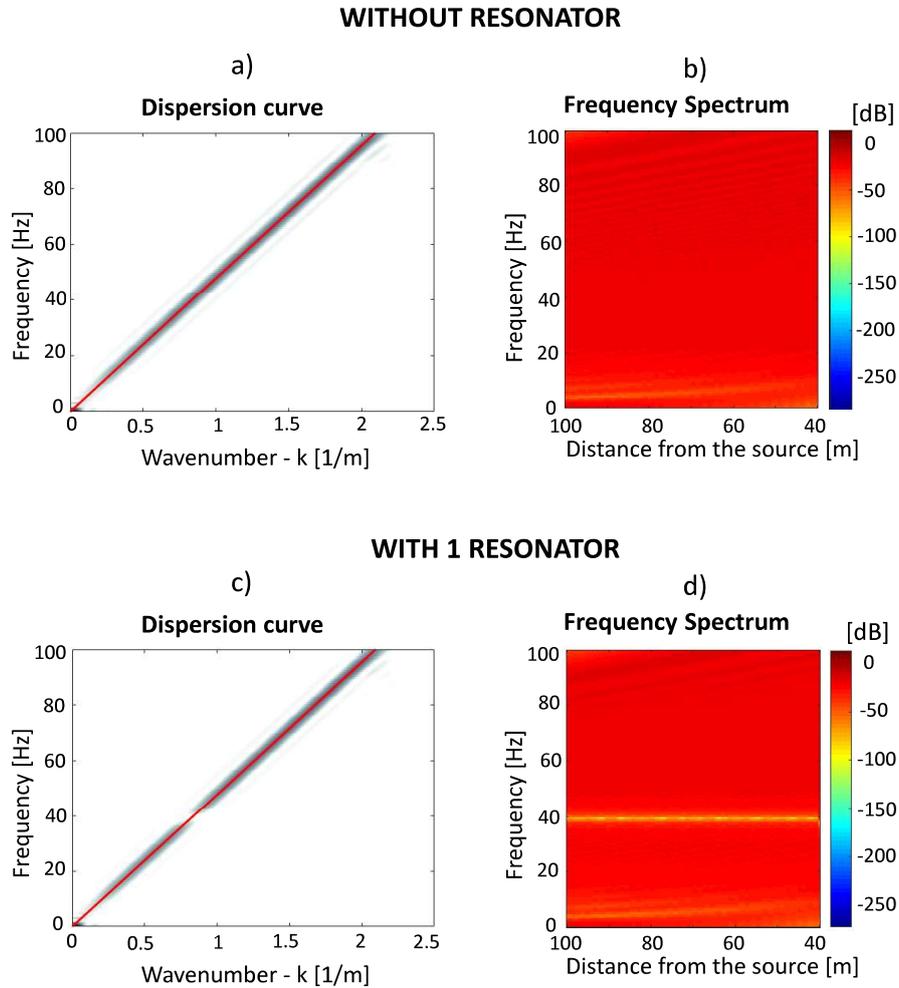
Figure 2.6: Comparison between the reference 1D problem without resonator and the case with only 1 resonator. In the frequency spectra the intensity of the wave energy through the range of colors displayed in the next color-bar. (a), (b) Results in frequency domain and frequency-wavenumber domain of the problem without any resonator. Since the medium is elastic, isotropic and homogeneous the dispersion curve obtained is linear (a) and the frequency spectrum (b) shows a constant amplitude between 20 and 100 Hz. (c), (d) Results referred to the problem with 1 resonator. The dispersion curve (c) is still linear with the exception of a bandgap at 39 Hz, due to the interaction with resonator. The same bandgap can be seen in the frequency spectrum (d), that shows a drop of energy at 39 Hz (the resonance frequency). The red line in (a) and (c) represent the Rayleigh wave velocity in a non-dispersive medium.

2.4 Wave Propagation in 1D truss coupled with an array of resonators

In this section I deal with 1D elastic waveguide, the truss coupled with an array of N resonators. The characteristics of the truss are referred to the same average soil described in the former example (Eq.2.4). The properties of each oscillator are the same shown in Eqs. 2.5 and 2.6. In this case the array of resonators represents a series of trees placed every two meters, that corresponds to an oscillator every two elements. With the seismic metamaerials the wave attenuation derives from the collective effect of many resonant units arranged at the sub-wavelength scale (referring to the incident wave). Thus, the spacing between every resonator should be smaller than $\frac{\lambda}{2}$, where λ is the wavelength that depends on the shear velocity in the ground and the fundamental frequency of the input wave:

$$\lambda = \frac{v_s}{f} = \frac{300 \ m/s}{40 \ Hz} = 7.5m \tag{2.31}$$

In this case the spacing is equal to $\frac{\lambda}{3.75}$. The system of equations that describes the wave propagation in an elastic 1D truss coupled with an array of N resonators is:

$$\mu \ \frac{\partial^2 u}{\partial x^2} - \rho \frac{\partial^2 u}{\partial t^2} = F(t) - K_r(u - u_r) \tag{2.32}$$

$$M_r \ddot{u}_r = K_r(u - u_r) \tag{2.33}$$

I use the SEM space-discretization and the Newmark method to solve the problem, as previously explained. The only difference is that I use a vector of attachment points to represent the coupling condition between truss and resonators and the boundary conditions are:s

1. continuity of displacements: $u_{truss} = u_{resonators}$

2. continuity of internal force:$f_{truss} = f_{truss} + f_{resonators}$

The Fig 2.7 shows the results in time domain: displacements of the truss and of the first mass and spring of the array. In particular, I displayed the results for three significant instants of time. Afterwards, I study the problem in the frequency domain using the same sweep wave introduced in the previous example (Eq.2.29) by applying the Fast Fourier Transform to the displacements of the truss. Thus, I obtain the frequency spectrum of the signal. Likewise in the previous case, the energy of the wave strongly decreases at the 39 and 75 Hz. The first bandgap is generated by the interaction with the array of resonators and is located around 39 Hz, which is the resonance frequency. On the contrary, the second one is due to the Bragg-Scattering, which explains the effects of the reflection of electromagnetic waves on periodic structures whose distances are in the range of wavelength.

In the frequency-wavenumber domain, the dispersion curve is not linear anymore: around the resonance frequency of 39 Hz a bandgap is generated due to the presence of the metamaterial and at 75 Hz the elastic waves are reflected for the Bragg-Scattering (see Fig.2.8).

The Bragg effect was discovered for crystalline solids, which are able to reflect specific range of frequency, as I have shown in the Fig 1.2. The same phenomena can be analyzed at the geophysical scale for periodic structures, as the array of resonators, where the distance between adjacent elements is equal to a multiple of wavelength of the incident elastic waves. In this case the Bragg's scattering occurs at 75 Hz, and the referring wavelength is:

$$\lambda = \frac{v}{f} = \frac{300m/s}{75Hz} = 4m \tag{2.34}$$

The incident wave is orthogonal to the truss, consequently $\sin \theta = 1$, the distance between adjacent elements is $d = 2$. The Bragg's law is respected with $n = 1$:

$$2d \sin(\theta) = n\lambda \longrightarrow 2 \cdot 2 \ m = 1 \cdot \frac{300 \ m/s}{75 \ Hz}$$

Therefore, at frequency of 75 Hz and for this specific resonators' distribution the elastic waves are reflected because of the Bragg-Scattering.
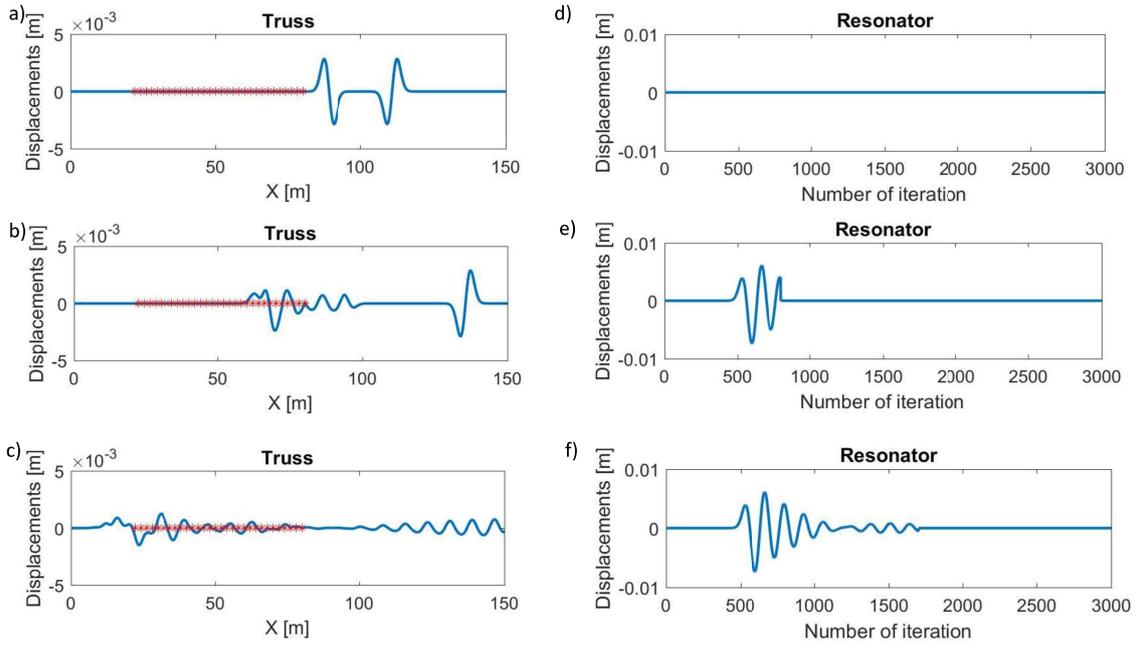
Figure 2.7: Time domain results for the truss coupled with an array of resonators. (a)-(c) Wave transmission in the truss for different instant of time, the red stars indicate the position of the 30 resonators. (d)-(f) First resonator's displacement for different iterations, referring to the same time's instance of the figure on the left. (a), (d) Show the time instance at 0.074 s after 380 iterations, before hitting the array of resonators the wave transmission is linear and undisturbed and the first resonator is steady at initial position. (b), (e) Show the time of instance after 800 iterations, after the interaction between the resonator and the front wave. The resonator starts to vibrate and the wave is trapped among the resonators, part of the energy is reflected.(c) ,(f) Configuration after 1700 iterations, proceeding with iterations the truss displacement shows that an important part of input wave energy is reflected and the displacement of the first oscillator becomes smaller.
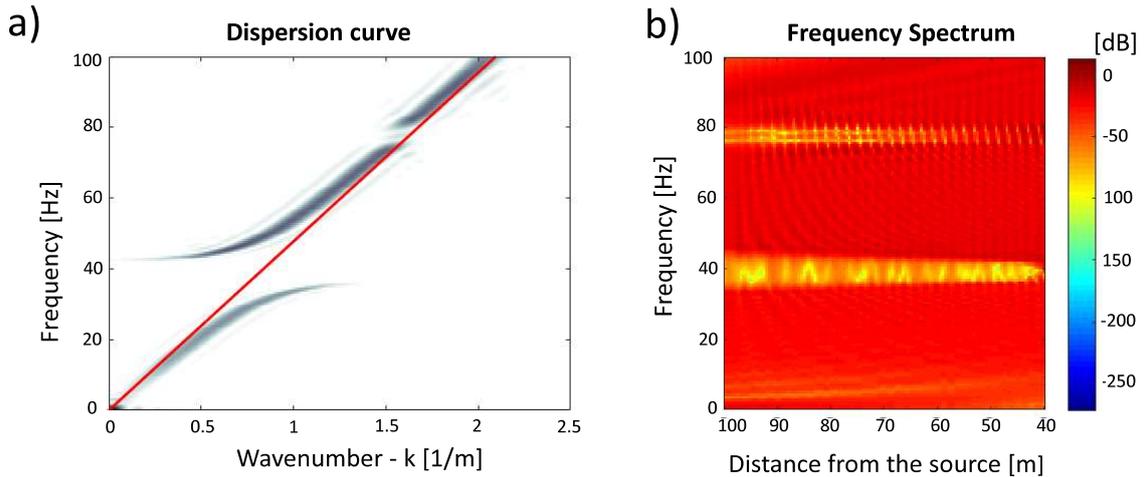

Figure 2.8: Results of the wave propagation in the 1D truss coupled with an array of 30 resonators with 2 m of spacing. (b) Frequency spectrum obtained applying the FFT to the truss' displacements (recorded along of the seismometers' array, placed between 20 and 80 m, with a point of measurement each 10 cm), which shows a bandgap of 90 dB around 40 Hz, due to the interaction with the array and another one at 75 Hz due to Bragg's effect. For the same reason the dispersion curve (a) shows a large bandgap between 35 and 40 Hz and a smaller one for 75 Hz. The red line represents the Rayleigh wave velocity in a non-dispersive medium.
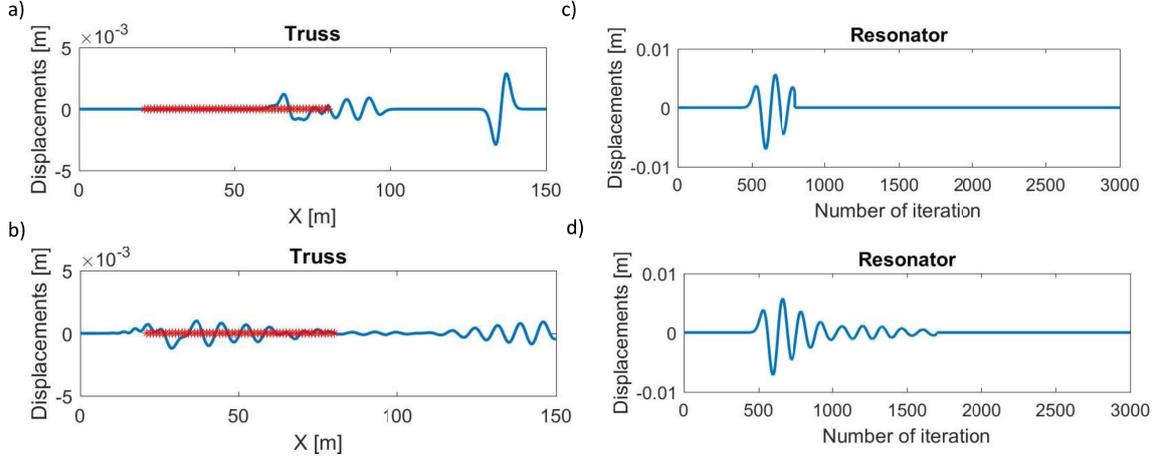
Figure 2.9: (a), (b) Wave transmission in the truss for different instant of time, the red stars indicate the position of 60 resonators. (c), (d) First resonator's displacement for different iterations, referring to the same time's instance of the figure on the left. (a), (c) Situation after the interaction between the resonator and the front wave: the resonator vibrates and the wave is trapped among the resonators, part of the energy is reflected. (b) (d) CConfiguration after 1700 iterations, proceeding with iterations the truss displacement shows that an important part of input wave energy is reflected, after interaction with the array, and the displacement of the first resonator becomes smaller. The results are similar to the former case (Fig 2.7).

2.4.1 Array of resonators with different spacing

Afterwards, I analyze the same problem changing the spacing between adjacent resonators, using a constant spacing of 4, 1 and 0.5 m to underline how the spacing influences metamaterials' behavior. Thus, I place in the same length used for the former example, between 20 and 80 m, respectively 15, 60 and 120 elements.
I report in Fig. 2.9 the results in time domain for the case with 60 resonators and a constant spacing of 1 m. But, from the study in time domain, it is impossible to see any difference related to increasing of resonators. Thus, I move to the study of the problem in the frequency domain, for the three different spacing. The Fig 2.10 shows the results obtained in the frequency domain and frequency-wavenumber domain from the problem with constant spacing of 4 m. Referring to a range a of frequency between 1 and 10 Hz and shear velocity $v_s = 300m/s$, the range of wavelength analyzed in this problem is computed as:

$$\lambda = \frac{v_s}{f} = \frac{300 \; m/s}{1 - 100 \; Hz} = 300 - 3m \tag{2.35}$$

Thus, the spacing of 4 m does not result effective to control the input wave, since metamaterials can manipulate wave propagation for specific frequency ranges if the spacing among elements are subwavelengths. For this reason, the dispersion curve presents a bandgap, generated by the resonators interaction , that is not clear as in the other examples with smaller spacings. For the same reason, the frequency spectrum in fig 2.10 presents a bandgap around the resonators resonance less deep than in other examples. On the contrary, the bandgap due to the Bragg's effect at 75 Hz is similar to the one obtained with s=2 m. Thus, referring to the Bragg's law at Eq. 1.1 for a perpendicular input wave ($\sin\theta = 1$) and setting $d = 4m$, the equality is satisfied for $n = 2$:

$$2d\sin(\theta) = n\lambda \longrightarrow 2 \cdot 4 \;\; m = 2 \cdot \frac{300 \;\; m/s}{75 \;\; Hz}$$

The frequency spectrum reported in Fig 2.10c is referred to the problem with a constant spacing of 1 m and presents a clear bandgap around 40 Hz, where the energy decreases up to 90 dB. Furthermore, changing the spacing, the bandgap around 75 dB due to Bragg disappears because the Bragg's scattering is related to periodicity and spacing of the elements. Indeed, considering always a orthogonal wave ($\sin\theta = 1$), with a distance between each element of 1 meter the Bragg's
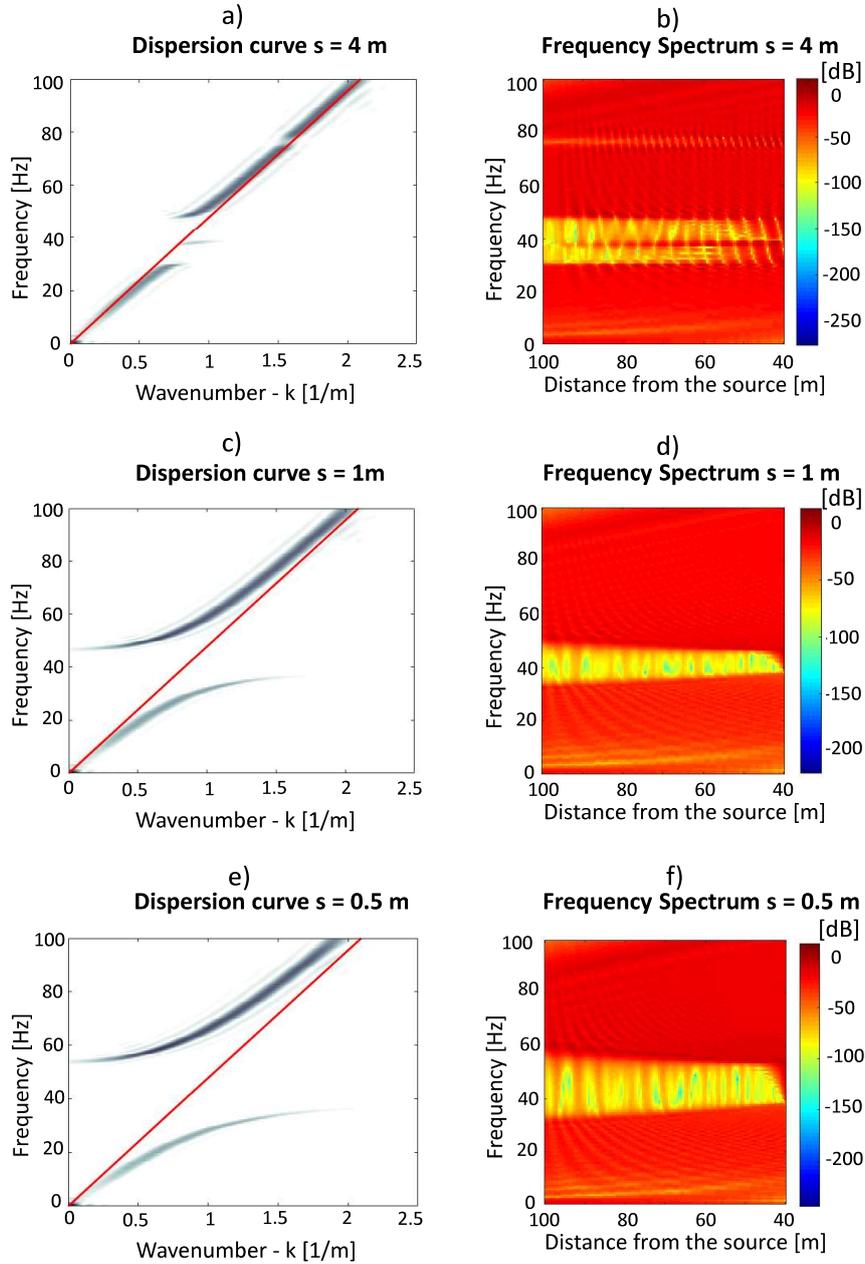
Figure 2.10: Results of the wave propagation in the 1D truss coupled with arrays of 15, 30 and 60 resonators, with a relative spacing between adjacent elements of 4, 1 and 0.5 m (similar to the results obtained in Fig. 2.8). (a), (c), (e) Dispersion curves for the three different cases and (b), (d), (f) are the frequency spectra referred to the same examples. (a), (b) Results for the constant spacing of 4 m, in both the representations the bandgap is between 35 and 45 Hz, due to the interaction with the array, but it is not well defined. Moreover, at 75 Hz the bandgap due to the Bragg-Scattering is clearly visible. (c), (d) Results for the problem with a constant spacing of 1 m, which show a bandgap between 25 and 45 Hz well defined. In that range of frequency, the drop of energy is up to 90 dB (d). Finally, (e), (f) represent the last example with a spacing of 0.5 m, the bandgap between 30 and 50 Hz is definitely larger than in all previous examples and the amplitude decreases up to 100 dB.

law becomes:

$$2d\sin(\theta) = n\lambda \longrightarrow 2 \cdot 1 \;\; = n \cdot \frac{300\ m/s}{f}$$

For the frequency range of 1-100 Hz doesn't exist a integer number which satisfies the equation. For the same reason, the dispersion curve shows only a bandgap around 40 Hz. The branch becomes flat around 35 Hz and there is no propagation to 45 Hz, thus the range of frequency without any displacement is broader than in cases with constant spacing of 4 and 2 m (see Fig 2.10d).
Finally, the Fig 2.10e,f report the results for the 1D problem with an array of a constant spacing of 50 cm. The bandgap generated by the interaction with the resonators is larger than all the previous examples, indeed in the dispersion curve the branch becomes flat at 35 Hz and there is not wave propagation up to 55 Hz. As in the example with s = 1, the bandgap due to Bragg's affect disappears because it is not possible to satisfy the Bragg's law (Eq 1.1) for the range of frequency analyzed (1-100 Hz). In conclusion, the effectiveness of resonators in reflecting the seismic waves deeply depends on the number of resonators and spacing between elements.

2.4.2   Array of resonators with a random distribution

After having analyzed the 1D problem with ordered distribution of resonators, I study wave propagation in the same 1D truss coupled with an array of disordered pattern of elements. Thus, the mechanical characteristics of the locally resonants are unchanged remaining the natural frequency of 39.38 Hz, but the spacing is not constant anymore. The 30 elements are located in the same region of the first problem between 20 and 80 meters, and their position is generated by the MATLAB function "rand", which creates a random series of numbers. Therefore, the current spacing among elements can be smaller or larger than 2 m.
The results in the time domain are shown in the Fig 2.11 and are similar the time analysis of the the truss coupled with the constant spacing array: part of the input wave energy is reflected and part passes through the array. Thus, it is necessary to pass in the frequency domain, to reach the differences between the random and ordered case.
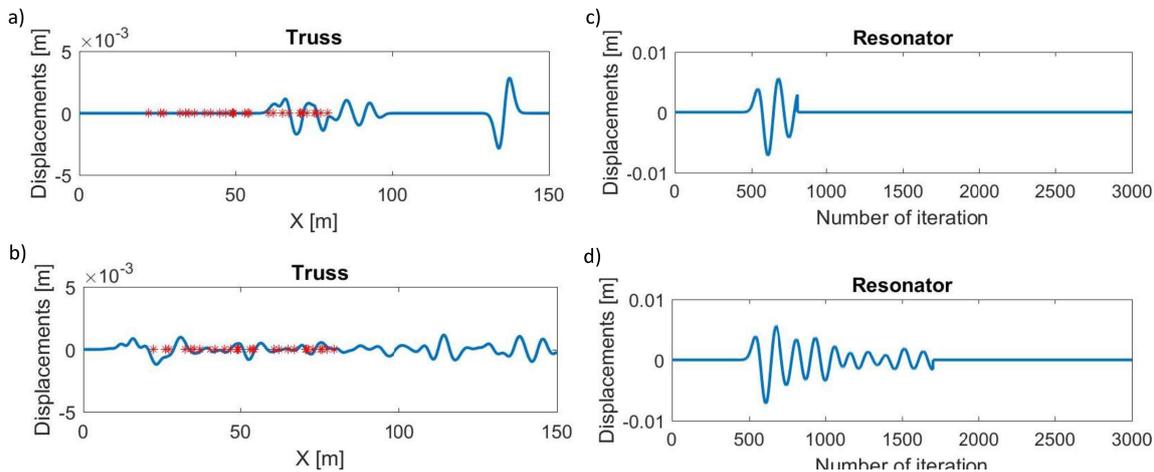

Figure 2.11:   Results in time domain for 1D truss coupled with random array. (a) Truss' displacements after 800 iterations, part of the energy is reflected by the array of disordered elements, which are represented by red stars. (c) The first resonator's displacement for the same time of instance. (b), (d) Same situation after 1700 iteration, part of the wave energy has passed through the array and another part is reflected. Therefore, in the time domain the results are similar to the case with the array of ordered elements.

After applying the FFT, I obtain the frequency spectrum of the truss, recorded along the array of seismometers. As in the previous examples there is a clear bandgap around 40 Hz, due to the interaction with the array. For the current problem the bandgap is larger and less deep in comparison with the same problem with a constant spacing. Furthermore, the diagram is more discontinuous than before, even if the the seismometers used to recording has the same length and
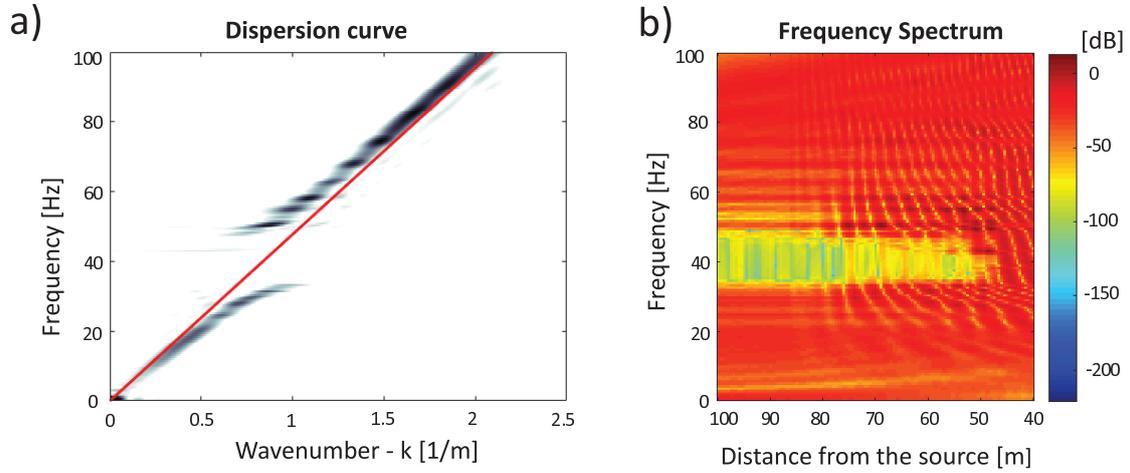
Figure 2.12: Results of 1D problem of the truss coupled with an array of 30 resonators with random distribution (similar to the results displayed in the Fig.2.8). (a) The frequency spectrum shows a bandgap around 40 Hz, larger than in the case with constant spacing (see Fig. 2.8a) and with a maximum drop of amplitude of 80 dB. (b) The dispersion curve shows a bandgap between round 40 Hz, similar to the case with constant spacing, even if the curve is less clear (see Fig. 2.8b).

location. In the frequency-wavenumber domain, the dispersion curve shows the bandgap around 40 Hz, as in the problem with constant spacing but the curve is not well defined like before. Moreover, the bandgap around 75 Hz, due to the Bragg's effect disappears, since it depends on the constant element's distribution . In conclusion, the bandgap created by the interaction with locally resonants does not depend on ordered or disordered spacing, even though the results obtained with random spacing array are less clear than in the examples with ordered elements distribution.

2.4.3 Array of damped resonators

In the former problems resonators are implemented as undamped single degree of freedom systems. This represents the abstract problem, since every type of system in nature has some energy dissipation due to friction. Thus, I introduce here an array of 30 resonators where each element has a damping coefficient, to investigate a more realistic problem, analyzing the damping effect for different levels. Therefore, I want to study the effect of attenuation , which has been neglected in the most of previous studies about seismic metamaterials, since implementing the damping effect usually involves an high computational cost. The discrete, FEM version of the 1D wave equation coupled with the array of resonators, implemented as damped systems, is written as [12]:

$$M\ddot{u} + Ku = F(t) - K_r(u - u_r) + C\dot{u}_r \tag{2.36}$$

$$M_r\ddot{u}_r = -C\dot{u}_r + K_r(u - u_r) \tag{2.37}$$

These equations are solved with the Newmark Method. Where C is the damping coefficient , which is related to the damping ratio ξ :

$$\xi = \frac{C}{2M_r\omega_r} \tag{2.38}$$

Furthermore, ξ is related to the Q factor, a dimensionless parameter which describes how damped a resonator is:

$$Q = \frac{1}{2\xi} \tag{2.39}$$

I analyzed the same problem for the following values of damping to examine how the damping influences the resonators' effect:

Level of damping	Q	ξ	C
High	1	0. 5	2.1766e+05
Medium	5	0. 1	4.3531e+04
Low	20	0. 025	1.0883e+04

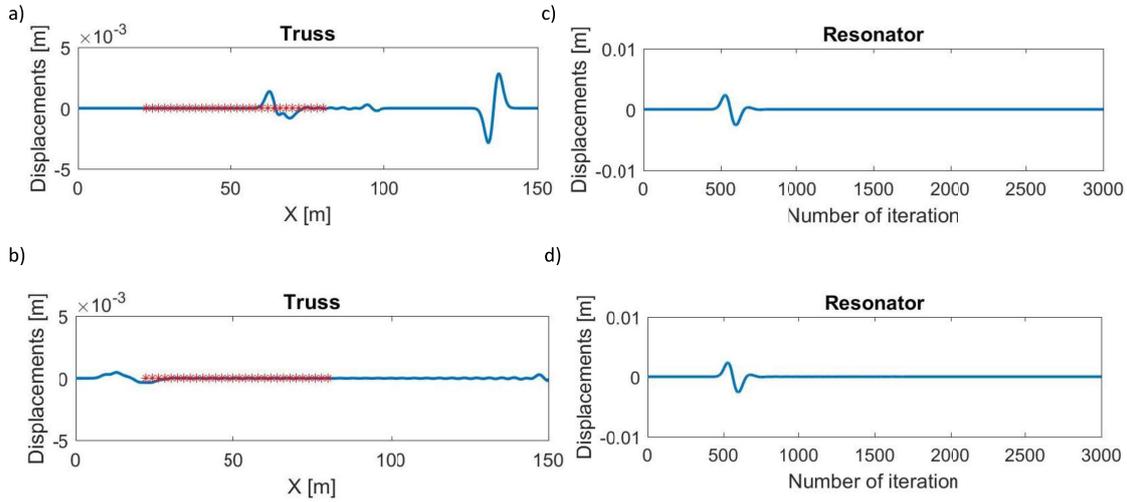The system is always underdamped because $\xi < 1$.

Figure 2.13: Results in time domain for 1D problem with an array of 30 damped resonators ($\xi = 0.5$). (a), (b) Truss' displacements after 800 and 1700 iterations, a small part of the energy is reflected by the array of resonators, since their effect is smoothed by the presence of damping. Thus, the most of the energy passes through the array (b). (c), (d) Displacement of the first resonators for the same time of instance, after 1700 iterations (d) the displacement is clearly smoothed by damping.

Therefore, I show in the Fig 2.13 the displacements of the truss and of the first resonator referred to the case with Q = 1. In particular, I show the results after 800 and 1700 iterations, as in the previous problem with an array of 30 elements without the damping effect (see Fig 2.7), to make a comparison between the two cases and to underline the effect of attenuation.
Then, I show in Fig 2.14 the results in the frequency domain and in the wavenumber-frequency domain for the three different levels of damping. Both the frequency spectra and the dispersion curves demonstrate that the bandgap due to the interaction with the locally resonants is smaller for higher values of damping, and it disappears for the problem with Q = 1. Thus, the damping effect is so strong to delete the locally resonants effect, even if this value of damping of $\xi = 0.5$ (Q = 1) is not common and the maximum value of damping ratio in civil structures is $\xi = 0.2$. On other hand, the bandgap due to the Bragg diffraction around 75 Hz is almost constant in all the cases because it does not depend on the properties of resonators but on their spacing and periodicity.
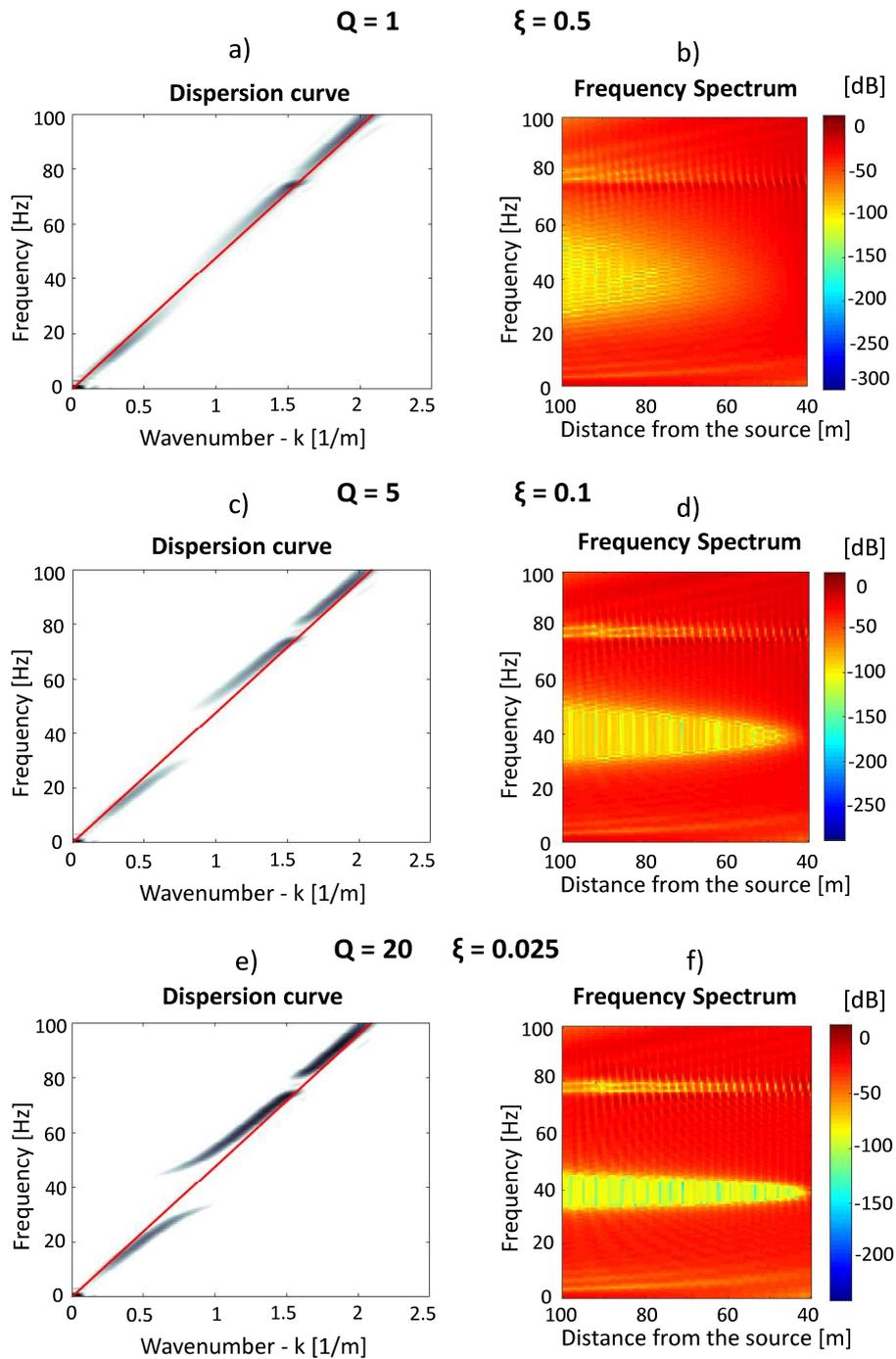
Figure 2.14: Results of the 1D problem of truss coupled with an array of 30 resonators, same as Fig. 2.8 but for the case of damped resonators. (a), (b) Dispersion curve and frequency spectrum referred the case with an high level of damping (Q = 1), both the diagrams show 2 bandgaps: around 75 Hz due to the Bragg's effect, and around 40 Hz due to the interaction with resonators, which results really smoothed. (c), (d) Same plots, but referred to the case with the medium value of Q, the bandgap generated by the interaction with the array is smaller than in the undamped case, but, the bandgap at 75 Hz due to the Bragg's effect remains almost constant.Finally, (e),(f) represent the results for system with a low damping (Q = 20), and the results in the frequency domain and wavenumber-frequency domain are similar to the undamped problem (see Fig. 2.8).

33

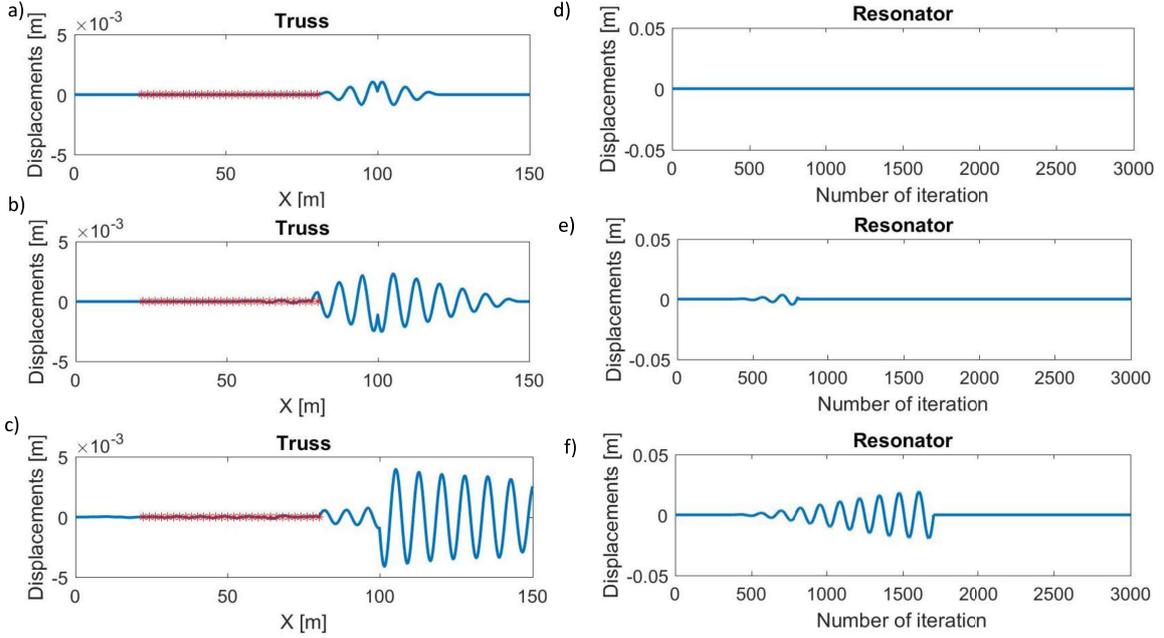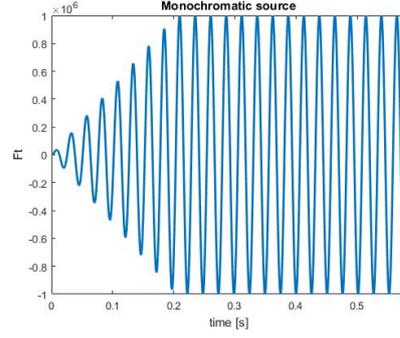Figure 2.15: Representation of the monochromatic wave as a function of time

Figure 2.16: Results in time domain for the sine wave propagation. (a),(d) Displacement of the truss and of the first resonator for the increasing sine wave ($t \leq \frac{16\pi}{\omega}$) , the array of resonators is still unshaken. After 800 iterations, (e) the first resonator starts to vibrate and (b) the sine wave is still increasing its amplitude . After 1700 iterations, (f) the first resonator vibrates increasing its amplitude as well as (c) the sine wave amplitude rise. Moreover, the wave it totally reflected by the array and there is not propagation through the resonators (c).

2.4.4   Array of resonators with monochromatic input wave

Afterwards, I analyze the propagation of a monochromatic wave in the same truss coupled with an array of 30 resonators. The wave source is a sine wave, which increases amplitude until $t < \frac{16\pi}{\omega}$ and remains constant for $t \geq \frac{16\pi}{\omega}$ as it is explained in the following expressions and it is shown in the figure 2.15:

$$F(t) = \frac{\omega t}{16\pi} \sin(\omega t) \qquad for \quad 0 \leq t < \frac{16\pi}{\omega} \qquad (2.40)$$

$$F(t) = \sin(\omega t) \qquad for \quad t \geq \frac{16\pi}{\omega}$$

Therefore, as the opposed to the previous cases, the input wave has just a specific frequency that I set equal to the natural frequency of the resonators $f = f_r = 39.38$ and consequently the circular frequency is:

$$\omega = 2\pi \cdot 39.38 Hz = 247.43 \ rad/s$$

I report in the Fig 2.16 the displacement of the truss and of the first resonator at the same instants of time reported for the Ricker wave propagation. In the time domain, the displacement of the
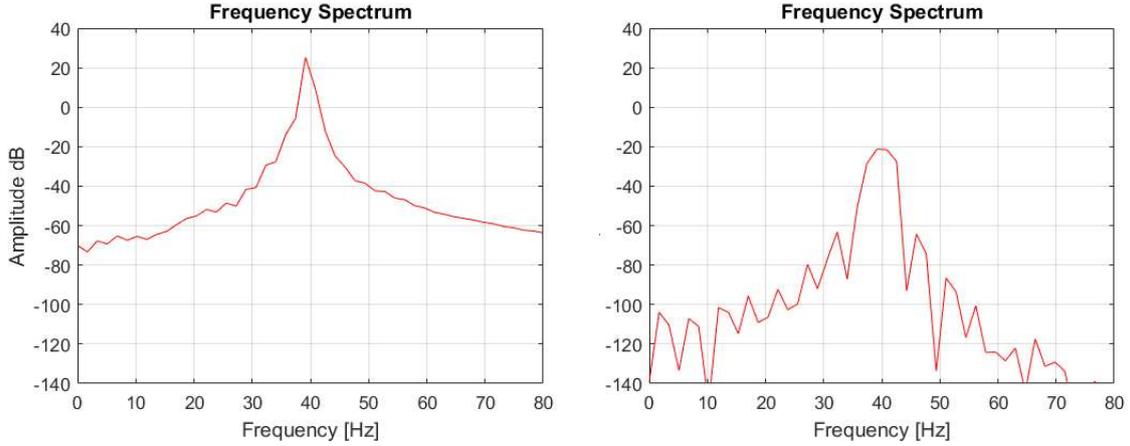
34

Figure 2.17: Frequency Spectra of sine wave propagation in 1D problem with an array of resonators and without any array. (a) Frequency spectrum of the problem without the array resonators, which presents a peak of 25 dB at the frequency of 39.38 Hz. (b) Frequency spectrum of the case with the array of resonators: the response is clearly smoothed by the presence of the array and the peak presents a maximum of -20 dB instead of 25 dB.

truss trough the resonators is almost zero because the wave is monochromatic and is set at the exactly same frequency of the array. If the input wave had a different frequency, part of the energy would pass trough the array.

In the frequency domain, the presence of resonators smooths the wave amplitude, in particular the peak of amplitude around 40 Hz, which corresponds to the fundamental frequency of the wave and the natural frequency of the trees. The Fig 2.17 shows the frequency spectrum, recorded at the position that corresponds to the end of the array with and without the presence of resonators, to underline their behavior.

Array with graded resonators

Since I proved that the wave propagation's control depends on the trees' natural frequency, I analyze an array of resonators with different frequencies in order to widen the bandgap [5]. Thus, I create an array of equally spaced resonators with different heights keeping the same cross section, density and Elastic Modulus. As before, I consider only the first longitudinal mode of resonators, neglecting the flexural modes contribute which participates very marginally to the dispersion properties. The height of the 60 elements smoothly increases from 10 meters to 20 meters and the related frequencies are between 55.13 Hz and 27.56 Hz. The spacing between elements is 1 m and the resulting increasing angle is 9°. The fig 2.18 shows the geometry of the pattern described. The split sweep wave (see Eq. 2.29) hits the shortest resonator and travels through the array with increasing resonator height.

The Fig 2.19 shows the displacements of the truss and the first resonator after 800 and 1700 iterations. The time domain results are similar to the 1D problem with 60 constant height resonators displayed in the Fig 2.9): part of the wave energy passes through the array and the rest is reflected by the locally resonants elements.

The frequency spectrum (Fig 2.20), obtained using the sweep input wave (Eq.2.29), shows a wide bandgap between 27 and 60 Hz with a maximum decrease of 80 dB. This bandgap is broader than the one obtained by a regular array of constant resonator height and it moves towards lower frequencies increasing the resonator height. The dispersion curve displays a bandgap between 40 and 60 Hz, which range of frequency seems to be controlled by the first part of the array (see Fig. 2.20).

Afterwards, I analyze the opposite problem with an array of decreasing resonator height between 20 and 10m. The natural frequencies of elements are between 27.56 Hz and 55.13 Hz, now the input wave hits the tallest element. The Fig 2.18 shows the geometry of the problem.

In the time domain, the displacements of the truss (Fig. 2.21) are similar to the problem with
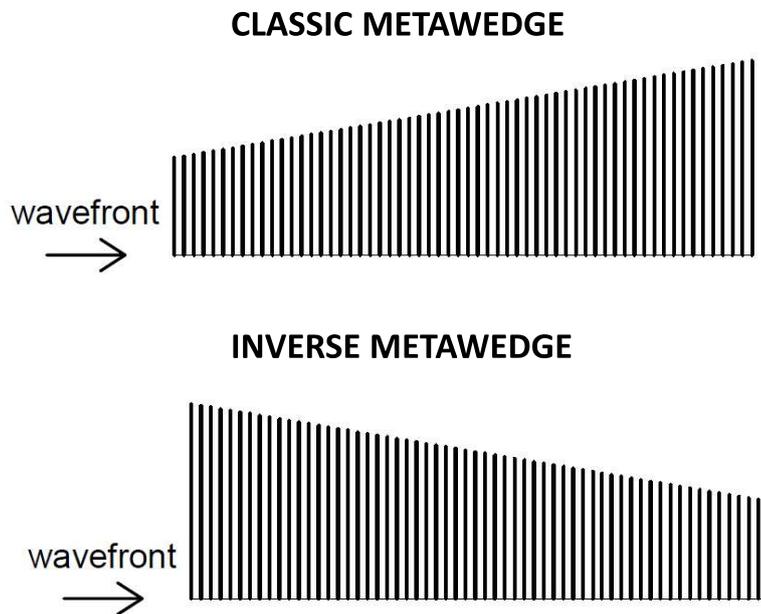
CLASSIC METAWEDGE

INVERSE METAWEDGE

Figure 2.18: Side view of arrays with increasing and decreasing resonator height (10-20 m) relative to the direction of the input wave. In both cases the array is composed by 60 elements with a constant spacing of 1 m.

Figure 2.19: Result in time domain referring to the array with increasing resonator height. (a), (c) Displacements of the truss and the first resonator after 800 iterations, the split Ricker wave is traveling through the array and part of the energy is reflected. (b), (d) Same displacements but after 1700 iterations, the wave is trapped inside the array and it is partially reflected.

GRADIENT

Figure 2.20: Results of the array with increasing resonator height. (a) The dispersion curve shows a bandgap between 43 and 60 Hz, where there is no propagation of energy. The red line represents the Rayleigh wave velocity in a non-dispersive medium. (b) The frequency spectrum shows large bandgap between 27 and 60 Hz with a maximum decrement of 90 dB, in particular, increasing the distance from the source the bandgap clearly moves towards lower frequencies, since the natural frequency of resonators inversely depends on their height.
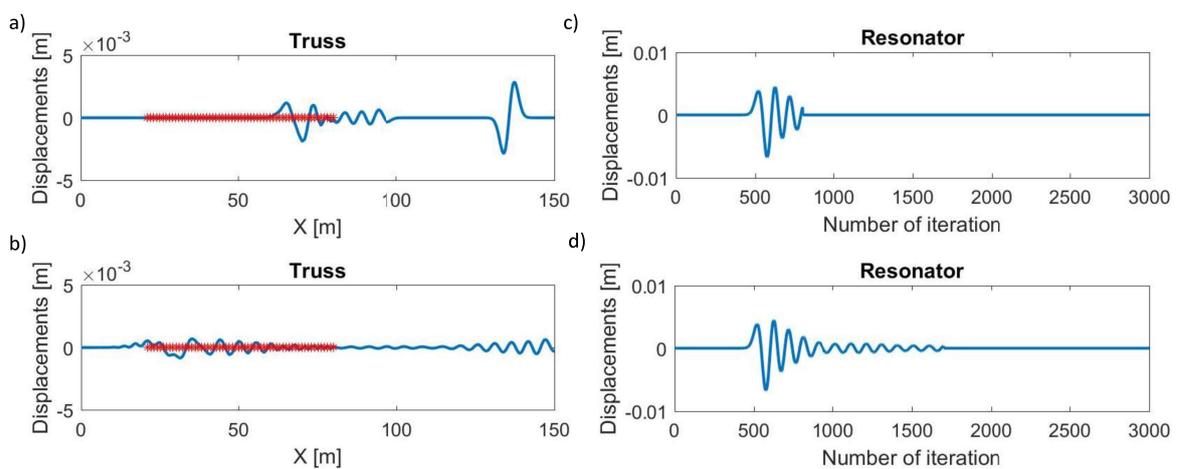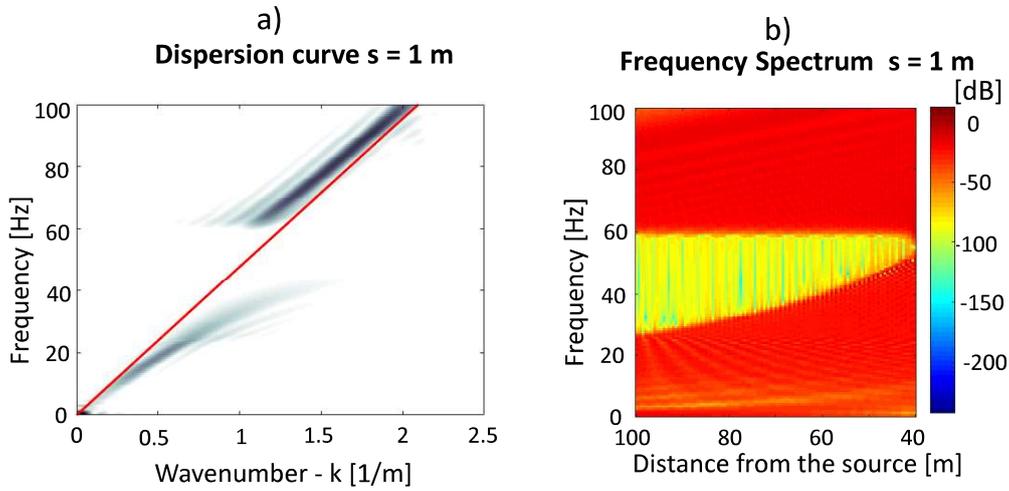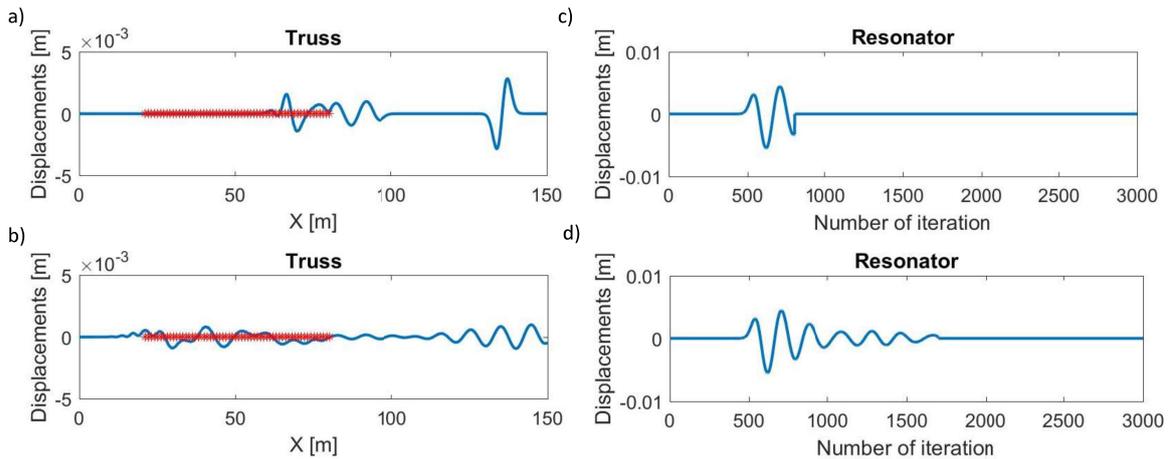

Figure 2.21: Result in time domain referring to the array with decreasing resonator height. (a), (c) Displacements of the truss and the first resonator after 800 iterations. The truss displacement (a) is similar to the previous case: the Ricker wave is traveling through the array with decreasing height and part of the energy is reflected. On the contrary, the displacement of the first resonator is slower because his natural frequency is lower than before (27.56 Hz). (b), (c) Same displacements but after 1700 iteration, the wave is trapped inside the array and it is partially reflected.

INVERSE GRADIENT

a)
Dispersion curve s = 1m

b)
Frequency Spectrum s = 1 m

Figure 2.22: Results of the array with decreasing resonator height. (a)The dispersion curve presents a bang-gap between 27 and 35 Hz, where the wave propagation is forbidden. (b) The frequency spectrum shows a bandgap between 27 and 60 Hz with a maximum decrement of 80 dB. In contrast to the previous example (see Fig 2.20), increasing the distance from the source the bandgap clearly moves towards higher frequencies.

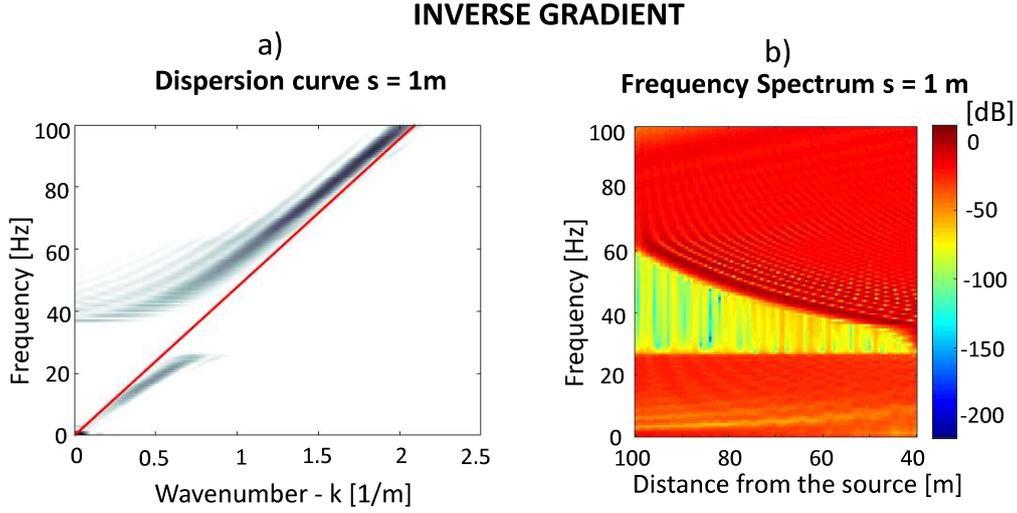an array of constant resonator height, but the first resonator's displacement is slower, since its frequency is lower than in the previous examples. Thus, it is necessary to analyze the problem in the frequency domain to properly investigate the phenomena.

In the frequency domain the amplitude drops between 27Hz and 60 Hz up to 80 dB. The bandgap moves towards higher frequencies increasing the distance form the source, since the resonator's height decreases at the same time (see Fig 2.22). The dispersion curve is reported in the Fig 2.22 and presents a bandgap between 27Hz and 38 Hz, which seems to be not influenced by the last part of the array characterized by higher natural frequencies.

Therefore, it is possible to extend, in terms of frequency, the bandgap generated by presence of the array of mass and spring elements, changing the natural frequency of the elements to obtain different values of resonance.

2.5 Wave Propagation in 2D plate coupled with a metabarrier

Once obtained results in 1D field, I move to the study of the 2D problem. Thus, I want to analyze the wave propagation in an elastic, homogeneous and isotropic plate. First of all, it is created a rectangular mesh in x-y plane (50x30 meters) implemented by 30 elements in x-direction and 20 elements in y-direction. The polynomials implemented are of sixth degree, therefore each element is described by 7 nodes (including the two geometrical end-nodes). The plate represents the soil with average characteristics and I set the properties of the medium using the same parameters of the truss:

$$\rho = 2000 \quad kg/m^3$$

$$v_s = 300 \quad m/s$$

$$\mu = \rho v_s^2 = 180 \cdot 10^6 \quad N/m^3$$

Therefore, I arrange a rectangular lattice of 84 resonators composed by 4 rows of 21 elements between 4 and 45 in x-direction placed each 2 meters. The resonators are placed orthogonally to
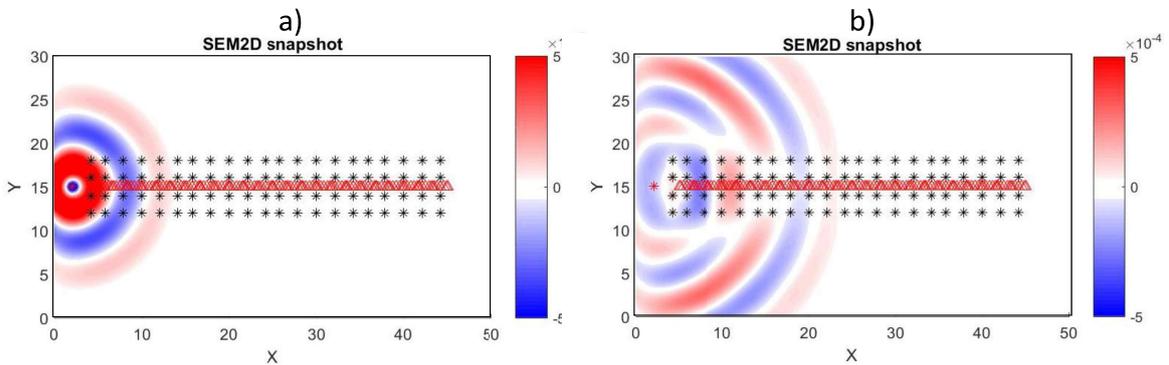
Figure 2.23: Spatial representation (x-y) of the wave propagation in terms of displacement after 200 and 450 iterations. Black stars symbolize the four rows of resonators with a constant spacing of 2 meters and the red line represents the points of wave recording with a spacing of 10 cm. (a) The snapshot after 200 iterations show that the wave is traveling through the metamaterials, since the resonators can control the wave propagation only for a specific range of frequency. (b) In the snapshot after 450 iterations the resonators are vibrating for the interaction with the wave, and the wave propagation is not homogeneous.
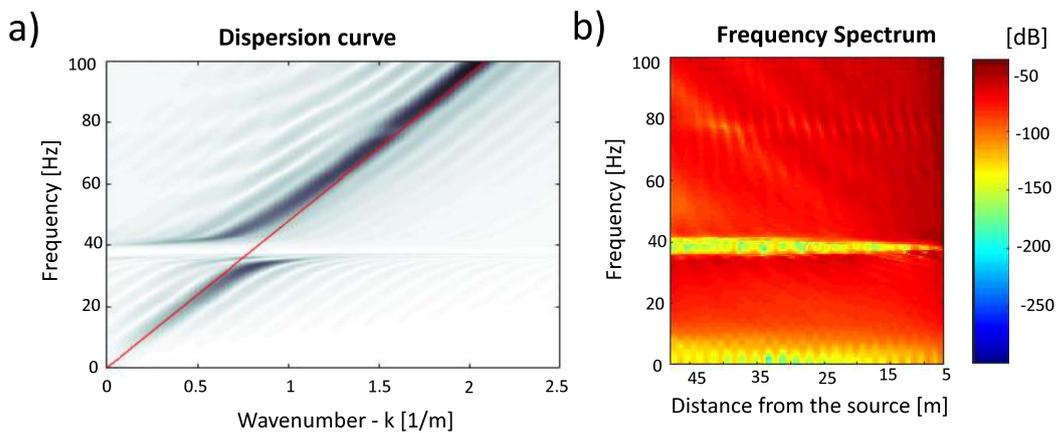
Figure 2.24: Results of 2D problem with rectangular metabarrier with constant spacing of 2 meters. (a) The dispersion curve in frequency-wavenumber domain shows a clear bandgap between 35 and 40 Hz, indeed, around 37 Hz the branch becomes flat and the wave transmission is not allowed to the frequency of 40 Hz. The straight red line represents the Rayleigh wave velocity in a non-dispersive medium. (b) The frequency spectrum represents the intensity of the wave energy through the range of colors displayed in the next color-bar. I plot the frequency spectrum of the signal measured by the array of seismographs. The amplitude is expressed in Decibel Units as a function of frequency and distance from the source and it is almost constant between 5 and 100 Hz in a range of [-50/-70] dB and decreases up to 100 dB around 40 Hz for the interaction with the metabarrier.

the plate and each element vibrates along its longitudinal axis. I want to simulate a forest of pine trees with the arrays of oscillators, as I previously described for the 1D problem. Thus, I set the resonator's parameters referring to the pine tree with the same properties used in the 1D case (see Eqs. 2.5 and 2.6).

The input wave is the same sweep wave used in the 1D problem to investigate the frequency domain, described in the Eq. 2.29 . The Fig 2.23 shows the wave propagation in terms of displacements and the geometry of the problem in the x-y domain: the wave propagations is partially reflected by resonators, that vibrate because of the interaction.

Then, I move to the study of the same problem in the frequency domain. I apply the FFT to the displacements recorded in the array of seismometers to obtain the amplitude as function of frequency. The amplitude is plotted as function of frequency and distance form the source, such as in 1D problems. The frequency spectrum reported in the Fig 2.24a shows the wave amplitude almost constant between 5 and 100 Hz with a drop of energy around 40 Hz, due to the interaction with the metabarrier.

Finally, I study the problem in the wavenumber-frequency domain in the same way shown for the 1D problem: applying the FFT2 to the displacements in space-time domain (see Eq. 1.37). I take the absolute value of the FFT2, that is the square root of the real and imaginary parts squared:

$$|FFT2| = \sqrt{Re^2 + Im^2}$$

The dispersion curve in Fig 2.24b shows a clear bandgap due to the interaction with the rectangular metabarrier, which interrupts the displacements of the plane for the specific range of frequency between 35Hz and 40 Hz . Without the presence of resonators, the curve would be linear, because the plate is elastic, homogeneous and isotropic.

2.5.1 Metabarrier of resonators with different spacing

I analyze the same problem of wave propagation in elastic, homogeneous and isotropic plate with a rectangular lattice of resonators located as before (between 4 and 45 m along x-axis and between 12 and 18 m along y-axis), changing only the spacing among elements. In particular, I studied the problem with a constant spacing of 4 m, 1 m and 0.5 m. The Fig.2.37 represents the geometry of the problem in x-y domain referred to the constant spacing of 4 and 1 m.
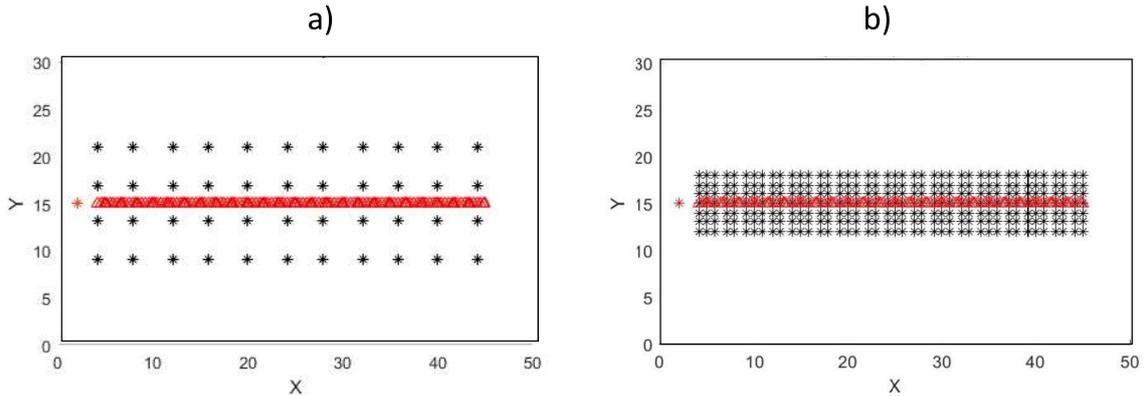
Figure 2.25: Spatial representation (x-y) of resonators' patterns. (a) Rectangular lattice with constant spacing of 4 m. (b) Rectangular lattice with constant spacing of 1 m. In both the spatial representation the resonators are symbolized by black stars and the red line represents the seismometers' array.

From data collected by seismometers, I compute the frequency spectra which show how the bandgap becomes larger decreasing the spacing between elements. Thus, increasing the density of resonators, their effectiveness improves , as it is shown in the Fig 2.26. Therefore, in terms of frequency-wavenumber domain, the dispersion curves demonstrate the same phenomena: even if the mechanical characteristics of resonators are the same in all the examples, the response is deeply effected by density of elements.
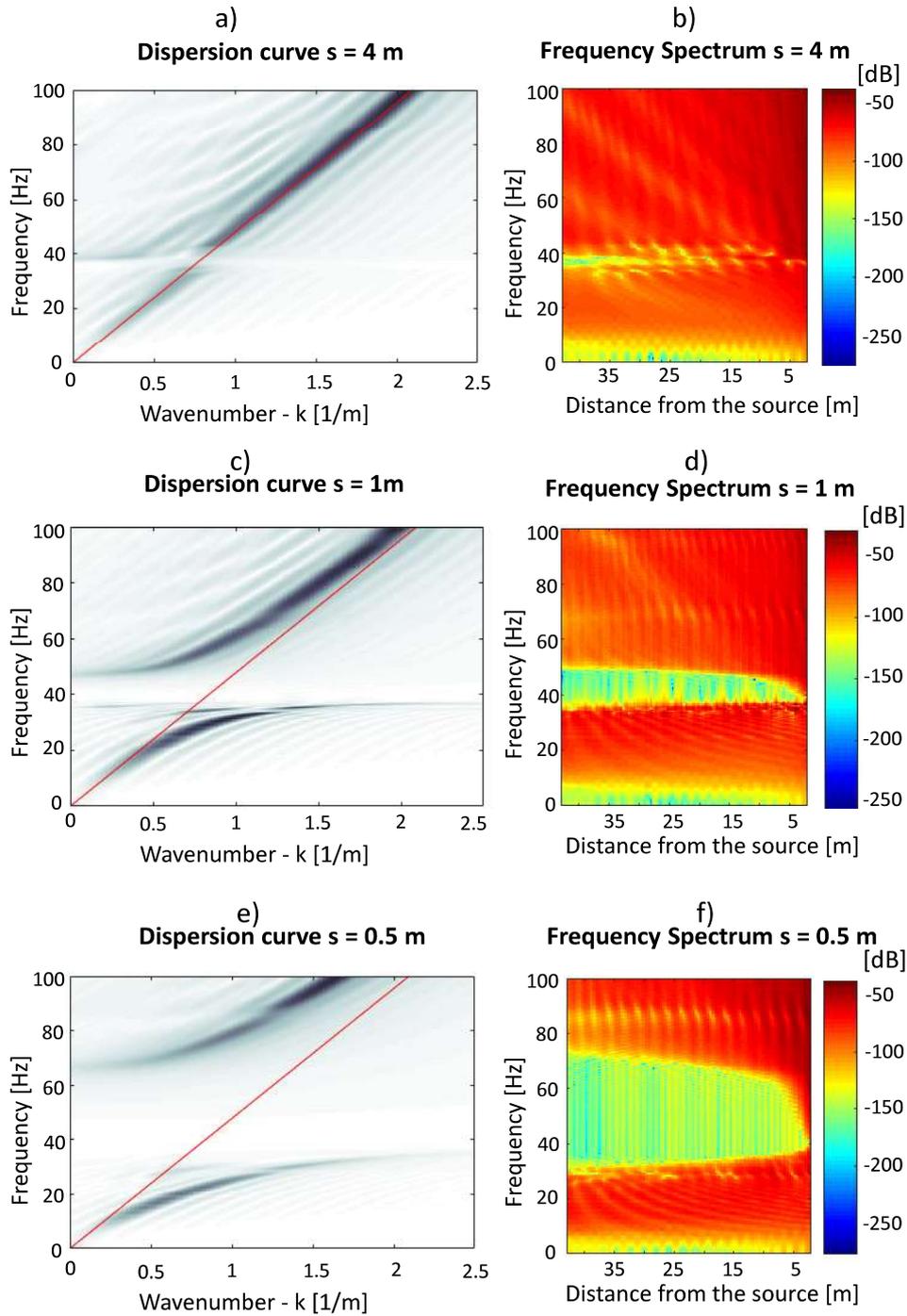
Figure 2.26: Results of 2D problem referred to a rectangular metabarrier with constant spacing of 4, 1 and 0.5 m. (a), (c), (e) Dispersion curves recorded for the three different cases, where the straight red line represents the Rayleigh wave velocity in a non-dispersive medium. (b), (d), (f) Frequency spectra for the same problems, the amplitude is almost constant between 5 and 100 Hz in a range of [-50/-70] dB and decreases up to 100 dB around 40 Hz for the interaction with the metabarrier. (a)-(b) For a constant spacing of 4 m the bandgap is narrow and the wave propagation is inhibited only at 39 Hz. Decreasing the spacing the bandgap become larger and for s = 0.5 (e),(f) there is no wave propagation between 30 Hz and 70 Hz. Therefore, the bandgap strongly depends on the number of resonators and on the spacing among elements.
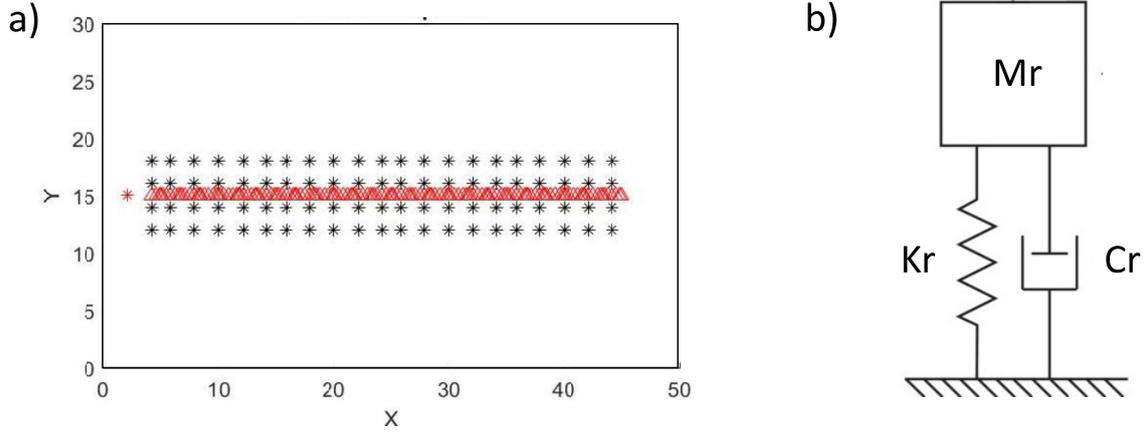
Figure 2.27: (a) Spatial representation (x-y) of rectangular lattice of resonators with a constant spacing of 2 m. (b) Representation of a single degree of freedom system with damping.

2.5.2 Metabarrier of damped resonators

After having studied the abstract problem with undamped resonators I introduce the effect of attenuation. Thus, referring to the rectangular pattern composed by 4 rows of 21 elements with a spacing of 2 meters between adjacent elements, I implement each element as a damped single degree of freedom system, such as in the 1D problem (see Fig. 2.27). I analyze the same problem for following value of damping to examine how the damping influences the resonators effect:

Level of damping	Q	ξ	C
High	1	0. 5	2.1766e+05
Medium	5	0. 1	4.3531e+04
Low	20	0. 025	1.0883e+04

Where:

- Q is the quality factor;

- $\xi = \frac{1}{2Q}$ is the damping ratio;

- $C = 2M_r\omega_r\xi$ is damping factor.

From data collected by seismometers, I represent the frequency spectra, which show the amplitude as a function of frequency and distance from the wave source. In all the three frequency spectra, the energy is concentrated between 5 Hz and 75 Hz and it decreases around 40 Hz for the cases with medium damping (ξ= 0.1), where the bandgap over 40 Hz is evidently smoothed, and with low damping (ξ= 0.025), where the results are similar to the undamped system problem. On the contrary, for high level of damping ($\xi = 0.5$) the metabarrier does not reflect the wave energy and the frequency spectrum does not present a bandgap for the resonance frequency.
The same phenomena is confirmed in the dispersion curves, which display a bandgap only for the cases with medium and low damping. Thus, since the medium is non-dispersive, the dispersion curve for high level of damping ($\xi = 0.5$) is linear because the wave propagation is not influenced by the metabarrier. Finally, dispersion curves are compared to the straight red line which represents the Rayleigh wave velocity in a non-dispersive medium (see Fig 2.28).
Therefore, the presence of damping makes the effect of metabarrier less efficient. Indeed, the effectiveness of the resonators is reduced by the increasing of their damping and it is important to reduce the damping effect as much as possible.

Figure 2.28: Results of 2D problems with rectangular metabarrier with a constant spacing of 2 m and different value of damping . (a), (c), (e) Dispersion curves computed for the three different values of damping, respectively Q =1, Q = 5 and Q = 20. (b), (d), (f) frequency spectra referred to the same cases. For Q = 1 (a) the dispersion curve is almost linear and (b) the frequency spectrum does not show a clear bandgap at the resonance frequency. For Q = 5 (c) the dispersion relation presents a bandgap for the interaction with resonator and the same phenomena is confirmed in the frequency domain (d). Finally, for Q = 20 (e)-(f) the results obtained are similar to the problem with the same spacing but undamped resonators (see Fig. 2.24), with a drop of energy inside the gandgap up to 90 dB.
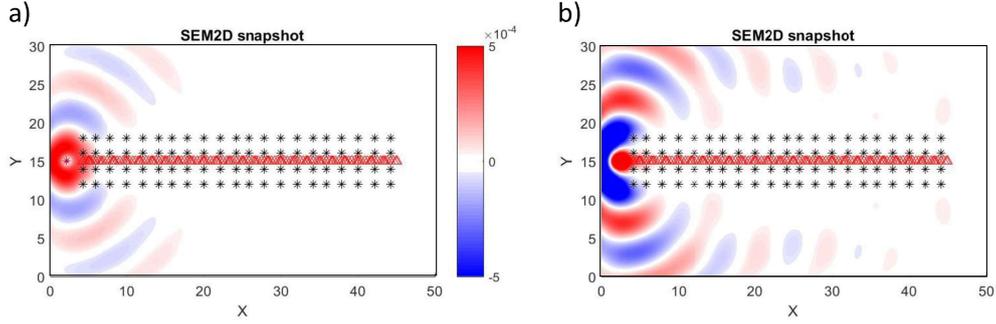
Figure 2.29: Spatial representation in x-y domain of the wave transmission, in terms of displacement, for two different time steps. (a) Snapshot after 500 iterations, the wave amplitude is still growing and the metabarrier completely reflects the wave propagation. (b) Snapshot a the end of the simulation (after 8000 iterations), the wave is completely reflected by the metabarrier.
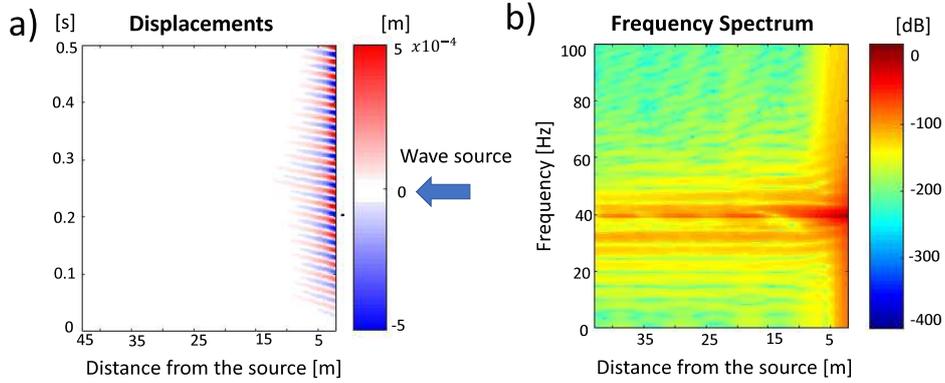

Figure 2.30: Results of 2D problem with rectangular metabarrier with constant spacing of 2 meters and sine input wave. (a) Displacements as function of time and distance from the source, while their intensity is represented through the range of colors displayed in the next color-bar and clearly decreases for the interaction with the metabarrier. (b) Frequency spectrum shows the amplitude, in terms of dB, centered around the frequency of the sine wave [39.38 Hz] and smoothed because of the presence of resonators.Thus, the amplitude decreases form the point source along the metabarrier for the interaction with resonators.

2.5.3 Metabarrier of resonators with monochromatic wave

Afterwards, I analyze the propagation of a monochromatic wave, as well as in the 1D problem. The wave source is a sine wave which amplitude increases until $t = \frac{16\pi}{\omega}$ and remains constant after this instant of time, (see Eq. 2.40). The frequency of the input wave is set equal to the natural frequency of the metabarrier: $f = f_r = 39.38$ and the point source wave is placed at x= 2 m, y = 15 m. Furthermore, the plate is coupled with a rectangular metabarrier composed by 2 rows of resonators with a constant spacing of 2 m, as the Fig. 2.29 shows.

The time domain results are presented in the Fig 2.29, where it is displayed the wave propagation in terms of displacement for two different instant of time. The wave transmission is completely blocked by the metabarrier during all the numerical simulation, as the input wave is monochromatic and its frequency perfectly matches the resonance frequency.

From the data collected in the seismometers, located along the x-axis inside the resonators lattice (see Fig. 2.29) I generated a move-out in terms of displacements (Fig. 2.30), which decrease to zero after 5 meters from the wave source because of the interaction with the metabarrier. (Fig 2.30). In the frequency domain (see Fig. 2.30) the wave amplitude is gathered around the input wave frequency, but is strongly smoothed by the metabarrier.
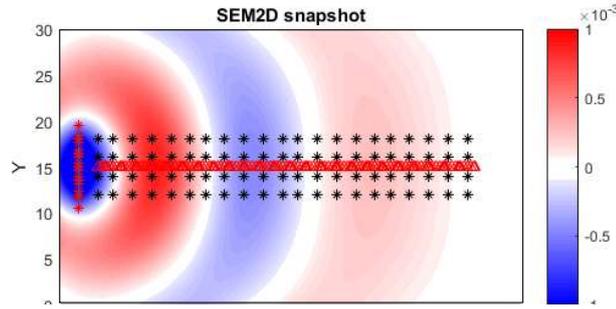
44

Figure 2.31: Spatial representation (x-y) of the plane wave propagation in terms of displacements. The plane wave is made by an array of point source waves and the resonators' lattice is rectangular with a spacing of 2 meters between adjacent elements.
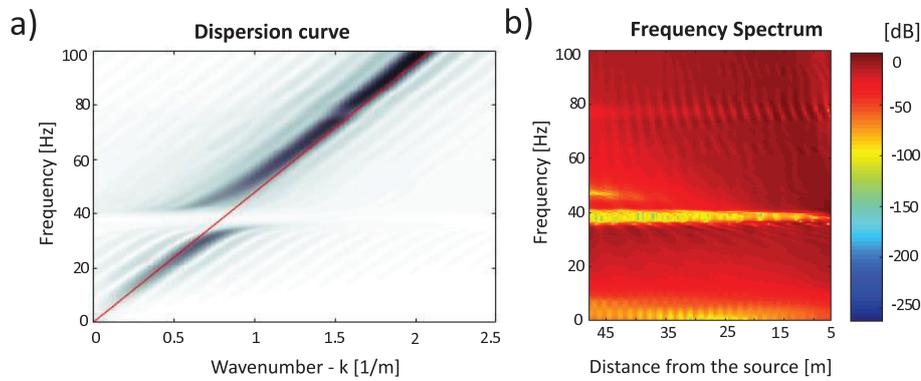

Figure 2.32: Results of 2D problem with rectangular metabarrier with constant spacing of 2 meters and plane input wave. (a) Dispersion curve shows a bandgap between 37 and 40 Hz, as in the 2D problem with the same lattice investigated by a point source wave (see 2.8). (b) Frequency spectrum presents the amplitude almost constant between 5 and 100 Hz in a range of [0/-25] dB and decreases up to 100 dB around 40 Hz for the interaction with the metabarrier. In comparison with the former examples the amplitude has higher values, because the input wave is made up of 21 point sources instead of one point source.

2.5.4   Metabarrier of resonators with plane wave

Then, I study the propagation of a plane wave in the same mesh of 50x30 meters implemented by 30x20 elements, without changing the lattice of rectangular resonators with a constant spacing of 2 m implemented in the last example and displayed in the Fig. 2.31 .Thus, I apply an array of point source wave to simulate the plane wave propagation. The input wave is the same sweep wave previously used and described by Eq. 2.29 .The array is set along y-direction from 10 to 20 meters and it is composed by 21 point sources, placed one every 50 centimeters.

  In the frequency spectrum the results follow the same trend of the previous problems, thus the most of the energy is between 5 Hz and 75 Hz with a clear decrease before of 40 Hz, due to the interaction with metamaterials. Furthermore, the bandgap becomes larger increasing the distance from the source, since the effect of resonators increases at the same time. Even the dispersion curve confirms the results with a clear bandgap before 40 Hz.

Hence, the behavior of the metabarrier is not influenced by the kind of input wave source, since in the frequency spectrum and in the frequency-wavenumber representation the bandgap, generated by interaction with metamaterials, is unchanged in comparison to the same example with a point source wave.
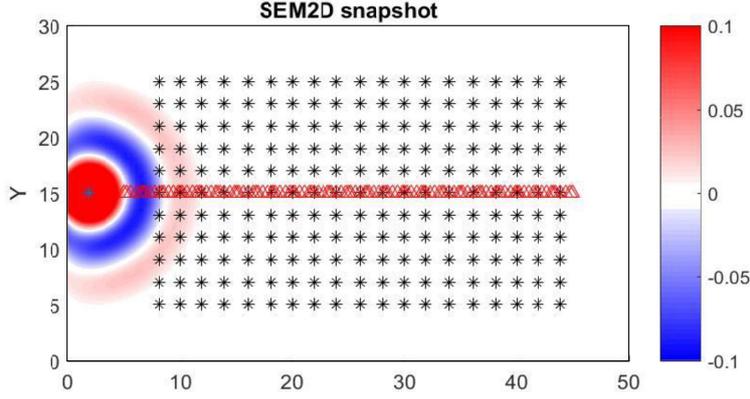
Figure 2.33: Representation in x-y domain of the wave propagation in terms of velocity. The resonators' lattice is composed by 20 columns along y-direction of 10 elements, and each column has resonators with the same height. Resonators are represented by black stars and the red line symbolizes the array of seismometers.

2.5.5 Metabarrier with graded resonators

Since I proved that the bandgap depends on the natural frequency of resonators, I implement a metabarrier with increasing resonator height [5] [4] in order to control the seismic waves widening the bandgap in terms of frequencies. I model a metabarrier of vertical resonators increasing the height between 10 and 19.5 meters. The resonators' rectangular lattice is composed by 20 columns along y-direction of 10 elements (see Fig.2.33), and each column is made by resonators with the same height and consequently with the same natural frequency, which is between 28.27 Hz and 55.13 Hz . The coupling between the seismic input sweep wave (see Eq.2.29) and the longitudinal resonances creates a bandgap, which frequency range is inversely proportional to the resonators' height. I consider only the first longitudinal mode, holding the same value of density, Elastic Modulus and cross section used in problems with constant height. Thus, I obtain the following values of mass, stiffness, circular frequency and frequency:

$$M_r = \pi(\frac{d}{2})^2 h\rho = 62.83 \cdot h \quad [kg]$$

$$K_r = \frac{EA}{h} = \frac{\pi(\frac{d}{2})^2}{h} = \frac{7.54 \cdot 10^8}{h} \quad [N/m]$$

$$\omega_r = \sqrt{\frac{K_r}{M_r}} = [346.41; 329.91; 314.92; 301.23; 288.67; 277.13; 266.47; 256.60; 247.43; 238.90;$$
$$230.94; 223, 49; 216.51; 209.94; 203.77; 197.95; 192.45; 187.25; 182.32, 177.64] \quad [rad/s]$$

$$f_r = \frac{\omega_r}{2\pi} = [55.13; 52.51; 50.12; 47.94; 45.94; 44.10; 42.41; 40.84; 39.38; 38.02; 36.75; 35.57;$$
$$34.46; 33.41; 32.43; 31.50; 30.63; 29.80; 29.02; 28.27] \quad [Hz]$$

Then, I implement the same problem with graded arrays of decreasing resonator height. Thus, the metabarrier and the concerned frequency range is exactly the same, but the input wave hits first the tallest column of resonators passing through columns with decreasing height (from 19.5 to 10 meters) and increasing frequency (from 28 to 55 Hz). For both the cases, I show the results in the frequency domain in Fig. 2.34, where the bandgap generated by the interaction with the metabarrier presents a triangular shape due to the range of trees resonance frequencies. Indeed, the bandgap moves towards lower frequencies in the first example with increasing hight and vice versa in the second one. In both the examples, the bandgap is larger than in the case with constant height because the effectiveness of the resonators depends on their natural frequencies.
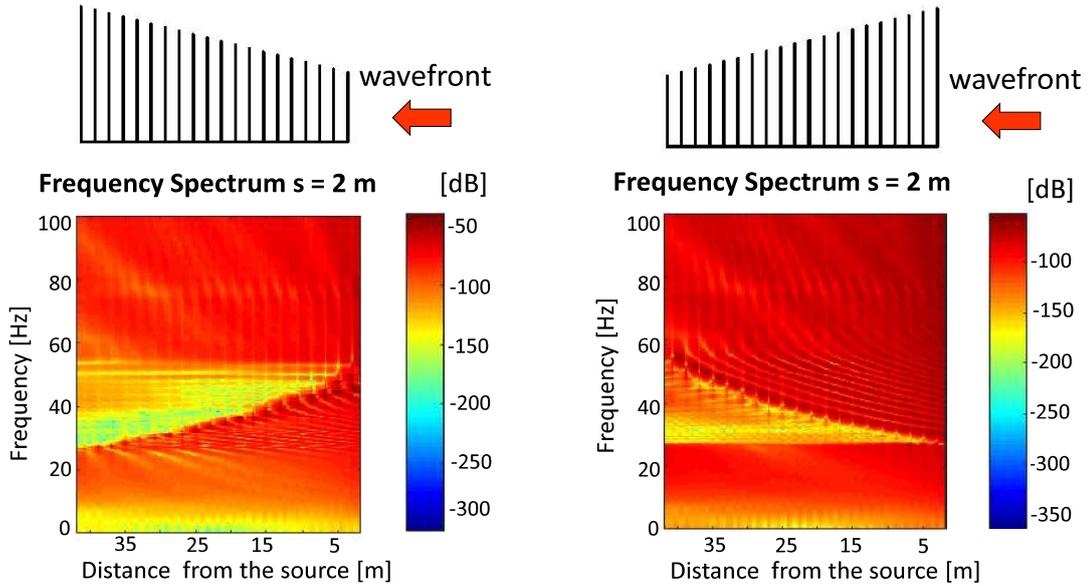
Figure 2.34: Frequency spectra of 2D problems with rectangular metabarrier made by spatially graded array of resonators coupled with the relative side view of metabarrier with increasing and decreasing respectively resonator height. The frequency spectrum on the left is referred to the case with increasing resonator height, rising the distance from the wave source the bandgap moves towards lower frequencies. The frequency spectrum on the right is referred to the case with decreasing resonator height and shows the opposite phenomena.

2.6   Filtered spatial representation in x-y domain

Afterwards, I analyze the same problems with a different input source to show the wave propagation in the x-y plane. The input wave is a Gaussian wave:

$$F(t) = e^{[-2\pi f_0 (t-t_0)]^2} \qquad (2.41)$$

$$t_0 = 0.0315 \ s$$

The fundamental frequency $f_0 = 40Hz$ is set almost equal to the natural frequency of the trees. From data collected in a grid of 20x20 meters in x-y domain I create a spatial representation in terms of displacements, for different time steps, referring to the same problems analyzed above. Thus, for the three time steps recorded I compare the snapshots to analyze the behavior of locally resonators. The square grid is located between 5 and 25 meters along both x and y axes, with a spacing of 0.5 m between adjacent points of measurements [32].

For all examples with constant resonator height, I apply a Butterworth bandpass filter with a lower cutoff frequency of 38 Hz and a higher cutoff frequency of 42 Hz. Therefore I represent the wave propagation related to the range of frequency of the bandgap to show how the wave propagation is forbidden in that frequency band.

In order to apply the filter in the time domain it is necessary to multiply the signal by the filter expressed in time domain :

$$x'(t) = x(t) \cdot w(t) \qquad (2.42)$$

In the frequency domain, on the other hand, it is necessary to perform a convolution to obtain the filtered signal:

$$X'(\omega) = X(\omega) \cdot W(\omega) \qquad (2.43)$$

The Butterworth filter is a type of signal processing filter designed to have as flat frequency response as is possible in the passband. The frequency response of the Butterworth filter is maximally flat in the pass-band and decreases towards zero in the stop-band. After having applying this filter, the following series of snapshots (Fig 2.36) clearly show how the wave transmission in x-y domain is effected by the metabarrier, which reflects part of the wave energy.
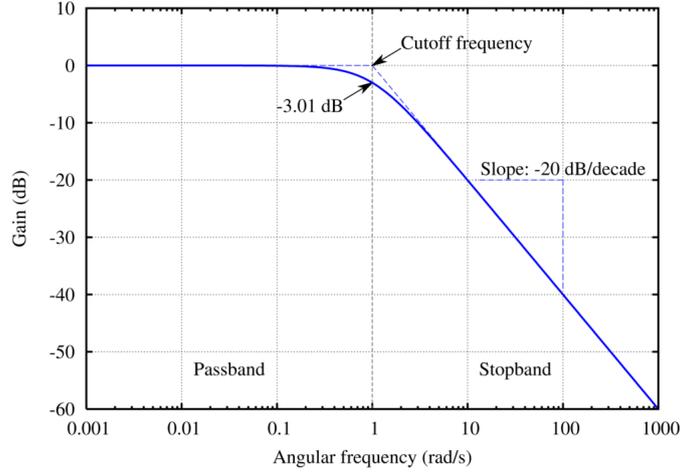
Figure 2.35: Frequency response of a low pass Butterworth filter of first order, whose cutoff frequency is normalized to 1 radian per second and whose response is in terms of Decibel Units is computed as $G(\omega) = \frac{1}{\sqrt{1+\omega^{2n}}}$ (ω is the angular frequency and n is the number of poles in the filter). The transition between the pass-band and stop-band of a first order filter (n=1) with cut-off frequency ω_c normalized ($\omega_c = 1/\tau$) is characterized by the slope of 20 dB per decade of frequency's change, as well as it is shown in the tutorial picture .

The fig 2.36 shows snapshots for three instants of time referring to the 2D wave propagation in the plane coupled with rectangular metabarrier with constant spacing of 2 meters among elements. I compare for the same time steps the wave transmission without the presence of resonators, to highlight their behavior. Indeed, in the second example, the wave travels homogeneously, while with the presence of resonators the wave is reflected.

Afterwards, I analyze the metabarrier's effectiveness for different spacing, studying the same problem with a constant spacing of 1 and 4 m. The snapshots in Fig 2.37 show that reducing the spacing between adjacent elements the metamaterials' success improves, indeed with a spacing of 1 m the most of the energy is reflected. On the contrary, the spacing of 4 m is not enough to control the wave transmission.

Then, I study the damping influence, computing the same 2D problem for the following values of damping ratio: $\xi = 0.5, 0.1 and 0.025$. I report the results in the fig 2.38. From this analysis, the main result is that the metabarrier looses its effectiveness by increasing the damping. Indeed, with $\xi = 0.5$ the metabarrier is not able to control the wave transmission anymore and with $\xi = 0.025$ the metabarrier has almost the same success obtained with undamped resonators.

Then, I study the effect of the damping with a input plan wave. In particular, I report the spatial representation of the wave propagation problem with a rectangular metabarrier with a constant spacing of 2 m at two different instants of time. I analyze the same problem with undamped resonators and resonators with damping (respectively $\xi = 0.1$ and $\xi = 0.5$). The results from the analysis prove that increasing the effect of attenuation the metamaterials become less efficient at controlling the wave propagation. Thus, with a different kind of source the metamaterials show the same behavior obtained in the previous examples with an input point source wave.

Finally, I represent in the Fig. 2.40 the wave propagation in x-y domain filtered at different frequency ranges to underline how change the wave shape increasing the speed. Moreover, I report the relative dispersion curve. The snapshots are referred to the 2D problem with a rectangular metabarrier with a constant spacing of 2 m, composed by undamped elements. The input point source wave is the same used before described in Eqn. 2.41. Therefore, applying the band-pass filter between 30 and 35 Hz (before the stop band) the wave shape is flat since for a low range of frequencies the wave is slow. On the contrary, applying the band-pass filter between 45 and 55 Hz (after the stop band) the wave shape is bended as the wave speed is higher than in the previous example. Furthermore, in both the examples the wave is not reflected by metamaterials because the two frequency ranges are outside the bandgap.
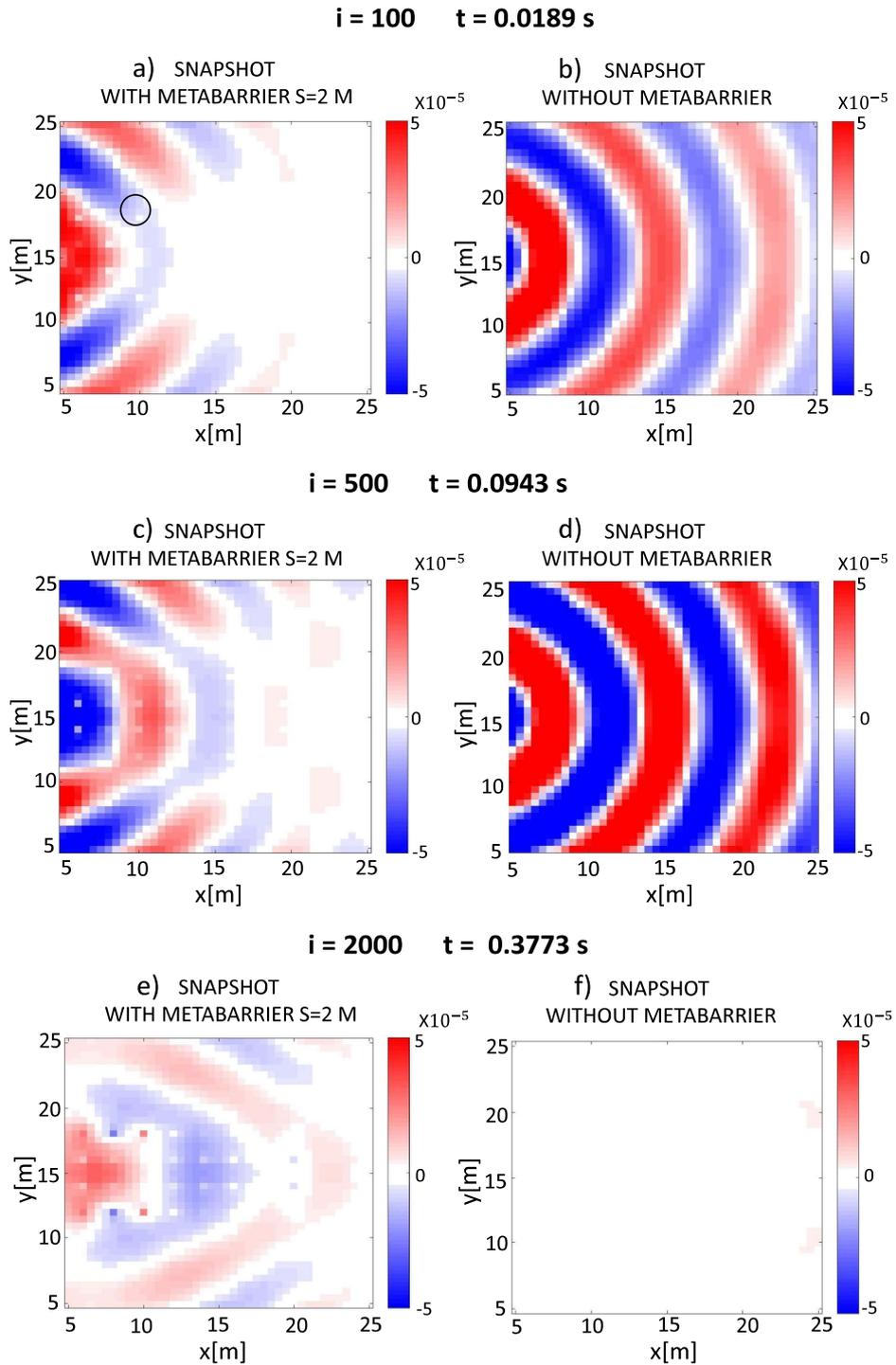
i = 100   t = 0.0189 s

a) SNAPSHOT
WITH METABARRIER S=2 M

b) SNAPSHOT
WITHOUT METABARRIER

i = 500   t = 0.0943 s

c) SNAPSHOT
WITH METABARRIER S=2 M

d) SNAPSHOT
WITHOUT METABARRIER

i = 2000   t = 0.3773 s

e) SNAPSHOT
WITH METABARRIER S=2 M

f) SNAPSHOT
WITHOUT METABARRIER

Figure 2.36:   Filtered spatial representation (x-y) at three different instants of time, referring to the same problem with and without the presence of the metabarrier. (a) Snapshot at t= 0.0189, the input Gaussian wave cannot travel through the metabarrier. It is possible to identify the position of single resonator, which are represented by white points (one of them is highlighted with a circle as example). (b) Snapshot at the same time steps for the case without any resonator, the input wave travels regularly. (c) After 500 iterations, part of the energy is reflected and part travels through the metabarrier, but it is smoothed by locally resonators. At the same instant of time in the problem without metabarrier (d) the input wave is travelling undisturbed. (e), (f) The last row represents the configuration after 2000 iterations, (f) there is not displacement since the input wave have passed through the metabarrier, on the other hand, in the problem with metabarrier (e) part of the energy is still trapped inside.
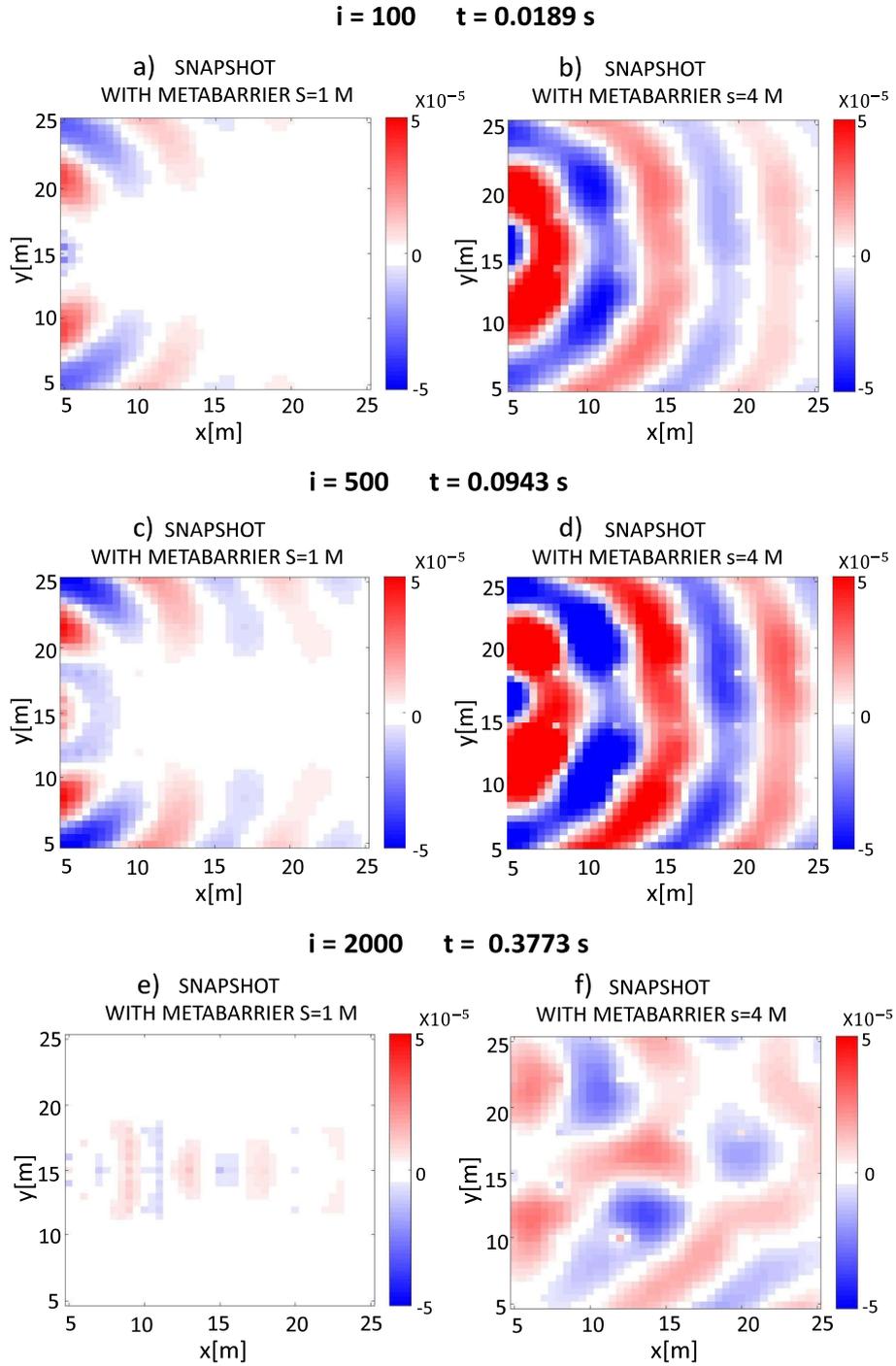
Figure 2.37: Filtered spatial representation (x-y) at three different instants of time (t= 0.0189 s, t = 0.0953 s and t = 0.03773 s), referring to the plate coupled with the metabarrier with constant spacing of 1 m and 4 m. (a), (c) Snapshots for the plate coupled with metabarrier with constant spacing of 1 m, which appears to be really effective to reflect the input waves. On the contrary, in the examples with constant spacing of 4 m (b),(f), the metabarrier loses its effectiveness and the most of the wave passes trough resonators, which location is clearly visible in these snapshots. Finally, after 2000 iterations (e),(f) the snapshots show that, after that the input wave has passed through it some energy is still trapped among resonators, mostly in the metabarrier with spacing of 4 m.
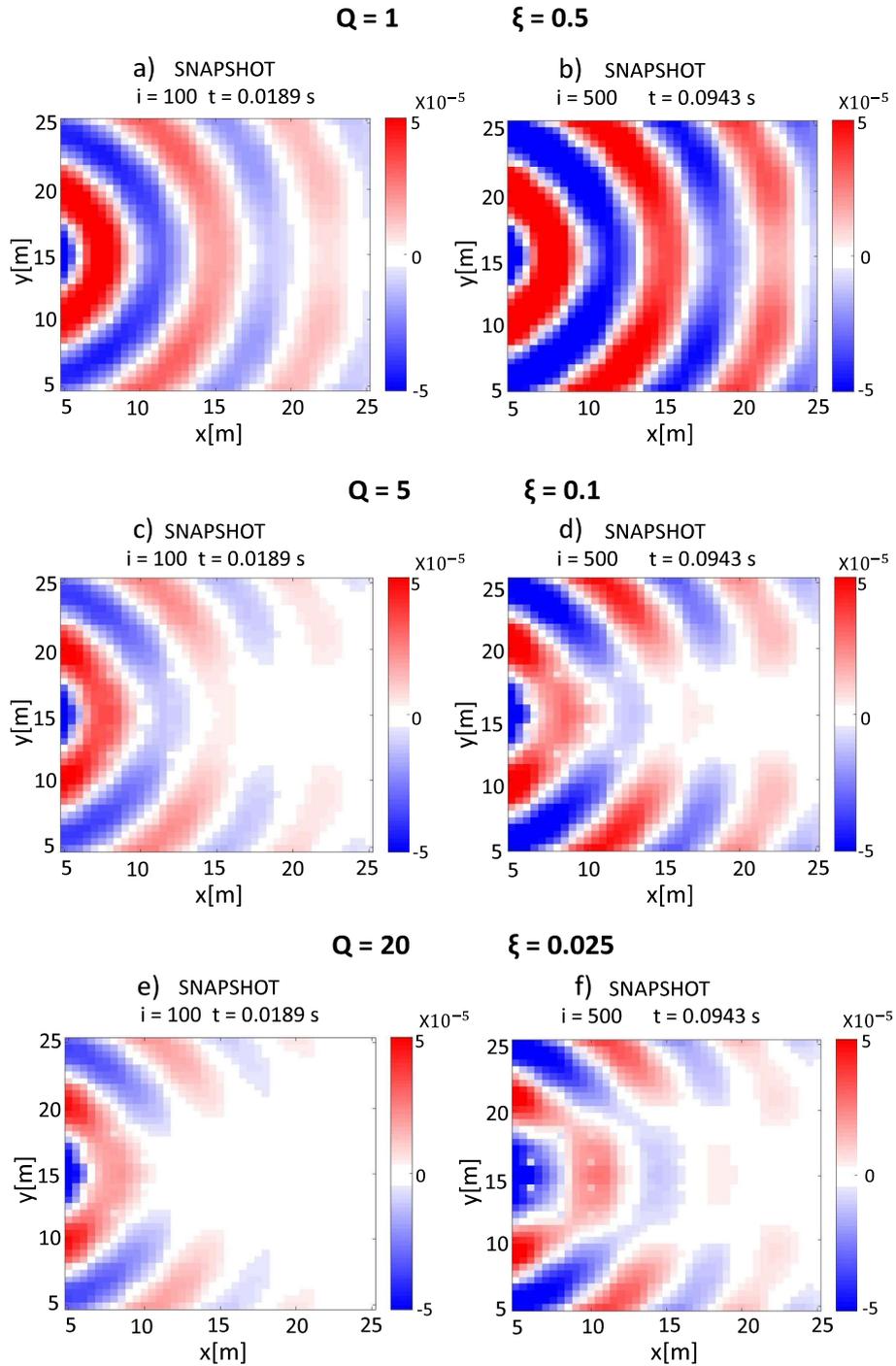
Figure 2.38: Filtered spatial representation in x-y domain for two different instants of time, referring to a metabarrier with three different value of damping. (a), (b) Snapshot at t= 0.0189 and t= 0.0943 s for resonators with a damping ratio of 0.5. Since the value of damping is high, resonators lose their effectiveness and the input wave travels inside in. (c), (d) Snapshots for the same instants of time with resonators implemented with ξ= 0.1, the most of the input wave energy is reflected by the metabarrier. Finally, (e), (f) represent the problem for damping system set at ξ= 0.025. Since the value of damping is really low the results are similar to the undamped problem (see Fig. 2.36) and the input wave is reflected by locally resonators.
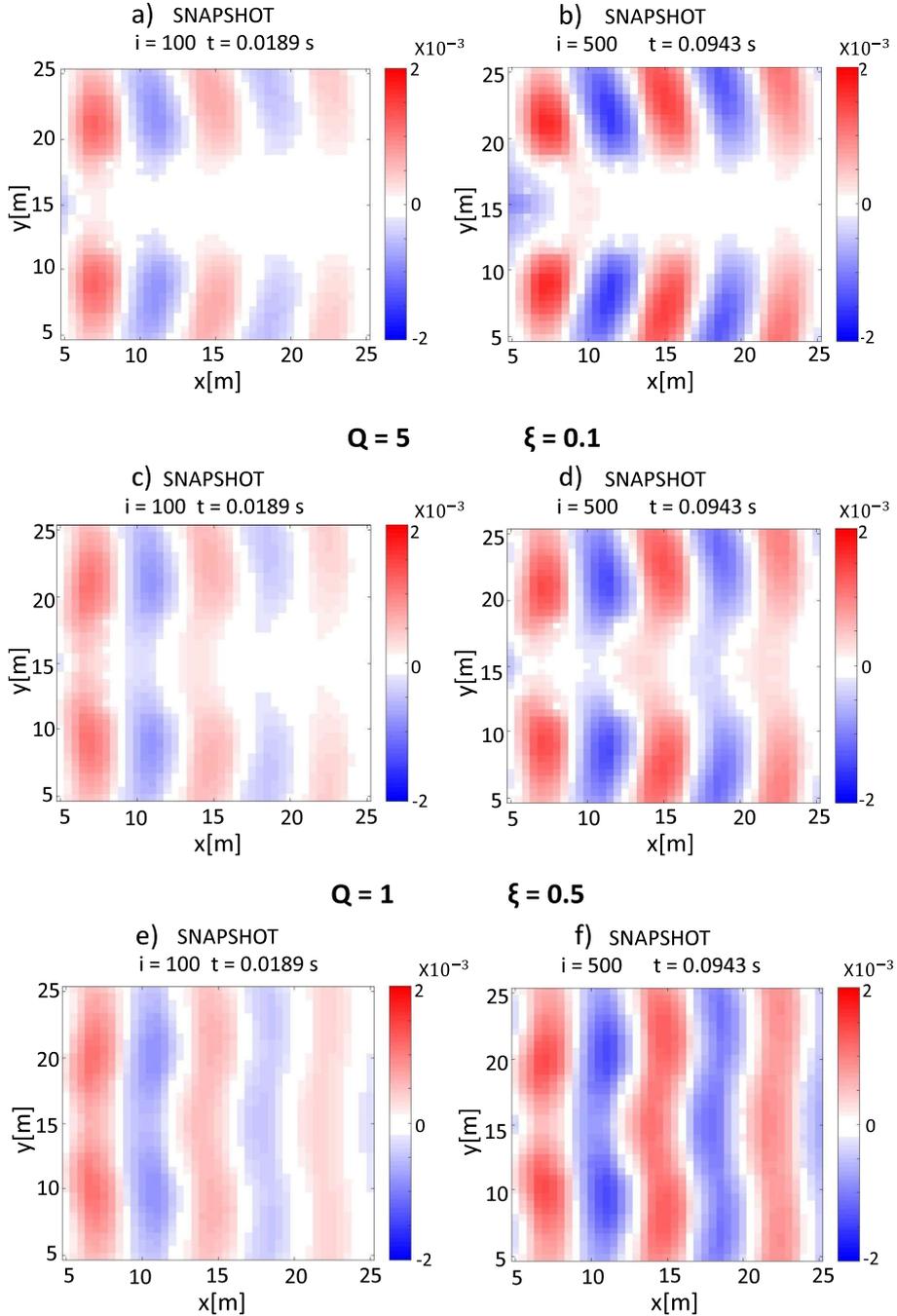
Figure 2.39: Filtered spatial representation (x-y) of a plane wave propagation referring to a metabarrier with undamped resonators and damped resonators ($\xi = 0.1$ and $\xi = 0.5$), at two different instants of time. The range of displacements is higher than in the previous examples, since the plane wave is generated from 21 point source wave. (a), (b) Snapshot at t= 0.0189 and t= 0.0943 s for the undamped system, which results to be effective to reflect the most of the energy of the plane wave. (c), (d) Snapshots for damped metabarrier with $\xi = 0.1$, which smooths the wave energy just in part. Finally, (e),(f) for low damped system ($\xi = 0.025$) the results are similar to the undamped system, thus the damping effect is the same with a plane wave or point source wave and the kind of wave does not influence the metabarrier's behavior.
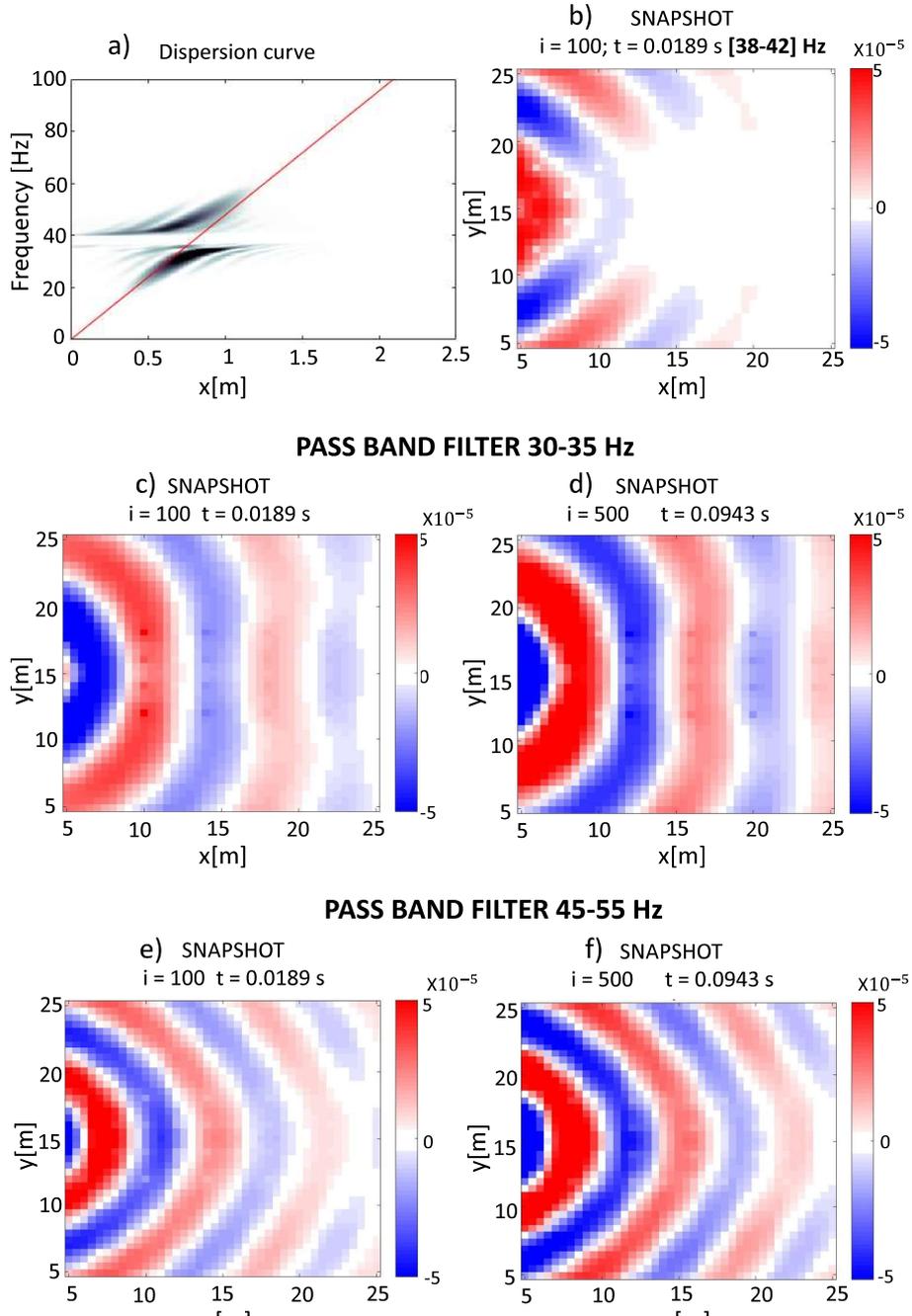
Figure 2.40: Spatial representation (x-y) filtered in different range of frequencies: before, inside and after the bandgap and the relative dispersion curve. The input wave is Gaussian with fundamental frequency of 40 Hz and the resonators' lattice is rectangular with a constant spacing of 2 m.(a) Dispersion curve shows that the wave energy is gathered between 20 and 60 Hz and at 40 Hz there is a clear bandgap due to the presence of resonators. (b) Snapshot after 100 iteration filtered for the range of frequency interested by the bandgap, the wave is clearly reflected by the metabarrier. (c), (d) Snapshots respectively after 100 and 200 iterations, the bandpass filter applied is between 30 and 35 Hz, before the stop band. The input wave is not reflected by metamaterials and travels through it, furthermore the flat wave shape is typical for slow waves. (e), (f) Snapshots at the same instants of time, filtered between 45 and 55 Hz (after the stop band), the wave is not reflected by metamaterials and the wave shape is bended since the wave speed increases for higher frequencies.
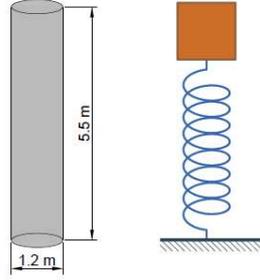
Figure 2.41: Representation of vulcanized rubber column and a simple resonator

2.7 Low seismic frequency example

Afterwards, I used the spectral element methods to investigate the wave propagation referring to a low seismic range of frequency. Thus, I change the mechanical characteristics of resonators and the fundamental frequency of the input waves in order to analyze the frequency range typical of earthquake events [1-10 Hz]. I study the wave propagation in 1D domain and 2D domain, referring to the vertical component of Rayleigh waves.

 The typical range of frequency for the seismic waves is between 1Hz and 10 Hz. Thus, starting with time domain of 1D domain problem, I set the fundamental frequency of the Ricker input wave at 6 Hz, as an average seismic frequency value. The Ricker wave is expressed as:

$$F(t) = [2(\pi F0(t - t_0))^2 - 1] \exp^{-\pi F0(t-t0)^2} \tag{2.44}$$

Where:

- $F_0 = 6Hz$, the fundamental frequency of the wave;

- $t_0 = \frac{1.5}{F_0}$ the delay.

Then, I implement an array of 30 resonators with a spacing of 5 m between adjacent elements. The elements' properties are set referring to columns made by vulcanized rubbers, shown in the Fig 2.41, which presents the following properties:

- height =5.5;

- diameter= 1.2 m;

- Elastic Modulus = 0.5 Gpa;

- density $(\rho) = 2200 \ kg/m^3$;

Thus, I obtain:

$$M_r = \pi(\frac{d}{2})^2 h\rho = 13700 \quad kg$$

$$K_r = \frac{EA}{h} = \frac{\pi(\frac{d}{2})^2}{h} = 2.056 \cdot 10^7 \quad N/m$$

$$\omega_r = \sqrt{\frac{K_r}{M_r}} = 38.76 \quad rad/s$$

$$f_r = \frac{\omega_r}{2\pi} = 6.17 \quad Hz$$

In the time domain representation, when the split Ricker wave hits the array of columns part of the energy is clearly reflected, as it is shown in the Fig 2.42. Thus, I obtain the same results of the previous examples where I investigated higher range of frequency.
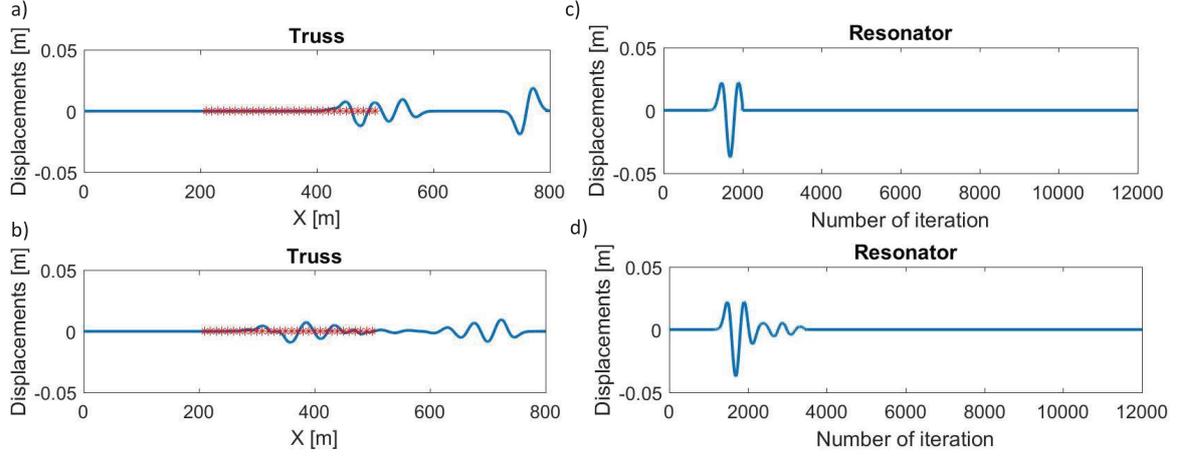
Figure 2.42: Time domain results for 1D low seismic frequency example. (a), (b) Wave transmission in the truss for two different instants of time, the red stars indicate the position of 30 resonators. (c),(d) First resonator's displacement referring to the same time's instances of the figure on the left.(a), (c) After 2000 iterations, because of the interaction between the resonator and the wavefront, the first resonator vibrates and the wave is trapped among the resonators, part of the energy is reflected. (b), (d) Same displacements after 3500 iterations, (b) part of the wave is reflected by the array of vulcanized rubber columns and (d) the first resonator' displacement becomes smaller.

Then, I move to the study of the same problem in the frequency domain and frequency-wavenumber domain, using the following input sweep wave:

$$F(t) = \frac{\omega t}{16\pi} \sin[2\pi(f_0 + bt)t] \qquad for \quad 0 \le t < \frac{16\pi}{\omega} \tag{2.45}$$

$$F(t) = \sin[2\pi(f_0 + bt)t] \qquad for \quad t \ge \frac{16\pi}{\omega}$$

Where:

- f_0=1 Hz, is initial input frequency;

- $b = 2$.

The range of frequency analyzed is between 1 and 15 Hz, and both the frequency spectrum and the dispersion curve show a clear bandgap around the resonance frequency (6.17 Hz). In the frequency-wavenumber domain, the branch becomes flat at 5 Hz and there is not wave propagation up to 8 Hz. Furthermore, the frequency spectrum shows a drop of energy of 50-70 dB at the bandgap. Hence, I obtain similar results to the previous examples but for a lower range of frequency.

Then, I move to the study of the same problem in 2D domain. I investigate the wave propagation of the sweep wave described above (see Eq:2.45) in a rectangular plate of 180x100 m coupled with a metabarrier, where each resonator is implementing referring to a vulcanized rubber column (see Fig.2.41). The resonators' lattice is composed by 12 rows of 29 resonators with a constant spacing of 5 m and is displayed in the Fig 2.44.

The frequency spectrum and the dispersion curve computed and reported in Fig 2.45 confirm the same results already discussed in 1D problem. The interaction with the metabarrier generates a clear bandgap around the resonance frequency of 6 Hz and the frequency spectrum shows a drop of energy up to 100 dB.
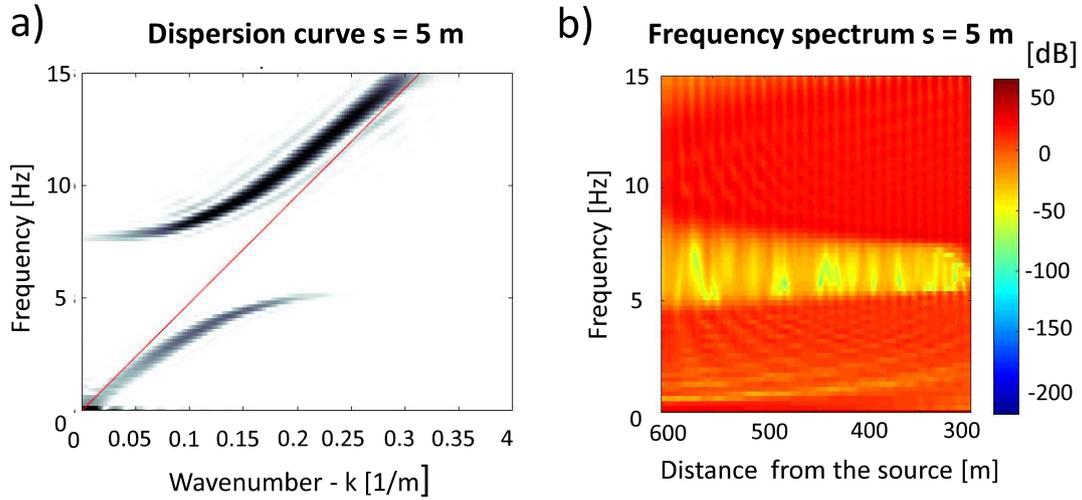
Figure 2.43: Results in frequency domain and frequency-wavenumber domain of the 1D truss coupled with an array of 30 resonators, which natural frequency is 6.17 Hz.(a) Dispersion curve shows a clear bandgap between 5 and 8 Hz, where the wave propagation is inhibited by the interaction with the array of vulcanized rubber columns. The red line represents the Rayleigh wave velocity in a no-dispersive medium. The same bandgap is represented in the frequency spectrum (b), where there is a drop of energy of 50-70 dB.
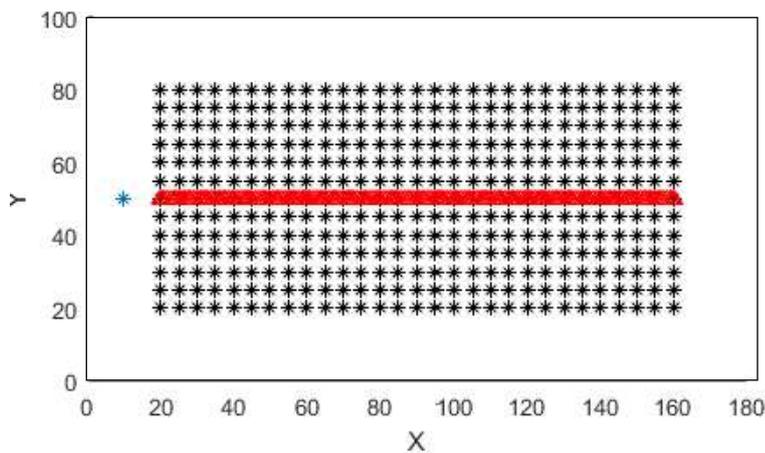

Figure 2.44: Spatial representation in x-y domain of resonators' lattice, with a constant spacing of 5 m between adjacent elements. The red line represents the array of seismometers used to the signal recording and the blue star symbolizes the input point wave.

a) **Dispersion curve s = 5 m**

b) **Frequency Spectrum s = 5 m** [dB]
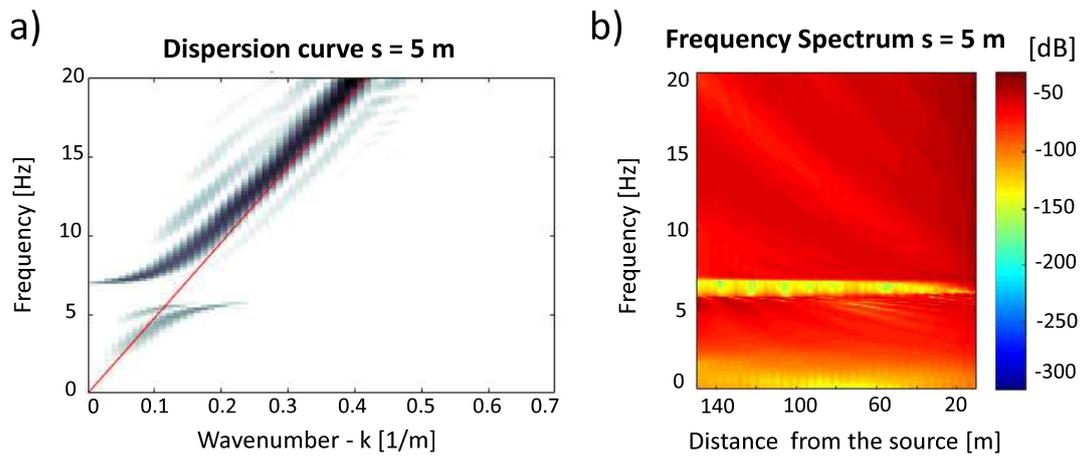
Figure 2.45: Results in frequency domain and frequency-wavenumber domain of the 2D plane coupled with metabarrier of resonators, which natural frequency is 6.17 Hz.(a) Dispersion curve shows a clear bandgap between 5 and 7 Hz, where the wave propagation is not permitted .The red line represents the Rayleigh wave velocity in a no-dispersive medium. The same bandgap is represented in the frequency spectrum (b), where there is a drop of energy up to 100 dB.

Chapter 3

Reciprocal space in 2D problems

Before discussing about the reciprocal space in 2D field, I will make some general remarks concerning the reciprocal space in 1 dimension. I have already analyzed the wave propagation in the reciprocal space (frequency-wavenumber domain) to obtain the dispersion curve, which allows to identify the bandgaps generated by the periodicity of the structure or by the interaction with resonators. The wave propagation in a 1D periodic structure presents the frequency as a periodic function of the wave number [3]:

$$\omega = f(k') \qquad period \ 2\pi \ in \ k' = 2\pi kd \tag{3.1}$$

$$f = F(k) \qquad period \ 1/d \ in \ k = 1/\lambda \tag{3.2}$$

Because the periodicity properties of the structure, it is sufficient to study the functions f and F inside only one period of k' or k to describe the whole behavior. As a wave always propagates to the right and to the left in the same way, f and F are even functions and the most convenient period for the analysis is:

$$-\pi \leq k' \leq \pi \tag{3.3}$$

$$-1/2d \leq k \leq 1/2d \tag{3.4}$$

Thus, if k or k' is positive the wave propagation is towards right and if k or k' is negative the wave is propagating to left. Therefore, if d is the length of the cell in the direct lattice which define the periodicity of the medium, in the reciprocal space $1/d$ give the frequency's periodicity, of the wave propagating into the medium, as function of the wavenumber. Then, I move to the description of the reciprocal space in 2D, using the 2D lattice in Fig 3.1, which is composed by particles with the same mass and equal distance to explain this concept. Thus, taking d_1 and d_2 as basis vectors, the vector coordinate of any point in the lattice is given by:

$$\mathbf{r_{l_1 l_2}} = l_1 \mathbf{d_1} + l_2 \mathbf{d_2} \tag{3.5}$$

Where l_1 and l_2 are positive integers. Thus, the lattice in x-y domain (direct lattice) is completely determined. For each direct lattice is possible to sketch a reciprocal lattice defined by b_1 and b_2 vector basis, which are determined by:

$$(\mathbf{b_i} \cdot \mathbf{d_k}) = \delta_{ik} \qquad i, k = 1, 2 \tag{3.6}$$

Where δ_{ik} is Kronecker symbol, defined by:

$$\begin{matrix} 1 & if & i = k \\ 0 & if & i \neq k \end{matrix}$$

Therefore, using in terms of Cartesian components, b_1 is perpendicular to d_1 and b_2 is perpendicular to d_1. The area of the elementary cell in the direct lattice and reciprocal lattice are reciprocals and are given respectively by:

$$S_d = |\mathbf{d_1} \times \mathbf{d_2}| = |\mathbf{d_1}||\mathbf{d_2}| \sin \theta \tag{3.7}$$

$$S_b = |\mathbf{b_1} \times \mathbf{b_2}| = |\mathbf{d_1}||\mathbf{d_2}| \sin \theta \tag{3.8}$$
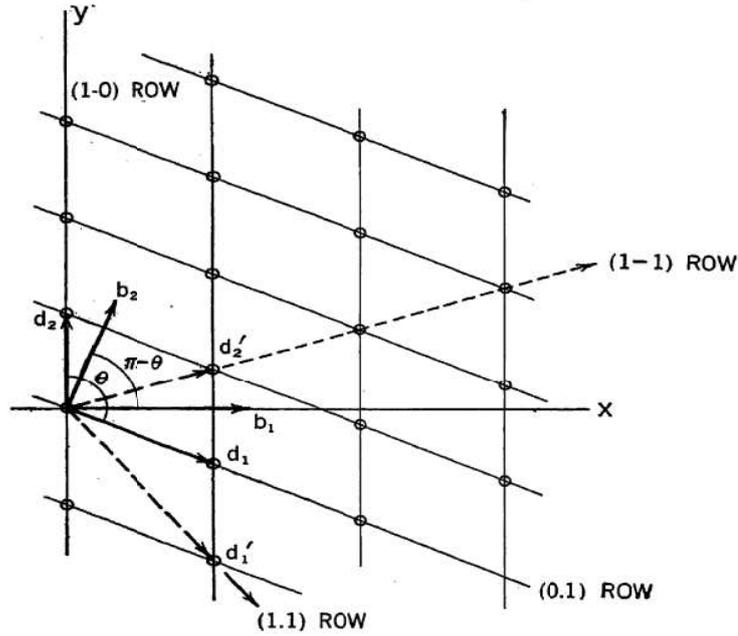
Figure 3.1: Example of two-dimensional periodic lattice [3]

In 1D it is possible to define into the frequency-wavenumber domain an interval containing one period in terms of the frequency. The same concept occurs in the 2D case, where it is possible to define different zones in the reciprocal lattice and the first zone is the elementary cell, named Brillouin zone after the French physicist Lèon Brillouin. When the structures is periodic studying a single elementary cell is enough to define the behavior of the whole structure. In the 2D reciprocal space the frequency is a function of the two components of the wavenumber: k_x and k_y. The Fig 3.2a is an example of isofrequency map in $k_x - k_y$ domain, where each line represent the locus of points characterized by the same frequency. Using a cross section of isofrequency map along Ox ($k_x = 0$), the frequency as a continuous function of k_x can be computed (Fig 3.2b), this amounts to the dispersion curves described in the previous chapter. The Fig. 3.2c,d show two different plots of the frequency, obtained respectively by a cross section at k_{y0} and a radial one along $O\rho$. In the last plot the frequency curve reach the boundaries with a no-zero normal derivate.

Therefore, I analyzed the $k_x - k_y$ domain trough numerical simulations computed with MATLAB. Using the same spectral element methods for two-dimensions described in the former examples. I computed a mesh of 100 x 100 m made by 100 x 100 elements, with a centered square resonators' lattice of 82 x 82 m with a constant spacing between adjacent elements of 2 m (see 3.3). The resonators' properties are set referring to a forest of pine trees, as before, but with a lower height. Since I want to investigate an higher range of frequencies I set parameters referring to the pine tree with the following characteristics:

- height = 9 m;

- density = 500 Kg/m^3;

- diameter = 0.4 m;

- Young's Modulus E= 3000 Mpa

Thus I obtain:

$$M_r = \pi(\frac{d}{2})^2 h\rho = 565.49 \quad kg$$

$$K_r = \frac{EA}{h} = \frac{\pi(\frac{d}{2})^2}{h} = 8.377 \cdot 10^7 N/m$$

$$\omega_r = \sqrt{\frac{K_r}{M_r}} = 384.9 \ rad/s$$

(a) ······ Locus of points where $-\frac{\partial \nu}{\partial \rho} = 0$

(b) Cross-section at $k_y = 0$

(c) Cross-section at $k_y \neq 0$
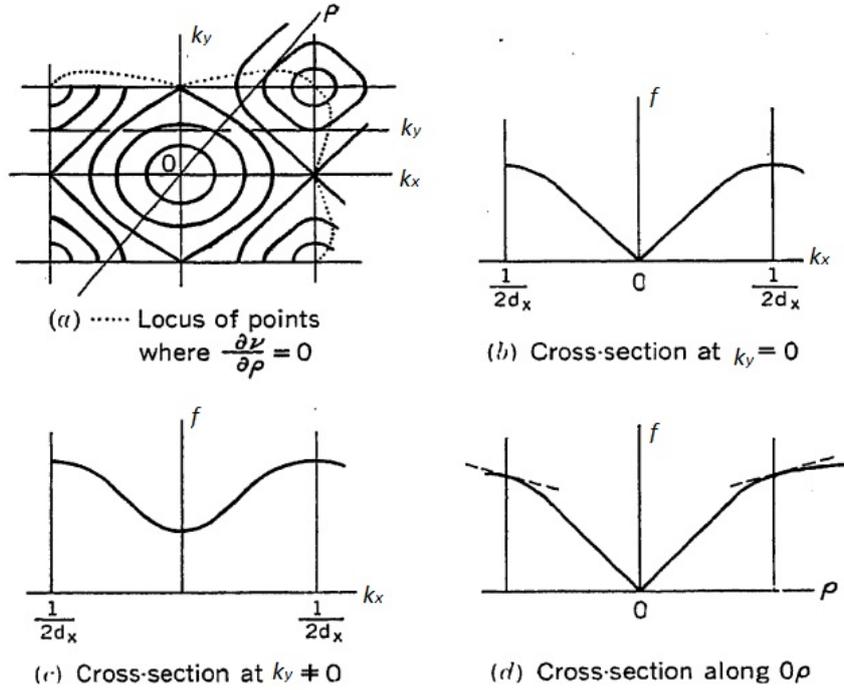
(d) Cross-section along 0ρ

Figure 3.2: Frequency representation in the reciprocal space in 2D domain [3]. (a) Isofrequency lines in $k_x - k_y$. (b), (c) Plots of $f - k_x$ obtained by cross sections of (a) along k_x at $k_y = 0$ and $k_y \neq 0$, where the frequency is a continuous function with a horizontal tangent at boundaries. Finally, (d) the $f - k_\rho$ diagram is computed by a radial cross section.[3]

$$f_r = \frac{\omega_r}{2\pi} = 61.26 \ Hz$$

The input wave is a a point source Gaussian wave:

$$F(t) = e^{[-2\pi f_0(t-t_0)]^2}$$

$$t_0 = 0.0473 \ s$$

The wave source is placed in plate's center and its fundamental frequency is set almost equal to the natural frequency of the trees ($f_0 = 60 \ Hz$). Then, I realized I centered square grid [82 x 82 m] of measuring points place every 0.5 m, for recording the wave propagation in x-y domain, as I have previously explained in the chapter " Filtered spatial representation in x-y". From data recording, I create a snapshot of the the wave propagation for different time of instance. Then, for a specific time of instance (0.127 s), I filtered the snapshot with a narrow pass-band of 0.1 Hz. In particular, I apply the same Butterworth filter explained in the Fig 2.35 in a range of frequency between 1 and 100 Hz. I report the spatial representation in x-y domain before the stop band and when it is entering inside in (see Fig 3.4). Before the bandgap (between 40.9 and 41 Hz) the wave propagation is homogeneous and is represented by increasing circles. On the contrary, applying the filter between 49.9 and 50 Hz, which corresponds to the beginning of the bandgap, the wave propagation presents anisotropic properties forming a cross, which represents the preference directions of propagation (see Fig 3.4c,e).

Afterwards, I compute the FFT2 (Fast Fourier Transform 2D) to the displacements in x-y domain, for a fixed time of instance, to achieve the wave propagation in the reciprocal space ($k_x - k_y$), which is defined by the elementary cell (Brillouin zone). The wave propagation is represented by circles, which color shows their amplitude's values (see Fig. 3.4). In particular, in each plot it is well highlighted the circle with the maximum amplitude, which grows increasing the frequency. Moreover, applying the passband filter between 50.9 and 51 Hz, where the displacements in the direct lattice show anisotropic properties, the circle becomes square (see Fig 3.4f).

The final goal is computing the different branches of the dispersion curve, which correspond to plot the frequency as a function of k_x ($\Gamma - X$ branch) , k_{xy} ($\Gamma - M$ branch) and k_y ($X - M$ branch). Thus, from the wave propagation in the reciprocal space, I compute the dispersion curves

60

for these branches. For this purpose, I use the same concept explained in the Fig. 3.2, where the $f - k$ diagrams are obtained by cross sections along x-axis (at y= 0), radial axis (specifically along the bisector) and y-axis (at x = X). Therefore, I implemented a simple algorithm to extract the maximum amplitude value and its position for each range of frequencies. The results are displayed in the Fig. 3.5, in particular FIg. 3.5e presents the dispersion curve for the all three different branches in the same diagrams. Therefore, using the spectral element method it has been possible to easily extract the dispersion relations along different directions and to analyze the anisotropic properties in the wave propagation.
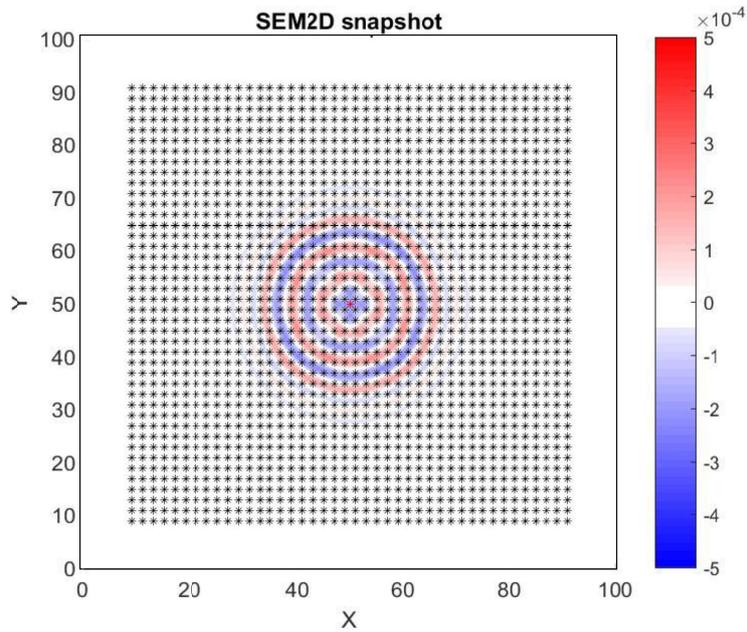

Figure 3.3: Spatial representation (x-y) of wave propagation in terms of displacements.The resonators' lattice (represented by black stars) is characterized by a constant spacing of 2 m.
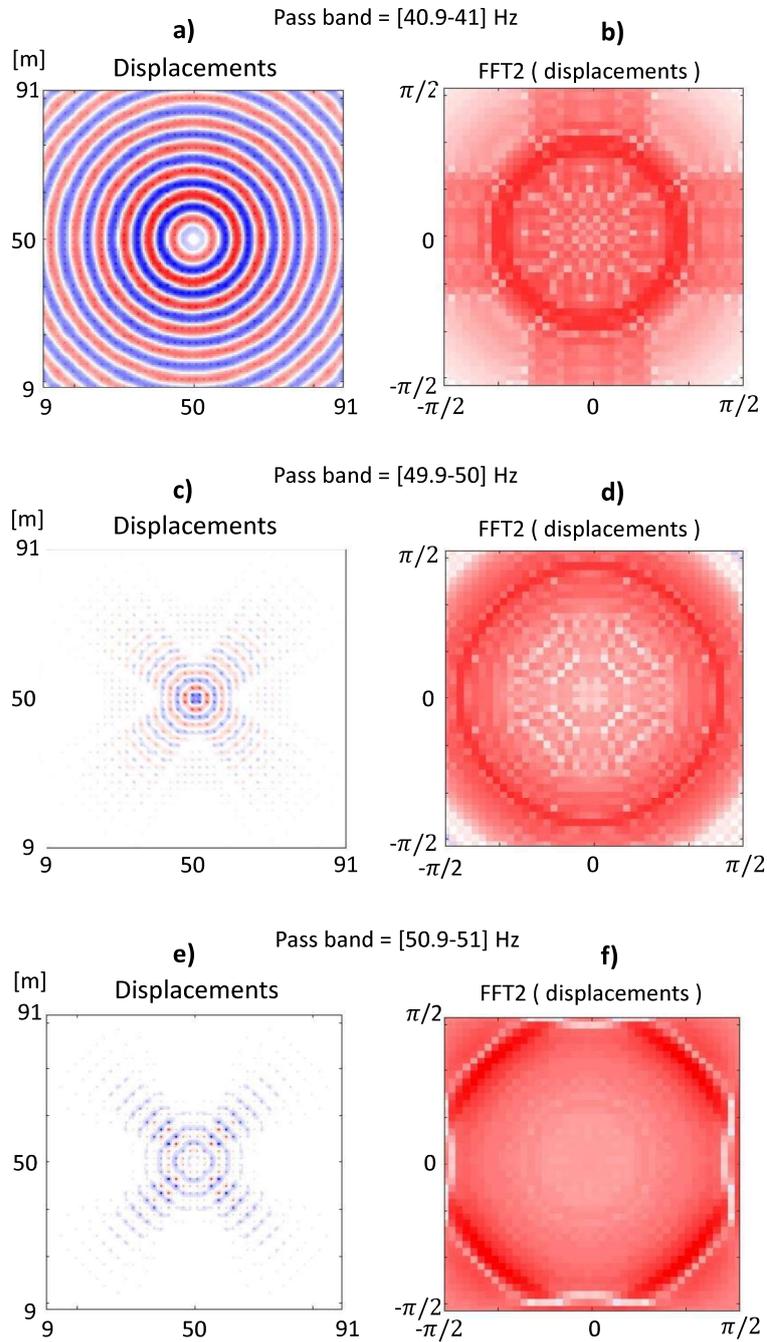
Figure 3.4: Displacements in x-y domain and in the reciprocal space $(k_x - k_y)$, filtered at different narrow passband. (a), (b) Results before the stop band, the wave propagation is homogeneous. (c), (d) Entering in the stop band the wave propagation shows anisotropic properties following preferential directions (c). Finally, inside the bandgap (e), (f) the wave is still traveling with 4 preferential directions and in the reciprocal space the circle becomes a square.

Γ-X

a)

Dispersion curve

b)

Frequency Spectrum

Γ-M

c)

Dispersion curve

d)

Frequency Spectrum
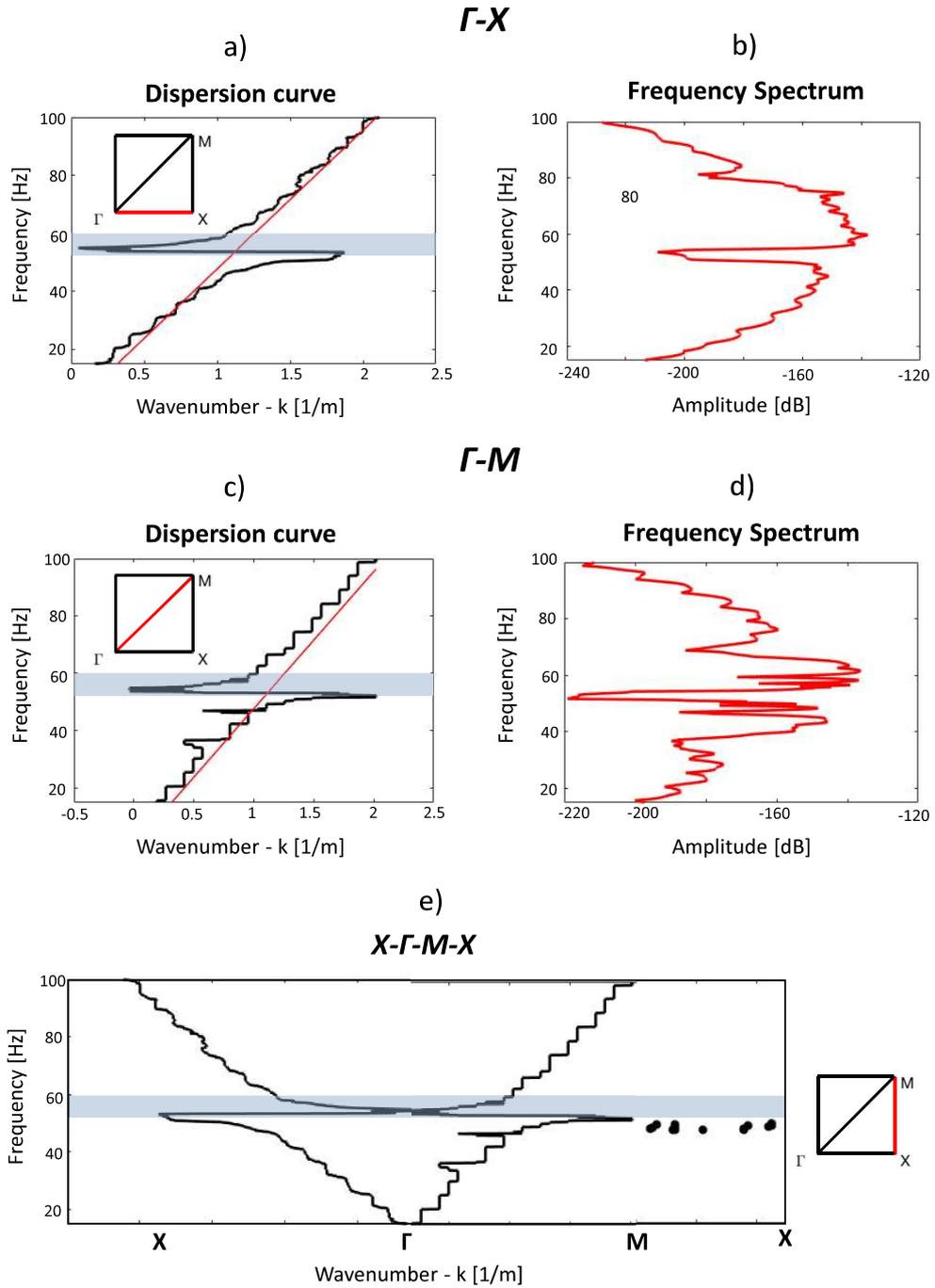
e)

X-Γ-M-X

Figure 3.5: Results in frequency-wavenumber domain and frequency domain. (a) The dispersion curve referred to the $\Gamma - X$ branch presents the maximum value of wavenumber around $\pi/2$, which corresponds to the boundary value defined by the elementary cell (see Fig. 3.4 d), and it shows a bandgap between 53 and 60 Hz and. At the same range, the frequency spectrum (b) presents a large drop of energy. (c) The dispersion curve referred to the $\Gamma - M$ branch presents the maximum value of wavenumber around $\sqrt{2}\pi/2$, since the branch $\Gamma - M$ is the bisector of the square and it shows a bandgap at the same range of frequency of the $\Gamma - X$ branch. (d) The frequency spectrum confirms the results, the energy decreases between 53 and 60 Hz. (e) Dispersion curves referred to the three branches together ($\Gamma - X$, $\Gamma - M$ and $M - X$) . The last branch $M - X$ is the most difficult to record, and it results more convenient its representation through points.

Chapter 4

Conclusion

The present thesis provides an efficient method for numerically studying the behavior of seismic metamaterials at different frequency ranges.

Seismic metamaterials are made by locally resonant units, able to partially control the wave transmission generating bandgaps, frequency ranges where the wave propagation is forbidden, related to the resonance frequency of locally resonators.

The numerical simulations presented in this work are performed in time domain with spectral element method, an efficient formulation of the finite element method that provides a numerical solution of partial differential equations with a low computational cost. Therefore, this method is really efficient to conduct a sensitivity analysis over design parameters, in order to study the metamateials' behavior and to improve their effectiveness.

The analysis carried out in both 1D and 2D domains, confirms the presence of bandgap related to the resonance frequency of resonators. Furthermore, from the sensitivity analysis the parameters that deeply influence the effectiveness of the seismic metamaterials are: the density of resonators and the damping effect. Indeed, decreasing the spacing between adjacent elements, resonators increases their efficiency opening bandgap wider in terms of frequency and deeper in terms of amplitude. Moreover, it is necessary to guarantee a distance among elements smaller than $\lambda/2$, referring to the wave they have an influence on. Even the damping effect strongly modify the metamaterials' behavior. Indeed, the control of seismic waves is clearly smoothed by the presence of damping, but the effect of attenuation disappears for low levels of damping. On other hand, it has been proved that implementing spatially graded arrays of vertical resonators with increasing or decreasing height, it possible to widen the stop band generated in terms of frequency. Thus, each resonator is tuned at a different resonant frequency and the efficiency of the entire metastructure improves. On the contrary the parameters that do not influence the metamaterials' performance are the periodicity and the kind of source. Thus, it has been demonstrated that this type of metamaterials, made by resonant units, properly work even with elements disordered distribution. Furthermore, their action does not change for different kind of source and it has been verified that their behavior is the same with a point source wave and with a plane wave.

Finally, it has been studied the reciprocal space in 2D field, with the same method explained above, to extract even the dispersion curves referred to the radial and vertical branches. Indeed, in the previous examples the study in the frequency-wavenumber domain had been restricted the wavenumber' horizontal branch.

The possible challenge for the future is to carry out a large-scale experiments to investigate the interaction between metamateirals and seismic waves in the frequency's range typical of seismic events, between 1 and 10 Hz. Indeed, it is possible to design resonators which natural frequency match this range, but it is necessary to test their structural integrity with high dynamic loads typical of devastating earthquakes. Moreover, another important challenge is to move to the study of Love waves, the other main group of seismic surface waves. Indeed, it would be extremely useful to design seismic metamaterials capable of reflecting the two main kinds of surface waves, which control represent the leading problem in Earthquake engineering.

Bibliography

[1] Absorbing boundary conditions for acoustic and elastic wave equations, December 1977.

[2] Spectral-domain decomposition methods for the solution of acoustic and elastic wave equations, August 1996.

[3] Lèon Brillouin. *Wave propagation in periodic structures*. Dover Publication, 1953.

[4] Andrea Colombi, Victoria Ageeva, Richard J. Smith, Adam Clare, Rikesh Patel, Matt Clark, Daniel Colquitt, Philippe Roux, Sebastien Guenneau, and Richard V. Craster. Enhanced sensing and conversion of ultrasonic rayleigh waves by elastic metasurfaces. *Scientific Reports*, 7(1):6750, July 2017.

[5] Andrea Colombi, Daniel Colquitt, Philippe Roux, Sebastien Guenneau, and Richard V. Craster. A seismic metamaterial: The resonant metawedge. *Scientific Reports*, 6:27717, June 2016.

[6] Andrea Colombi, Philippe Roux, Sebastien Guenneau, Philippe Gueguen, and Richard V. Craster. Forests as a natural seismic metamaterial: Rayleigh wave bandgaps induced by local resonances. *Scientific Reports*, 6:19238, January 2016.

[7] D.J. Colquitt, A. Colombi, R.V. Craster, P. Roux, and S.R.L. Guenneau. Seismic metasurfaces: Sub-wavelength resonators and rayleigh wave interaction. *Journal of the Mechanics and Physics of Solids*, 99:379 – 393, 2017.

[8] Ezio Faccioli, Fabio Maggio, Roberto Paolucci, and Alfio Quarteroni. 2d and 3d elastic wave propagation by a pseudo-spectral domain decomposition method. *Journal of Seismology*, 1:237–251, November 1997.

[9] Ake Bjorck Germund Dahlquist. *Numerical Methods*. Prentice-Hall, 1974.

[10] Thomas J. R. Hughes. *The Finite Element Method: Linear Static and Dynamic Finite Element Analysis*. Dover Publications Basel, 2000.

[11] Sajeev John. Strong localization of photons in certain disordered dielectric superlattices. *Physical Review Letters*, 1987.

[12] Antil K-Chopra. *Dynamics of structures: Theory and Applications to Earthquake Engineering*. Prentice-Hall, 1995.

[13] D. Komatitsch and R. Martin. An unsplit convolutional perfectly matched layer improved at grazing incidence for the seismic wave equation. *GEOPHYSICS*, 72(5):SM155–SM167, September 2007.

[14] Dimitri Komatitsch and Jeroen Tromp. Introduction to the spectral element method for three-dimensional seismic wave propagation. *Geophysical Journal International*, 139(3):806–822, 1999.

[15] Ming-Hui Lu, Liang Feng, and Yan-Feng Chen. Phononic crystals and acoustic metamaterials. *Materials Today*, 12(12):34 – 42, 2009.

[16] Fabio Maggio and Alfio Quarteroni. Acoustic wave simulation by spectral methods. *East-West Journal of Numerical Mathematics*, 2, January 1994.

[17] G.W. Milton. *The Theory of Composites*. The Theory of Composites, 2002.

[18] Andrey E. Miroshnichenko, Sergej Flach, and Yuri S. Kivshar. Fano resonances in nanoscale structures. *Rev. Mod. Phys.*, 82(3):2257–2298, August 2010.

[19] Nathan M. Newmark. A method of computation for structural dynamics. *Journal of the Engineering Mechanics Division*, 1959.

[20] Antonio Palermo, Sebastian Krödel, Alessandro Marzani, and Chiara Daraio. Engineered metabarrier as shield from seismic surface waves. *Scientific Reports*, 6:39356, December 2016.

[21] J. B. Pendry, D. Schurig, and D. R. Smith. Controlling electromagnetic fields. *Science*, 312(5781):1780–1782, 2006.

[22] Yan Pennec and Bahram Djafari Rouhani. *Phononic Crystals, Fundamentals and Applications*. Springer, 2016.

[23] Daniel Peter, Dimitri Komatitsch, Yang Luo, Roland Martin, Nicolas Le Goff, Emanuele Casarotti, Pieyre Le Loher, Federica Magnoni, Qinya Liu, Céline Blitz, Tarje Nissen-Meyer, Piero Basini, and Jeroen Tromp. Forward and adjoint simulations of seismic wave propagation on fully unstructured hexahedral meshes. *Geophysical Journal International*, 186(2):721–739, August 2011.

[24] C. Pozrikidis. *Introduction to Finite and Spectral Element Methods using MATLAB*. Taylor & Francis Group, 2005.

[25] Robert W. Ramirez. *The FFT Foundamental and Concepts*. Tektronix, 1985.

[26] Philippe Roux, Dino Bindi, Tobias Boxberger, Andrea Colombi, Fabrice Cotton, Isabelle Douste Bacque, Stephane Garambois, Philippe Gueguen, Gregor Hillers, Dan Hollis, Thomas Lecocq, and Ildut Pondaven. Toward seismic metamaterials: The metaforet project. *Seismological Research Letters*, January 2018.

[27] Matthieu Rupin, Fabrice Lemoult, Geoffroy Lerosey, and Philippe Roux. Experimental demonstration of ordered and disordered multiresonant metamaterials for lamb waves. *Phys. Rev. Lett.*, 112(23):234301, June 2014.

[28] S. Stein and M. Wysession. *An introduction to seismology, earthquakes, and earth structure*. Blackwell Publishing, 2003.

[29] Kosmas L. Tsakmakidis, Allan D. Boardman, and Ortwin Hess. 'trapped rainbow' storage of light in metamaterials. *Nature*, 450:397, November 2007.

[30] Viktor G. Veselago. The electrodynamics of substances with simultaneously negative values of ϵ and μ. *Soviet Physics Uspekhi*, 10(4):509, 1968.

[31] Wikipedia. *Bragg diffraction*.

[32] Wikipedia. *Butterworth filter example*.

[33] Earl G. Williams, Philippe Roux, Matthieu Rupin, and W. A. Kuperman. Theory of multiresonant metamaterials for A_0 lamb waves. *Phys. Rev. B*, 91(10):104307, March 2015.

[34] Eli Yablonovitch. Inhibited spontaneous emission in solid-state physics and electronics. *Physical Review Letters*, 1986.